Linking cell dynamics with coexpression networks to characterize key events in chronic virus infection

María Graciela Riera Domínguez

TESI DOCTORAL UPF / 2018

DIRECTORS DE LA TESI

Dr. Andreas Meyerhans i Dr. Jordi Argilaguet

DEPARTAMENT DE CIÈNCIES EXPERIMENTALS I DE LA SALUT

Universitat Pompeu Fabra Barcelona

A mis papás,

ACKNOWLEDGEMENTS

Todavía no me creo que estoy escribiendo esta página. Ha llegado el momento de agradecer a todas esas personas que de una u otra manera han sido parte de este gran desafío.

I would like to thank all the people who have helped and supported me over all these years, for without you none of this would have been possible.

First and foremost, I want to thank my thesis director, **Andreas Meyerhans**, for giving me the opportunity to work in his lab, for his patience, motivation, and immense knowledge.

Quiero agradecer también a **Jordi** por la paciencia y la confianza. Gracias por tomarte el tiempo de enseñarme y guiarme durante todos estos años. Tu ayuda y apoyo moral han sido fundamental para que haya terminado este doctorado.

Quiero agradecer a mi catalana favorita, **Mireia**, por tomarte el tiempo en enseñarme cómo trabajar amb els ratulins. Gracias por las risas y las clases de catalán, por compartir mis tonterías, escuchar mis historias y hacer que las horas sean más cortas en el laboratorio. He tenido la suerte del mundo de tenerte como compañera de laboratorio. Merci!

I also want to thanks to all the lab members, past and present that have trained and helped me along the way. From the Infectious Biology group: **Valentina**, **Mie**, **Eva**, **Javier**, who have contributed immensely to my personal and professional time.

No quiero olvidarme de agradecer al grupo de Molecular Biology: **Juana**, gracias por darme la oportunidad de dar clases, ha sido una de las experiencias más desafiantes e increíbles de este 2018. **Gemma**, **Leire** y **Marc**, que siempre me han ayudado con todo. Gracias por dejarme robarles materiales y reactivos. **Jenni** no te imaginas todo lo que he aprendido y me he divertido contigo durante las prácticas de Microbiología.

Special thanks to **Katarina**. Barcelona has given me the greatest friend/accomplice/partner in crime/labmate I couldn't possibly ask for. You know what you mean to me.

A l'**Eva**, l'**Erika**, l'**Òscar** i a l'**Alex** pel suport tècnic, les classes de català i per fer més entretingudes les hores davant del citòmetre.

Durante estos 3 años en Barcelona, he conocido gente increíble, con la que he disfrutado tanto de esta ciudad y han estado a mi lado siempre. Ustedes saben quienes son, no se preocupen que les haré llegar el cariño que les tengo de forma personal. Gracias!
Josep, gracias por acompañarme durante estos años. Conocerte me ha cambiado la vida.

No quiero olvidarme de la más genia de todas, **Agostina**, mi argentina favorita. Gracias por las horas al teléfono, por los audios de 5 minutos, por los viajes juntas, por los mates, por las terapias en el balconcito y por hacerme el aguante mientras escribía esta tesis.

Carmen, eres una persona excepcional. No se que hubiese hecho sin ti, sin nuestras salidas, nuestras cañitas, las horas interminables hablando de la vida. Como te voy a extrañar!

Quiero agradecer también a mis amigas de Paraguay, **Ga**, **Ade**, **Tuli**, **Nati** y **Yoli**, gracias por hacer que la distancia no se sienta tan distancia y por estar ahí siempre.

New York me ha regalado personas con quienes siempre he contado de forma incondicional, hasta el día de hoy.

Doc, gracias por tomarte el tiempo de escucharme siempre, sentarte conmigo en el los banquitos de Washington Square Park y las horas interminables hablando por Skype, las cervezas y el psicoanálisis.

Niko, I'm the luckiest girl in the world to have you in my life. Thank you for always being there for me and for all your help and support throughout my days in New York and here in Barcelona. Also, thank you for taking the time to review this thesis. You are the best!

Quiero agradecer también a mi hermosa familia. Durante todos estos años fuera de casa me he dado cuenta que lo más importante son ustedes. A mis hermanos, por el apoyo y aguante durante todos estos años lejos de casa. **Mane**, sabes que todo empezó con el foco azul? Eres mi ejemplo de estudio, constancia y perseverancia. Gracias por tu ejemplo, tus consejos y por darme una mano con este documento. **Vero**, has sido el pilar que me ha mantenido en pie

todos estos años de estudio y fuera de casa, gracias por hacer que las distancias no se sientan tan distancias. **Chi**, gracias por tus palabras de aliento, por tu apoyo emocional siempre, por escucharme y ser honesta conmigo. A mis cuñados: **Nino**, gracias por nuestras conversaciones intelectuales. **Arie**, gracias por estar ahí siempre. **Germán**, bienvenido a la familia, felices de tenerte.

No me quiero olvidar de **Tío Enri** y **Tía Cruz**, que me acompañaron en este desafío desde día cero. Gracias por las hermosas palabras de aliento, por las conversaciones profundas y los abrazos y besos cuando más necesitaba.

Por último, quiero agradecer a mis papás, por estar conmigo en cada paso, por ser incondicionales y por apoyarme siempre en todas mis decisiones.
Papi, te admiro y te quiero. Orgullosa de tenerte como papá/asesor jurídico/referencia. Gracias por guiarme y acompañarme todos estos años.
Mami, sos una mamá excepcional, gracias por las horas del otro lado del teléfono, las comidas calentitas, por estar a mi lado siempre.

Nada de esto hubiese sido posible sin ustedes. Esto va por y para ustedes. Les quiero, son mi mundo entero.

Gracie Riera,

Barcelona, September 28th, 2018.

SUMMARY

The host immune response against infection requires the coordinated action of many diverse cell subsets that dynamically adapt to a pathogen threat. Due to the complexity of such a response, most immunological studies have focused on a few genes, proteins, or cell types. With the development of "omic"-technologies and computational analysis methods, attempts to analyze and understand complex system dynamics are now feasible. However, the decomposition of transcriptomic data sets generated from complete organs remains a major challenge. Here, we combined Weighted Gene Coexpression Network Analysis (WGCNA) and Digital Cell Quantifier (DCQ) to analyze time-resolved mouse splenic transcriptomes in acute and chronic Lymphocytic Choriomeningitis Virus (LCMV) infections. This enabled us to generate hypotheses about complex immune functioning after a virus-induced perturbation. This strategy was validated by successfully predicting several known immune phenomena, such as effector cytotoxic T lymphocyte (CTL) expansion and exhaustion. Furthermore, we predicted and subsequently verified experimentally that virus-specific $CD8^+$ T cells with an early effector transcriptome profile participate in the host adaptation to an overwhelming virus threat. Thus, the linking of gene expression changes with immune cell kinetics provides novel insights into the complex immune processes within infected tissues.

RESUMEN

La respuesta inmune del huésped contra una infección requiere la acción coordinada de varios tipos de células que, de forma dinámica, se adapta a la amenaza del patógeno. Debido a la complejidad de dicha respuesta, la mayoría de los estudios inmunológicos se han centrado en pocos genes, proteínas o en células específicas. Con el desarrollo de tecnologías "ómicas" y métodos de análisis computacionales, los intentos de analizar y comprender sistemas complejos ahora son más factibles. Sin embargo, la descomposición de datos de transcriptomas, generados a partir de órganos completos sigue siendo un desafío importante. Aquí he combinado Weighted Gene Coexpression Network Analysis (WGCNA) y Digital Cell Quantifier (DCQ) para analizar los perfiles transcriptómicos de bazos de ratón, a diferentes tiempos, durante la infección aguda y crónica por el virus de la Coriomeningitis Linfocítica Aguda (LCMV). Este método nos ha permitido generar hipótesis sobre funcionamiento del complejo sistema inmune después de una perturbación inducida por el virus. Esta estrategia fue validada al predecir con éxito varios fenómenos inmunes conocidos, como la expansión de los linfocitos T citotóxicos (CTL) y el fenómeno conocido como agotamiento. Además, he predicho y posteriormente verificado de forma experimental que las células efectoras T $CD8^+$ específicas de virus, con un perfil de transcriptoma efector temprano, participan en la adaptación a la amenaza del virus. Por lo tanto, la conexión entre la expresión de genes y la cinética de las células del sistema inmune, proporciona nuevos conocimientos sobre los complejos procesos inmunes en tejidos infectados.

PROLOGUE

The host immune response against infection is a complex multi-level interaction network of hundreds of different cell subsets that maintain a fine balance between host defense and inflammatory disease. Traditionally, immunological studies have focused on specific cell subsets and individual components of the immune system. Therefore, our current understanding lacks a systemic perspective on the dynamic changes involved in creating a concerted immune response. Omics-technologies that have emerged during the last several years, have helped to overcome this obstacle. Together, with the development of novel analytical tools, it is now feasible to extract relevant information from large amounts of data that capture the complexity of a biological system. One example is Weighted Gene Coexpression Network Analysis (WGCNA), a tool increasingly used to explore the system-level functionality of genes. It gives information about the expression patterns of highly interconnected genes, which are organized in clusters or modules. We have previously shown that WGCNA is a powerful tool to study system level infection-fate-specific gene signatures from splenic transcriptomes. This research has shown that whole organ signatures can be a valuable, phenotype correlating data set. Furthermore, we have identified infection-fate-specific networks among the gene coexpression modules that might provide novel mechanisms that influence the outcome of an infection. This approach, however, does not provide information about the cell subsets involved in biological pathways. To this end, a novel algorithm called Digital Cell Quantifier (DCQ) has proven to be effective to infer global dynamic changes in immune cell quantities from genome-wide transcription profiles of a specific organ, thus elucidating information that WGCNA could not provide. Here, we proved that combining WGCNA and DCQ it is possible to link gene expression changes to cell kinetics giving a global view of the transcription and cell dynamic changes happening in a specific organ. We use this approach to generate hypotheses on genetic changes that occurs in different immune cell subsets, and therefore, to understand fate-decision regulation and the coordinated action of the immune system.

TABLE OF CONTENTS

INTRODUCTION

1. System-level understanding of biological systems

Systems biology is an interdisciplinary approach to understand the interrelationships between networks of biological processes over time (Diaz-Beltran et al., 2013). The coordinated response of the cells of the innate immune system is the first line of defense against invading pathogens, and along with the adaptive immune responses, they play a critical role in the establishment of long-term protective immunity (Janeway and Medzhitov, 1998). The immune system is well suited for systems analysis as relevant cells can be isolated in different functional states and their interactions can be reconstituted in a biological meaningful manner (Zak and Aderem, 2009). Application of the tools of systems biology to the immune system will enable comprehensive analyses of the complex interactions that maintain the fine balance between host defense and inflammatory disease (Diercks and Aderem, 2013; Kitano, 2001).

One of the first uses of the system biology approach were over a decade ago, with the studies of the correlation between protein and mRNA abundance using exponential-phase batch culture of yeast (Gygi et al., 1999) and studies focusing on integrated analysis of the yeast galactose assimilation pathways (Fell, 2001; Ideker et al., 2001). In the infectious disease field, advances have been made with the first genomic analysis of HIV-infected cells in culture using cDNA microarrays (Geiss et al., 2000). Other reports of transcriptional profiling of virus infected cells and tissues have followed (Chakrabarti et al., 2010; Ertl and Klein, 2014; Lederer et al., 2009; Speranza and Connor, 2017; Sun et al., 2017), showing the importance of more exhaustive and comprehensive integrative methods for elucidating complex regulatory networks and the interrelationships between them.

1.1. Systems immunology: Putting the pieces together

The immune system has a high degree of interdependence and interconnection between hundreds of different cell subsets to maintain the fine balance between host defense and inflammatory disease (Davis and Shen-Orr, 2013; Katze, 2013). A particular biological function can be rarely attributed to a single cell. Rather, immunological processes are undoubtedly more complicated and are determined by a complex interaction among different components of the immune system (Davis and Shen-Orr, 2013; Diaz-Beltran et al., 2013; Robinson et al., 2014). Therefore, instead of analyzing individual components, the field of

systems immunology may provide a comprehensive understanding of how these components function together as a whole (Davis and Shen-Orr, 2013). One of the major goals of systems immunology is to quantitatively measure these complex interactions, allowing the development of computational models to predict responses to perturbations (Subramanian et al., 2015).

The new "omics"-technologies that have emerged during the last years have enabled to address fundamental questions in systems immunology. Together with the development of novel analytical tools, it is now feasible to extract relevant information from large amounts of data that capture the complexity of a biological system at a genome-wide scale and reveal underlying mechanisms involved in complex immune responses (Kidd et al., 2014).

1.2. Gene Coexpression Network Analysis

The construction and analysis of gene networks has been a valuable platform to study gene expression levels of thousands of genes simultaneously and the interconnectedness between them (Zhao et al., 2010). These networks represent the complex functional organization of biological systems in a genome-wide manner (Barabási and Oltvai, 2004; Serin et al., 2016). One of the methods increasingly used to explore the function of genes from a systemic point of view is the Weighted Gene Coexpression Network Analysis (WGCNA). WGCNA is a powerful system biology method to construct gene networks of clusters (modules) of highly interconnected genes and to identify central players (i.e., hub genes) within these modules.

The WGCNA workflow is as follows: (i) Construct a gene coexpression network represented mathematically by an adjacency matrix, the element of which indicates coexpression similarity between a pair of genes. (ii) Identify modules: WGCNA uses hierarchical clustering to identify modules. To measure the dissimilarity between clusters, WGCNA uses a topological overlap measure that can result in biologically meaningful modules in real data analysis. (iii) Relate modules to external information (phenotypes): several methods can be used to measure the association of a module to a phenotypic trait. For instance, one can test the association between the module eigengene (ME) and the phenotypic trait. The ME of a module is defined as the first principal component of the module. One can also use the module significance (MS), which is defined as the average gene significance (GS) of all genes in the module, to assess the association of a module to a phenotype. The GS of a node

is defined as the correlation between the node and the phenotypic trait. Modules with high trait significance may represent pathways associated with the phenotypic trait. (iv) Study inter-module relationships: WGCNA uses ME as a representative profile of a module and quantifies module similarity by eigengene correlations. Studying the relationship of the modules can help to find which modules are highly related. (v) Find key drivers in interesting modules: the nodes having the largest number of edges are most important because the malfunction of these genes would affect all connected genes (Langfelder and Horvath, 2008; Zhang and Horvath, 2005). The WGCNA workflow is depicted in Figure I1.

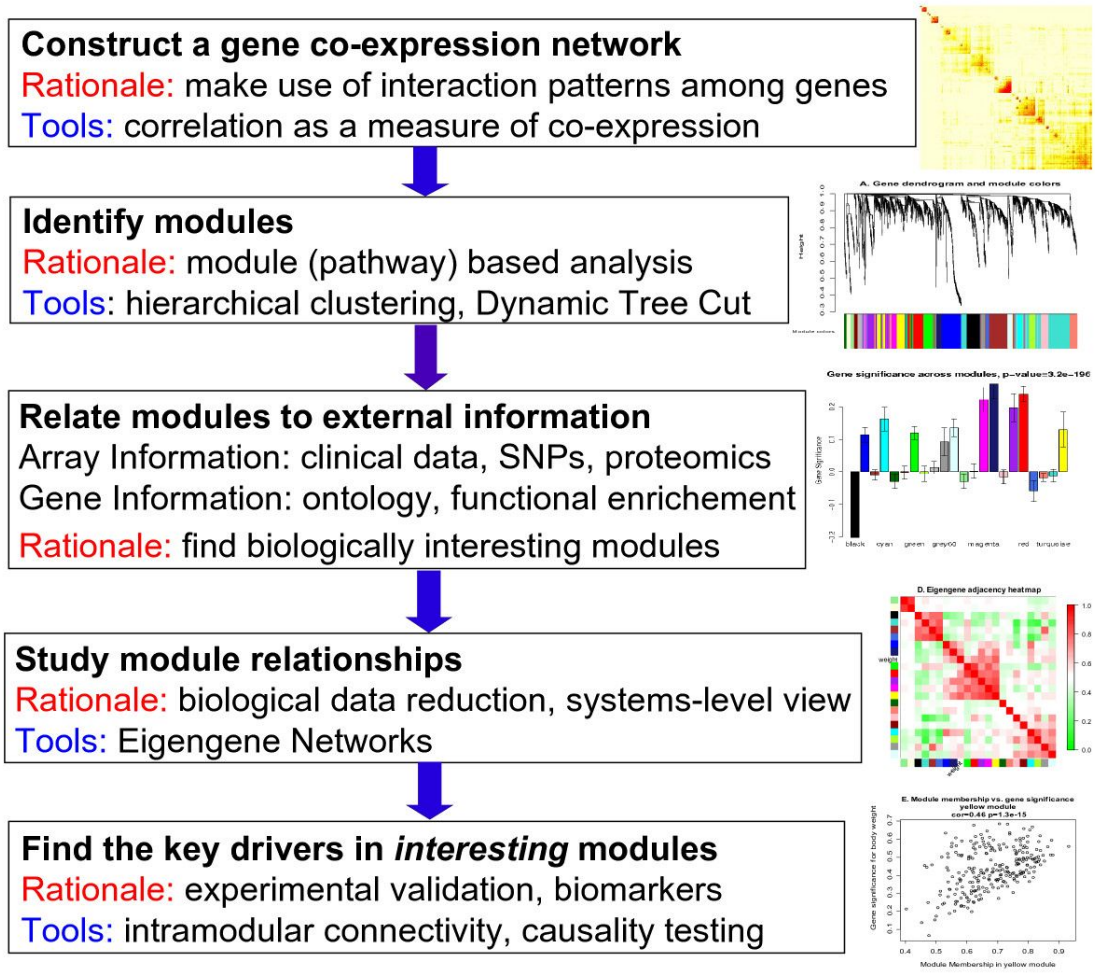

Figure I1: Overview of WGCNA workflow. Flowchart representing an overview of the main steps of Weighted Gene Coexpression Network Analysis. Figure obtained from Langfelder and Horvath, 2008.

In contrast to the traditional analyses of transcriptome data, WGCNA allows to better understand a biological system as a whole. This is accomplished by a biologically meaningful reduction of high dimensional data based on the identification of clusters (modules) of highly coexpressed genes sharing expression patterns. Analyses of these modules and their hub genes can provide insight into the underlying biological processes they represent (Langfelder and Horvath, 2008). Coexpression network analysis offers three major features, making this approach a valuable tool to analyze highly complex transcriptome data. First, in the analysis are included genes with low changes in their expression levels that might be highly connected to genes in a defined module. Second, trait-module relationships are identified, permitting to characterize the molecular mechanisms underlying a phenotype of interest. And third, the analysis of the degree of preservation between modules from independent data sets, allowing the identification of highly conserved and highly-specific modules. WGCNA has been used at both cell and tissue levels, allowing to identify pathways associated with effector and exhausted $CD8^+$ T cells (Doering et al., 2012), with different simian immunodeficiency virus (SIV) infection phenotypes using whole blood transcriptome data (Yang et al., 2016) and with hepatocellular carcinoma and breast cancer (Cheng et al., 2017; Guo et al., 2017). Thus, bioinformatic analysis based on gene coexpression networks enables to extract the main temporal events that are involved in complex biological systems.

1.3. Global Cell Dynamics

Several techniques have been developed to study the changes in the quantities in a particular immune-cell types within a complex tissue in the context of health and disease. High-throughput profiling technologies, such as fluorescence-activated cell sorting (FACS; (Ibrahim and van den Engh, 2007), cytometry by time-of-flight (CyTOF; (Bjornson et al., 2013)), confocal/two photon imaging (Cahalan et al., 2002), among others, have enabled the understanding of the immune system across multiple cellular components and time points. However, these methods are restricted to a small number of cell subsets. To address this obstacle, computational deconvolution methods were developed to infer changes in different cell-type quantities from gene expression data of a complex tissue.

Digital Cell Quantifier (DCQ) is an algorithm to study the changes in immune cell dynamics between two or more study conditions using as an input gene expression data from whole tissue. DCQ takes as input (i) differential genome-wide transcription profiles of organs that

were measured in two or more conditions (e.g., time points, perturbations) and (ii) a precompiled compendium of prior information about the abundance of each cell surface marker in each immune cell type. The outputs are interpretable hypotheses about changes in quantities of specific immune cell types between the two conditions. This method has been proven to be effective when applied to infer the dynamics of hundreds of immune cell subsets in mouse spleens upon influenza virus infection (Altboum et al., 2014). The DCQ algorithm is depicted in Figure I2.

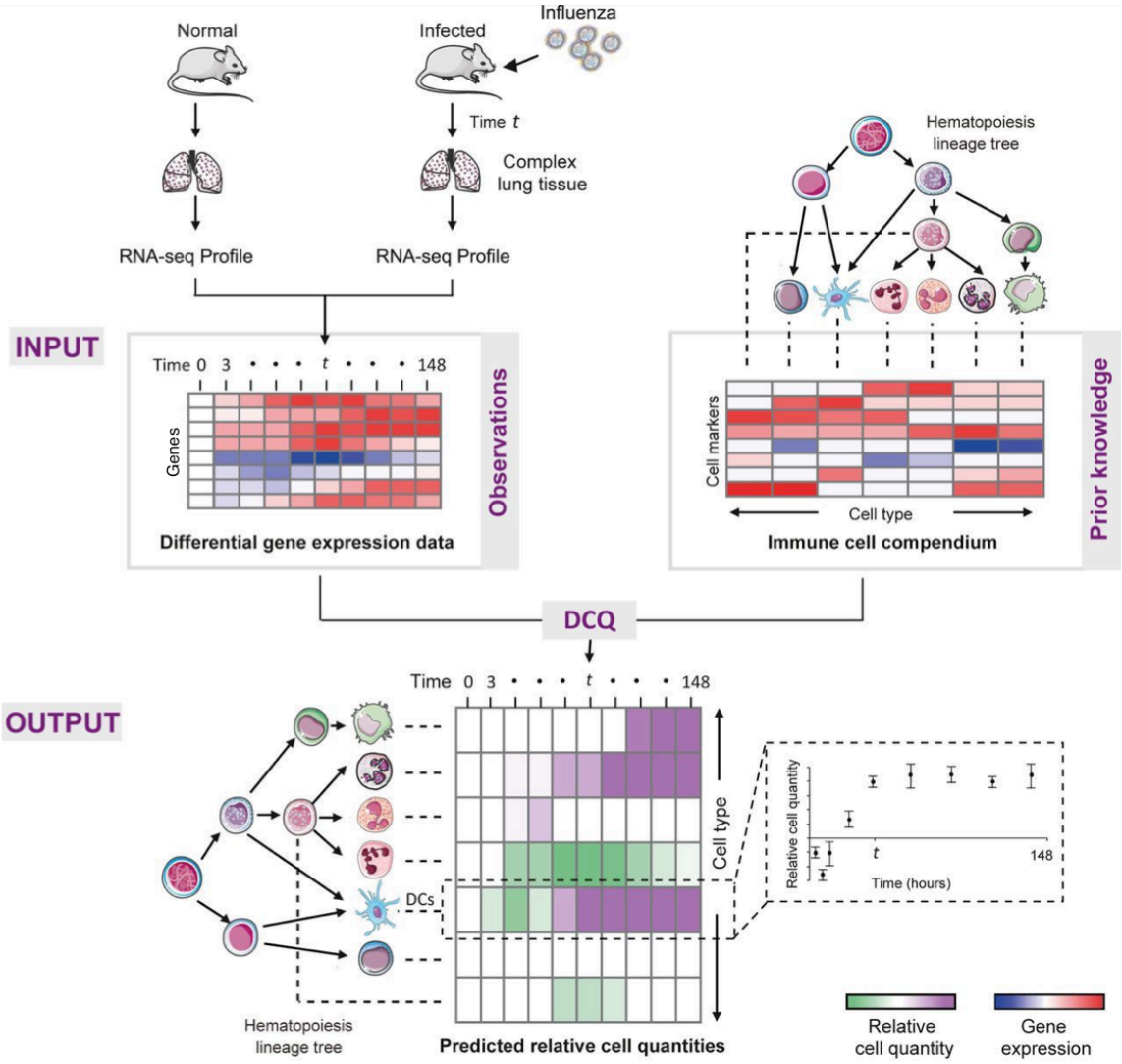

Figure I2. Overview of the Digital Cell Quantifier (DCQ) algorithm. DCQ method takes two gene expression datasets as input: First (top left), differential genome-wide expression data from a complex tissue (i.e., the lung). The rows represent the genes and the columns represent samples (i.e. timepoints postinfection). High and low transcript level are color-coded in red and blue, respectively. Second (top right), a precompiled compendium of prior information about the abundance of each cell surface marker in each immune cell type, where rows represent surface cell markers and columns represent immune cell types. Immune cell types are illustrated together with their hierarchical hematopoietic cell lineages. DCQ provides as output a matrix (bottom) of predicted relative cell quantities for each immune cell type (row) in each sample (column). Increase or decrease in cell quantity is color-coded in purple and green, respectively. Scatter plots (bottom right) as an example, show the inferred amount of dendritic cells (y-axis) during the time course of infection (x-axis). Here, DC's quantity is reduced during the initial few time points and then elevated during latter time points. Figure obtained from Altboum et al., 2014.

2. Chronic viral infections

2.1. Chronic viral infections: a persistent threat to human health

Viral infections can be fundamentally categorized as acute or persistent according to their temporal relationships with their hosts (Virgin et al., 2009). Acute infections in humans are usually resolved within a few weeks. In contrast, persistent infections are not resolved and, instead, develop when innate and adaptive immune responses are not sufficient to eliminate the invading virus during the primary infection phase. A consequence of this later condition is the establishment of a dynamic equilibrium between virus expansion and virus-specific adaptive responses that may be stably maintained for years without major pathological consequences or disrupted in a way that rapidly leads to overt disease. Viruses of both categories continue to threat human health. Notable examples are the regular recurrences of influenza virus strains that cause acute infections with partly critical illness or death every year (Fukuyama and Kawaoka, 2011; Oldstone, 2013) and infections with the Human Immunodeficiency Virus (HIV) or the Hepatitis B and C viruses (HBV, HCV) that cause a tremendous disease burden with more than 500 million people infected worldwide. These viruses can establish persistence in their hosts with different probabilities and pathogenic consequences. Whilst nearly all HIV infections lead to virus persistence, 50-80% of HCV and only about 5% of HBV infections in adults are persistent. The level of persistence of HBV-infected newborns is massively increased to about 95% indicating that the state of the immune system is an important component in determining infection fate (Feinberg and Ahmed, 2012; Rehermann and Nascimbeni, 2005).

2.2. Immune responses during chronic viral infections

Various viral and host factors in the early infection phase are involved in the fate decision between an acute and chronic infections. These includes virus strain and escape variants (Zinkernagel, 2002), viral dose and route of infection (Asabe et al., 2009; Moskophidis et al., 1995) and effector cell and virus expansion capacities (Bocharov et al., 2004; Ehl et al., 1998; Li et al., 2009). In the case of chronic infections, a decision is taken by the host in which the immune system undergoes a functional adaptation to a new virus-host equilibrium. Both suppressive and effector mechanisms participate in this immune adaptation, avoiding immunopathology while maintaining virus replication at low level (Wilson and Brooks, 2010). A relevant feature of this adaptation is T cell exhaustion, defined as the deletion and

functional impairment of virus-specific T cells (see section 2.3) (Barber et al., 2006; Moskophidis et al., 1993). Concomitant with T cell exhaustion, other regulatory elements also participate in the downregulation of the antiviral effector responses during chronic infections. Relevant factors are IL-10, regulatory T cells and myeloid derived suppressor cells (MDSCs) (see section 2.4) (Brooks et al., 2006; Norris et al., 2013; Schmitz et al., 2013). The appearance of large numbers of MDSCs during chronic inflammation appears to be a common feedback mechanism in both mice and humans. In fact, MDSCs have been also documented in patients with HIV, were the number of MDSCs correlated positively with viral titers and regulatory T cells and negatively with the number of $CD4^+$ T cells (Vollbrecht et al., 2012). Finally, there is a dual role of type I interferons (IFNs) during viral infections (Snell et al., 2017). Type I IFNs is a family of antiviral cytokines induced early after viral infection. They promote viral clearance by antiviral effects of IFN-stimulated genes, activation of dendritic cells (DCs), NK cells and enhanced B- and T- cell responses. However, during persistent infections such as HIV, SIV and LCMV, they are associated with a sustained production of low amounts of type I IFNs and activation of IFN-stimulated genes (ISGs) that trigger unwanted inflammatory responses. Indeed, blockade of I IFN signaling restores immune function and decreases viral loads in both LCMV and HIV mice infection models (Cheng et al., 2017; Teijaro et al., 2013; Wilson et al., 2013; Zhen et al., 2017).

Besides the functional adaptation undergone by the immune system, several immunological abnormalities might affect innate and adaptive immune cell subsets in a chronic infection. Plasmacytoid dendritic cells (pDCs), highly specialized cells for secreting IFN-I cytokines more than any other cell type, are able to directly recognize nucleic acids from several persistent viruses, including HIV and HCV in humans and LCMV in mice, through Toll-like receptor 7 (TLR7) and TLR9 (Gilliet et al., 2008; Zuniga et al., 2015). However, pDCs functionality is disrupted in LCMV, HIV, and HBV chronic infections, affecting their capacity to produce IFNα and therefore affecting the overall immune response (Bergthaler et al., 2010; Fitzgerald-Bocarsly and Jacobs, 2010; Macal et al., 2012). In the case of conventional DCs (cDCs), $CD8\alpha^-$ and $CD8\alpha^+$ DC subsets are responsible for the activation of naive T cells by presenting antigen on major histocompatibility complex (MHC) I and MHC II. Moreover, $CD8\alpha^+$ DCs have the additional ability of cross-presentation, whereby extracellular antigen is taken up and presented on MHC I to $CD8^+$ T cells. During chronic LCMV infection with variant clone 13 (CL13), $CD8\alpha^-$ and $CD8\alpha^+$ DCs exhibit a reduced cell-surface expression of MHC I, MHC II and costimulatory molecules, CD80, CD86, and

CD40. Therefore, the DC functionality is impaired, resulting in a reduced capacity to present antigen and stimulate naive T cells (Ng and Oldstone, 2012; Ng et al., 2013; Sevilla et al., 2004).

Even though there is more known about T cell exhaustion during chronic viral infections, B cells may also be negatively impacted (Virgin et al., 2009). B cell and antibody responses are altered (Ng et al., 2013), exhibiting a delayed production of virus-specific neutralizing antibodies and elevated levels of non-specific antibodies (hypergammaglobulinemia) (Hangartner et al., 2006; Hunziker et al., 2003). Extensive B cell dysfunction is observed during HIV infection (Moir and Fauci, 2009) and during persistent LCMV infection, where the production of virus-specific neutralizing antibodies is altered, leading to defect in the B cell repertoire (Hangartner et al., 2006; Ng et al., 2013). Finally, another factor promoting immunological abnormalities is the disruption of the lymphoid tissue architecture mediated by collagen deposition and/or the loss of lymphoid stromal cells. This alteration impairs immune responses by affecting T cell survival and lymphocyte trafficking in immune tissues (Boehm, 2016; Kityo et al., 2018; Zeng et al., 2012).

2.3. Cardinal features of exhausted T cells

Failure of the immune system to eliminate the invading pathogen results in a persistent infection. A major determinant of persistent infections is the appearance of "exhausted" $CD8^+$ T cells, a phenomenon characterized by the loss of effector function of virus-specific $CD8^+$ T cells (Dunn et al., 2002; Glazer et al., 1983), upregulation of inhibitory receptors, an altered transcriptional program and perturbations of functional effector or memory T cells and homeostasis (Zehn and Wherry, 2015). Exhaustion is a state of progressive dysfunction that occurs as a consequence of high antigen exposure (Pauken and John Wherry, 2015; Wherry, 2011). The severity of this dysfunction during chronic infections correlates with the level of infection, a prolonged and high expression of inhibitory receptors and with the lack of help from $CD4^+$ T cells (Virgin et al., 2009). Exhausted T cells was first described in lymphocytic choriomeningitis virus (LCMV) infection of mice, and has been extended to other chronic infections (Barber et al., 2006) such as HIV- (Khaitan and Unutmaz, 2010), HBV- (Penna et al., 2007; Ye et al., 2015) and HCV-infections in humans (Penna et al., 2007).

During exhaustion, $CD8^+$ T cell dysfunction develops in a hierarchical manner. Some functions, such as *ex vivo* killing, high proliferative capacity and IL-2 production, are lost in an early stage of exhaustion. Other functions are lost in a more advanced stage of exhaustion such as cytotoxicity and TNFα and IFNγ production (Virgin et al., 2009; Wherry and John Wherry, 2011). During exhaustion, T cells also lose their ability to proliferate in response to IL-7 and IL-15, thus they depend on TCR signals for their maintenance (Shin et al., 2007). T cell exhaustion ultimately ends with the apoptosis of the cell (Kahan et al., 2015).

During chronic infections, exhaustion has been described as a causative factor for the lack of pathogen control. However, exhausted T cells still contribute to the containment of chronic infections (Kahan et al., 2015). Therefore, exhaustion might be an adaptation to reduce the sensitivity of virus-specific T cells to antigen and promote their survival in an antigen-rich environment. In this way, the immune response could balance effector control of the virus and immunopathology, while at the same time maintaining the adaptability of T cell responses to subsequent viral bursts (Barnaba and Schinzari, 2013; Pauken and John Wherry, 2015; Peligero et al., 2015; Radziewicz et al., 2009).

2.4. Intrinsic and extrinsic regulatory pathways of exhaustion

Exhaustion is associated with a prolonged and high expression of inhibitory receptors. The number and type of inhibitory receptors determine the degree of dysfunction. The pattern of inhibitory receptors differs between CD4- and CD8- T cells, as well as the type of infection. Inhibitory receptors involved in exhaustion include PD-1, Lag-3, Tim3, CD244 (2B4), CD160, TIGIT, CTLA4, BTLA, KLRG1 and others. The protein programmed cell death-1 (PD-1) plays a major role during chronic LCMV infection in mice. PD-1 is highly overexpressed by virus-specific exhausted $CD8^+$ T cells, and blockade of the PD-1-PD1 ligand (PD-L1) pathway showed a restoration of impaired effector T cells and a reduction of viral loads (Barber et al., 2006). However, none of inhibitory receptors described above are exclusive markers for exhausted T cells because activated T cells can transiently express them (Crawford and Wherry, 2009; Nguyen and Ohashi, 2015; Okoye et al., 2017).

In addition to inhibitory receptors, multiple extrinsic factors influence T cell exhaustion, such as altered antigen presentation, immunosuppressive cytokines and several cell subsets (Jin et al., 2011; Kahan et al., 2015; Wherry, 2011). There is a reduced response to cytokines

including IL-7, IL-2 and IL-15, that normally promote proliferation and survival in effector and/or memory $CD8^+$ T cells. In addition, $CD8^+$ T cell responsiveness to IL-12, IL-18, and IL-21 has recently been shown to be reduced during chronic LCMV infection (Zuniga et al., 2015). Effector responses are influenced by deletion or alteration of DCs, such as decrease in MHC molecules and costimulatory ligands, and increase in coinhibitory ligands (Jin et al., 2011). Likewise, effector responses are influenced by suppressive cytokines such as transforming growth factor beta (TGF-β) and IL-10 and inflammatory cytokines such as type I IFNs. For example, in the LCMV mouse model, the blockade of TGF-β (Jin et al., 2011; Tinoco et al., 2009) or IFN α/β during the first days of infection (Teijaro et al., 2013; Wilson et al., 2013) prevents from severe exhaustion, and the blockade of IL-10 improves T cell functionality and promotes viral control (Brooks et al., 2006; Richter et al., 2013). In the case of HIV-infected individuals, IL-10 production by monocytes, impairing $CD4^+$ T cell activation (Said et al., 2010).

Depletion of $CD4^+$ T cells is another important factor influencing exhaustion. $CD4^+$ T cells provide help to $CD8^+$ T cells and are major producers of IL-21, which influences $CD8^+$ T cell and B cell differentiation and restricts regulatory T cell expansion (Lichterfeld et al., 2007; Matloubian et al., 1994; Schmitz et al., 2013; Zajac et al., 1998). Furthermore, NK cells and immunoregulatory cells such as MDSCs and regulatory T cells (Tregs) have a detrimental impact on virus-specific $CD8^+$ T cells further contributing to exhaustion (Dietze et al., 2011; Dittmer et al., 2004; Norris et al., 2013; Penaloza-MacMaster et al., 2014; Waggoner et al., 2011). NKs have been shown to act as master regulators of $CD4^+$ T cells which subsequently control $CD8^+$ T cells during LCMV infection (Waggoner et al., 2011). $CD4^+$ $CD25^+$ regulatory T cells exert key negative regulatory mechanisms of the immune system to prevent autoimmunity and T cell-mediated inflammatory disease (Belkaid and Rouse, 2005; Dietze et al., 2011; Schmitz et al., 2013; Suvas et al., 2003). They have been shown to negatively regulate $CD8^+$ T cell responses during HIV- (Nilsson et al., 2006), HBV- (Xu et al., 2006) and HCV- (Cabrera et al., 2004) chronic infections. Furthermore, elevated numbers of Treg cells have also been associated with persistent viral infections in humans (Belkaid and Rouse, 2005; Cabrera et al., 2004; Dietze et al., 2011; Schmitz et al., 2013; Suvas et al., 2003).

2.5. Maintenance of an effector response during chronic infection

Despite the various suppressive mechanisms induced during a chronic virus infection, the effector T cell shutdown is only partial and some T cell functionality remains to restrain the expansion of a persisting virus. In this sense, it has been shown that polyfunctional T cell responses in chronic HIV, HBV and HCV infections are linked to low viremia (Bertoletti and Ferrari, 2012; Hiroishi et al., 1997; Thimme et al., 2002). Moreover, depletion of $CD8^+$ T cells in rhesus macaques infected with the simian immunodeficiency virus (SIV) results in an increase of virus loads (Jin et al., 1999; Schmitz, 1999). Finally, despite the presence of exhausted T cells, ongoing selection of virus mutants within epitope regions have been observed (Allen et al., 2005; Draenert et al., 2004). Recent studies characterizing $CD8^+$ T cell subsets that are present during chronic viral infection have identified a virus-specific population expressing the C-X-C chemokine receptor type 5 (CXCR5) that retain cytotoxic antiviral activities during chronic LCMV infection (He et al., 2016; Im et al., 2016; Leong et al., 2016). Expression of the inhibitory receptors Tim3 and PD-1 is slightly lower in $CXCR5^+$ $CD8^+$ T cells than in their $CXCR5^-$ counterparts, suggesting that these cells are less susceptible to exhaustion. In fact, $CXCR5^+$ $CD8^+$ T cells provide the proliferative burst after anti-PD-1 therapy (Im et al., 2016). Importantly, HIV-infected patients also have a virus-specific $CXCR5^+$ $CD8^+$ T-cell subset, and its number inversely correlates with viral loads (He et al., 2016; Im et al., 2016). Moreover, our group has recently shown using the LCMV-infection model that, in the time of exhaustion appearance, this $CD8^+$ T cell subset mediates the recruitment of cross-presenting dendritic cells (DCs) by expressing the chemokine XCL1. Importantly, we demonstrated the crosstalk between this cell subset contributes to the maintenance of an antiviral cytotoxic T cell response and participates in viral control in the chronic infection phase (Argilaguet et al. 2018, submitted).

3. Lymphocytic Choriomeningitis Virus (LCMV) as model for chronic infections

3.1. The virus

LCMV is noncytopathic RNA virus, member of the Arenaviridae family. It causes a persistent infection in the mouse, its natural host, but it can also infect a wide range of other animals, including humans. Although there is no quantitative data on the relative threats of

the different LCMV virus strains to humans, it can cause a variety of symptoms that go from a mild respiratory infection to encephalitis or meningitis. Death from LCMV infection is rare, and patients usually recover without any sequelae (Farmer and Janeway, 1942). LCMV was isolated by the American physician Charles Armstrong, when studying an epidemic in St. Louis, MO, US. Since its discovery in 1933, infection of mice with several LCMV strains has been a widely used tool in scientific laboratories for examining mechanisms of viral persistence and basic concepts of virus-induced immunity and immunopathology (Farmer and Janeway, 1942; Wilson and Brooks, 2010; Zhou et al., 2012).

LCMV is an enveloped RNA virus with a bisegmented negative single-stranded RNA genome. Its life cycle is restricted to the cytoplasm of the infected cell. Each of the RNA genome segments, designated as large (L, 7.3kb) and small (S, 3.5kb), uses an ambisense coding strategy to produce two viral gene products, in opposite orientation, and separated by a non-coding intergenic region (IRG) that folds into a stable hairpin structure (de la Torre, 2009). The S RNA encodes the nucleoprotein (NP), the most abundant protein, and the viral glycoprotein precursor (GPC). The NP is the main structural element and plays an essential role in viral RNA synthesis. NP has been also associated with a type I IFN counteracting activity (Martínez-Sobrido et al., 2007, 2009). The GPC is post-translationally cleaved into GP1 and GP2, and GP1/2 together make the spike of the virion. The L RNA segment encodes for the viral RNA dependent RNA polymerase (RdRp, also referred to as L polymerase), and a small RING finger protein Z that localizes in the plasma membrane. The Z protein is a structural component of the virion that interacts with host proteins, inhibits RNA synthesis by the RdRp, and is the main driver of LCMV budding (de la Torre, 2009).

α-dystroglycan (α-DG) is the main cellular receptor protein for LCMV and the majority of arenaviruses. α-DG is a highly conserved and ubiquitous cell surface molecule that links the extracellular matrix with the cytoskeleton (Cao, 1998; Kunz et al., 2003; de la Torre, 2009). Within immune cell populations, α-DG is mainly expressed DCs (Oldstone and Campbell, 2011). Virus strains and variants that bind α-DG with high affinity are associated with virus replication in the white pulp of the spleen, with preferential replication in DCs. LCMV infection of mature DCs has as consequence the failure of DCs to present viral antigens and therefore to arm and expand immune-specific T and B cell responses (Oldstone and Campbell, 2011). After interaction of α-DG with the viral GP1, LCMV virions are endocytosed. The subsequent fusion between the viral and cell membranes is triggered by the

acidic environment found in the late endosome and GP2 (Gallaher et al., 2001). Upon release of viral genomic RNA, protein synthesis and genomic RNA replication starts. Formation and budding of arenavirus infectious progeny requires assembly of the viral ribonucleoproteins (RNPs) and the cellular membranes enriched with viral GPs. Finally, there is the assembly and cell release of the infectious virions (Kunz et al., 2002; Perez and de la Torre, 2003).

3.2. Understanding viral immunity: Contribution from the LCMV mouse model system.

The concept of persistent viral infection evolved from an observation Traub made in 1936. Mice infected with LCMV in the utero or shortly after birth neither died or eliminated the virus (Traub, 1936a, 1936b). In that time, three different LCMV isolates were originated: the Armstrong strain isolated from monkeys, the Traub strain isolated from a laboratory colony of persistently infected mice, and the WE strain, isolated from a human after exposure to persistently infected mice. Many different variants of these strains exist, but the most used are Clone 13, which derives from the Armstrong strain, and Docile, a derivative of the WE strain (Welsh and Seedhom, 2008). LCMV infection fate varies dramatically depending on the virus strain, age and genetic background of mice, route of infection, as well as the dose used for infection (Spiropoulou et al., 2002; Zinkernagel, 2002). In fact, one of the key features of the LCMV system is the ability to compare two different immune responses (Klenerman and Hill, 2005; Wilson and Brooks, 2010). Armstrong and Clone13 are genetically closely related strains but they differ in their ability to establish an acute and persistent infection, respectively (Ng et al., 2013). Interestingly, Armstrong and Clone13 viral strain genomes only differ by two amino acids, a K to Q substitution at position 1079 (polymerase gene) and a F to L substitution at position 260 (glycoprotein gene). The latter substitution alters receptor tropism, enabling Clone13 to infect more efficiently $CD11c^+$ DCs than the Armstrong strain (Matloubian et al., 1993). Viral targeting of these $CD11c^+$ DCs is associated with defective antigen presentation and costimulation, and results in impaired T cell responses and ultimately, viral persistence (Bergthaler et al., 2010). Furthermore, infection with low doses of LCMV Docile ($LCMV_{Doc}$) induced a robust response of virus effector specific $CD8^+$ and $CD4^+$ T cells that results in viral clearance within 8-10 days postinfection (p.i). In contrast, infection with high doses of $LCMV_{Doc}$ results in higher titer and clonal exhaustion of T cells and viral persistence (Cornberg et al., 2013).

Since Traub's discovery in the 1930s, LCMV infection of mice has been used as an important model system and allowed numerous key findings about innate and adaptive immune responses during acute and persistent viral infections. First, the MHC-restricted function of cytotoxic T lymphocytes was demonstrated by Rolf Zinkernagel and Peter Doherty, for which they were awarded the Nobel Prize in 1996 (Zinkernagel, 1975; Zinkernagel and Doherty, 1974). Second, the mechanism of CTL-mediated lysis of virus-infected target cells was shown to be via by perforin secretion (Kägi et al., 1994; Masson and Tschopp, 1985). Third, the concept of "memory" of adaptive immune responses where T cells remember their cognate antigen after initial antigen encounter was developed (Murali-Krishna et al., 1998). Forth, the key role of NK cells as important regulators of CD4 T-cell-mediated support for antiviral CD8 T cells was shown (Waggoner et al., 2011). Fifth, the role of organized secondary lymphoid organs in the induction of naive T and B cells, and subsequent virus control was established (Karrer et al., 1997). Sixth, the concept of immunopathology was developed in which the damage of the tissue and organs is associated with or directly caused by the immune response and not as a direct result of the pathogen burden or toxicity from the infected cell. Mediators of immunopathology include CTL, macrophages, neutrophils and interferons (Cole et al., 1972; Kim et al., 2009; Rivière et al., 1977). Seventh, the state of dysfunction of effector T cells, a phenomenon known as "immune exhaustion" (see section 2.3) was established (Welsh and Seedhom, 2008; Zhou et al., 2012). Eighth, the role of host immunoregulatory proteins such as PD-1 in directly inhibiting antiviral immune functionality and maintaining the immunosuppressive state was shown (Barber et al., 2006; Okoye et al., 2017; Waggoner et al., 2011). Thus, the LCMV mouse model system has proven to be an excellent platform for immunological studies.

3.3. Similarities between LCMV and HIV immunology

LCMV and HIV are inherently different viruses regarding genetic composition, replicative strategies and mechanisms of infection. Despite that, they both elicit comparable antiviral responses at least under certain LCMV infection conditions. For this reason, some of the immune features described in LCMV were then extended to the understanding of persistent HIV infections in humans (Klenerman and Hill, 2005). Some examples are: (i) Exhausted $CD8^+$ T cell responses in persistent LCMV infection are comparable to the exhausted $CD8^+$ T cell responses found in HIV infection, specifically the failure to proliferate and produce cytokines in responses to viral antigen (Klenerman and Hill, 2005); (ii) PD-1 expression on

virus-specific $CD8^+$ T cells are increased in LCMV and HIV infections, correlating with T cell exhaustion (Barber et al., 2006). PD-L1 blockade results in an increase of $CD8^+$ T cells functionality in both viral infections (Blackburn et al., 2008; Day et al., 2006; Petrovas et al., 2006); (iii) IL-10 plays an immunomodulatory role during persistent LCMV and HIV infection. Blockade of this cytokine enhances virus-specific T cell responses in both persistent infections (Clerici et al., 1994; Landay et al., 1996); (iv) $CD4^+$ T cells are required to sustain virus-specific $CD8^+$ CTL during chronic LCMV infection (Battegay et al., 1994; Matloubian et al., 1994); (v) The role of IL-2 as a regulator of effector and memory CTL generation has been pinpointed (Pipkin et al., 2010). IL-2 expression is suppressed by both $CD4^+$ and $CD8^+$ T cells in persistent LCMV and HIV infection, diminishing the expansion and generation of lasting memory $CD8^+$ T cells (Aiuti and Mezzaroma, 2006); and finally (vi) IL-21 production by $CD4^+$ T cells is necessary for the maintenance of $CD8^+$ T cell effector responses during persistent LCMV infection (Frohlich et al., 2009; Yi et al., 2009) as well as in HIV infection (Yue et al., 2010). Thus, LCMV has been proven to be a valuable experimental tool to address meaningful mechanistic correlations between the mouse system and what one observes in human HIV infection.

OBJECTIVES

The host immune response against an infection requires the coordinated action of hundreds of cell subsets that dynamically adapt to the pathogen threat. Due to the complexity of such response, most immunological studies are based on non-dynamical analyses focused on few genes, proteins or cell subsets. During the last years, “omic”-technologies have become a powerful tool to perform systematic analysis of dynamic biological processes. However, there is a need to develop novel methods that facilitate the interpretation of the generated “omics” data. This thesis has 3 objectives:

1. To study the global immune cell dynamics during acute and chronic LCMV infection of mice using Digital Cell Quantifier (DCQ).

2. To combine Weighted Gene Coexpression Network Analysis (WGCNA) and DCQ to link gene expression changes to cell kinetics.

3. To validate hypotheses generated by combining WGCNA and DCQ using gene coexpression modules relevant to LCMV chronic infection.

MATERIALS AND METHODS

1. Media, buffers and solutions

Ammonium chloride (NH_4Cl) - Lysing Solution

0.15M NH_4Cl (Merck), 10mM $KHCO_3$ (Sigma-Aldrich), 0.1mM Na_2EDTA (Sigma-Aldrich). pH 7.2-7.4.

FACS Buffer

Phosphate buffered saline (PBS) (Gibco), 5% heat-inactivated fetal bovine serum (FBS), 0.5% Bovine serum albumin (BSA) (Sigma-Aldrich), 0.07% sodium azide (Sigma-Aldrich).

FACS Fix Buffer

Deionized water, 1% paraformaldehyde (Sigma-Aldrich), 150mM NaCl (Sigma-Aldrich), pH 7.4.

Complete RPMI media

RPMI 1640 with L-glutamine (Sigma-Aldrich), 10% FBS (Sigma-Aldrich), 1U/mL penicillin, 1µg/mL streptavidin, 0.05mM β-Mercaptoethanol, 1mM Sodium Pyruvate (Sigma-Aldrich).

Perm Wash Buffer

Phosphate-buffered saline (PBS) (Gibco), 1% FBS, 0.1% NaN_3 (Sigma-Aldrich), 0.1% Saponin.

Fixation/Permeabilization (Fix/Perm) Buffer 1X:

Diluted from Fix/Perm concentrate (4x) (eBioscience) in Fix/Perm diluent (eBioscience)

Permeabilization (Perm) Buffer 1X:

Diluted from Perm concentrate (10x) (eBioscience) in deionized water.

2. Digital Cell Quantifier (DCQ)

The DCQ was performed as described in Altboum et al. 2014. Briefly, the DCQ took as an input: (i) an immune cell compendium of transcriptional profiles, consisting of 213 different immune cell subsets and their corresponding cell surface markers (prior knowledge about the mRNA quantities of each gene in different cell types); and (ii) differentially expressed genes from spleens from acute-and chronic-LCMV infected mice (Argilaguet et al. 2018, submitted). This prior immune cell compendium contains naive and effector cell subsets, isolated from 22 different tissues in both resting and activated immune states. As an output, DCQ predicted for each cell type and time point, a relative cell quantity (based on the change in cell quantity between a sample at a specific time point and a sample at time point zero). We used the glmnet R package (Friedman et al., 2010) with the parameters $\alpha = 0.05$, lambda.min.ratio = 0.2.

To evaluate the robustness of the predicted results, DCQ was run 100 times using only a random collection of 50% of the cell types in the compendium on each run, resulting in 100 different solutions. Standard deviations were calculated across these 100 solutions. The robustness score (significance of a predicted change in quantity) was assessed by evaluating whether the sample of relative quantities is significantly different from zero (P-value score). Significantly changing cell types were defined as those whose –log10 P-value score between at least two consecutive time points is lower than -20 (cell decrease) or higher than 20 (cell increase) (Supplementary Table 1 and 2).

3. Processing of RNA-Seq data for DCQ

Between 30-63 millions of single-end reads were produced after sequencing, and approximately 91% mapped against the reference mouse genome (GRCm38) using the GEM software (Marco-Sola et al., 2012), allowing for split maps. Gene quantification was performed using the GEMTools RNA-Seq pipeline with the gencode.vM2 mouse annotation. Around 90% of the reads were exonic, 5% intronic and 5% intergenic. The TMM method (Robinson and Oshlack, 2010) of the edgeR software (Robinson et al., 2010) was used for normalization of the gene expression. To apply the DCQ, the transcriptional profiles were pre-processed as follows: First, the $\log_2$-transformed profiles of the same time point were

averaged. Second, for each given gene, all its values were normalized by its median and standard deviation among the different time points. Finally, DCQ was applied on the transformed spleen RNA-seq data with robustness cutoff = 20.

4. ImmGen data

To compare gene expression levels between early and late effector $CD8^+$ T cells, the tool "Population Comparison" from ImmGen data browser (http://www.immgen.org/) was used. This tool provided a ranked table of genes that are always expressed in OVA-specific effector $CD8^+$ T cells analyzed 12 and 24 hours postinfection with LisOva and never expressed in the same cells analyzed at days 5, 6 and 8 postinfection with LisOva or VSVOva (Supplementary Table S8). Default thresholds from the ImmGen tool were used. To analyze the pattern of expression of the genes *Xcl1*, *Tnfsf8*, *Tlr7*, *Ccr9* and *Cd83* across OVA-specific $CD8^+$ T cells in ImmGen compendium, we used the tool "My GeneSet" using Microarray V1 data set. Expression values were obtained as the log2 of each gene expression value/average expression value of all genes.

5. Mice and viruses

All mice were maintained in pathogen-free conditions in the Parc de Recerca Biomèdica de Barcelona (PRBB) animal facility, and handling conformed to the requirements from Generalitat de Catalunya. All of the animal protocols were reviewed and approved by the ethical committee for animal experimentation at PRBB (CEEA-PRBB, Spain). Male C57BL/6J mice (4-8 weeks of age, obtained from Charles River Laboratories) were infected intraperitoneally (i.p.) with either $2x10^2$ (low dose, LD) or $2x10^6$ (high dose, HD) plaque-forming units (PFU) of the strain Docile of LCMV (4-6 animals per group) to induce an acute or chronic infection, respectively.

6. Tissue processing and splenocyte stimulation

Spleens were harvested at the indicated time points and placed directly in complete RPMI buffer supplemented with 10% fetal bovine serum (FBS). If analysis of cytokines was needed, complete RPMI buffer was also supplemented with Brefeldin A (10µg/ml), a protein

transport inhibitor. After collection, spleens were homogenized into a single-cell suspension and filtered through a 40µm nylon cell strainer (Falcon) to remove cells clumps. Splenocytes were then resuspended in ammonium chloride (NH_4Cl) lysing solution for 5 minutes at room temperature to lyse erythrocytes, washed twice, and resuspended either in complete RPMI medium supplemented with 10% FBS for stimulation or cell sorting, or in FACS buffer for flow cytometry staining.

7. Cell staining and Flow cytometry

7.1. Splenocytes stimulation

For intracellular detection of IFN-ɣ, splenocytes were seeded at 1.5-2x10^6 cells/well in 96 wells round-bottom plates (Sigma-Aldrich) and incubated with gp33 (1µg/ml) peptide for two hours at 37ºC. After incubation, 10µL of Brefeldin A (10µg/ml) was added to the cells, following incubation at 37ºC for another three hours. After the second incubation, cells were removed from the incubator and cell surface and intracellular staining were performed following the steps described in sections 7.2.

7.2. Cell staining

Splenocytes were seeded at 1.5-2x10^6 cells/well in 96 wells round-bottom plates (Sigma-Aldrich), washed twice with PBS and stained with a viability stain Live/Dead fixable violet dye (Vivid) (Invitrogen) or Fixable viability stain 620 (BD Biosciences) for 20 minutes at room temperature to exclude dead cells from the analysis. After, splenocytes were washed twice with FACS buffer and pelleted cells were then incubated for 20 minutes on ice in a total volume of 50µL with CD16/CD32 Fc block (BD Biosciences) to block non-antigen-specific binding of immunoglobulins to the Fc receptors. After blocking, cells were washed twice with FACS buffer and stained with 50µL of fluorochrome-labelled monoclonal antibodies against: CD4, CD8a, CD45R, NK1.1, CD11c, CD11b, Ly-6G, Ly-6C, CD25, CD3e, CD27, CD44, CXCR5, CD83, CD199 (CCR9) and CD153 (TNFSF8). After surface antibody staining, cells were washed twice with FACS buffer and fixed with FACS fix.

For intracellular staining, cells were permeabilized for 20 minutes with 100µL of Perm Wash buffer. Once permeabilized, cells were washed twice with Perm Wash buffer and pelleted

cells were then incubated for 20 minutes on ice with 50µL of fluorochrome-labelled monoclonal antibodies against IFNɣ, TLR7 or XCL1. After, cells were washed with Perm Wash and resuspended in FACS fix.

For intracellular detection of FOXP3, cells were fixed and permeabilized using FOXP3 staining kit (eBioscience) according to manufacturer's instructions. Briefly, cells were washed twice with Perm Buffer (eBioscience) and centrifuged. Pelleted cells were then incubated 25 minutes, at room temperature, with a 100ul of fluorochrome-labelled monoclonal antibodies against FOXP3. After 25 minutes, cells were washed twice with Perm Buffer (eBioscience) and finally resuspended in FACS Fix Buffer.

Stained cells were acquired in a flow cytometer within two hours after staining. Prior to acquisition, cells were kept protected from light at 4ºC. Flow cytometry data were collected on a LSR Fortessa (BD biosciences) and analyzed with FlowJo software (Tree Star). Data were analyzed using FlowJo 10.1 software. Flow cytometry panels can be found in Table M1.

7.3. Sorting of monocytes/macrophages, neutrophils and $CD8^+$ $CD44^-$/ $CD8^+$ $CD44^+$ T cells.

For sorting of monocytes/macrophages, neutrophils and $CD8^+$ $CD44^-$/$CD8^+$ $CD44^+$ T cells, cells were seeded in polypropylene round bottom test tubes (Falcon) at $50x10^6$ cells/tube, rinsed with FACS buffer and incubated for 20 minutes on ice in a total volume of 100µL with CD16/CD32 Fc block (BD Biosciences) to block non-antigen-specific binding of immunoglobulins to the Fc receptors. Cells were then washed twice with FACS buffer and stained with 100µL of fluorochrome-labelled monoclonal antibodies against: CD45R, NK1.1, CD11c, CD11b, Ly-6G and Ly-6C (for Monocytes/Macrophages and neutrophils) and CD4, CD8a, CD3e and CD44 (for $CD8^+$ $CD44^-$/$CD8^+$ $CD44^+$ T cells). After surface antibody staining, cells were washed twice with FACS buffer and resuspend with RPMI supplemented with 10% FBS. Flow cytometry panels can be found in Table M1.

Stained cells were sorted in a FACSAria II SORP (BD Biosciences) right after staining. Sorted cells were collected in complete medium and kept on ice during and after sorting. Sort purity was > 95% for all populations.

Table M1. Flow cytometry panels.

Table M1. Flow cytometry panels. (BD: Biosciences, Dil: dilution; Cat.#: Catalog number)

IFNγ in $CD4^+$ and $CD8^+$ T cells					
Antigen	**Fluorochrome**	**Company**	**Cat. #**	**Clone**	**Volume**
CD4	PE	BD	553653	H129.19	0,12µL
CD8	PECy5	BD	553034	536.7	0,12µL
IFNγ	FITC	BD	554411	XMG1.2	0,03µL

Monocytes/Macrophages and Neutrophils					
Antigen	**Fluorochrome**	**Company**	**Cat. #**	**Clone**	**Volume***
Live/Dead	FVS620	BD	564996	-	Dil 1:1000
CD45R	PE-CF594	BD	562313	RA3-6B2	0.15µL
NK1.1	PE-CF594	BD	562864	PK136	0.3µL
CD11c	PerCP-Cy5.5	BD	560584	HL3	5µL
CD11b	Pe-Cy7	BD	552850	M1/70	1.25µL
Ly-6G	PE	BD	551461	1A8	0.625µL
Ly-6C	FITC	BD	561085	AL-21	0.625µL

*For sorting analysis, the volume of antibody was doubled and the quantity was tripled.

$CD4^+$ Regulatory T cells					
Antigen	**Fluorochrome**	**Company**	**Cat. #**	**Clone**	**Volume**
CD4	PE	BD	553653	H129.19	0,12µL
CD25	APCCy7	BD	557658	PC61	0,75µL
FOXP3	AF647	BD	560401	MF23	0,75µL

Natural Killer cells					
Antigen	**Fluorochrome**	**Company**	**Cat. #**	**Clone**	**Volume**
Live/dead	Vivid	Invitrogen	L34955	-	Dil 1:5000
CD3e	PE-Cy7	BD	561100	145-2C11	1,25µL
NK1.1	PE-CF594	BD	562864	PK136	0,3µL
CD11b	APC	BD	553312	M1/70	0.625µL
CD27	FITC	ThermoFisher	11-0271-81	LG.7F9	0,25µL

$CD8^+$ $CD44^-$ and $CD44^+$ T cells					
Antigen	**Fluorochrome**	**Company**	**Cat. #**	**Clone**	**Volume***
CD4	PerCPCy5.5	BD	550954	RM4-5	0.15µL
CD8a	FITC	BD	553030	53-6.7	0.5µL
CD3e	PE-Cy7	BD	561100	145-2C11	1.25µL
CD44	eFl450	ThermoFisher	48-0441-80	IM7	0.625µL

*For sorting analysis, the volume of antibody was doubled and the quantity was tripled.

Effector $CD8^+$ T cells					
Antigen	**Fluorochrome**	**Company**	**Cat. #**	**Clone**	**Volume***
Live/Dead	FVS620	BD	564996	-	Dil 1:1000
CD8a	PerCP-Cy5.5	BD	551162	53-6.7	0.31µL
CXCR5	PE-Cy7	ThermoFisher	25-7185-80	SPRCL5	2.5µL
CD83	AF488	BD	563539	Michel-19	2.5µL
CD199	BV421	BD	565412	CW-1.2	1.25µL
Xcl1	-	BD	MAB486	80222	0.5µL
anti-rat IgG2a	AF647	Abcam	ab172333	2A 8F4	Dil 1:2000

*For sorting analysis, the volume of antibody was doubled and the quantity was tripled.

Effector CD8+ T cells					
Antigen	**Fluorochrome**	**Company**	**Cat. #**	**Clone**	**Volume***
Live/Dead	FVS620	BD	564996	-	Dil 1:1000
CD8a	PerCP-Cy5.5	BD	551162	53-6.7	0.31µL
CXCR5	PE-Cy7	ThermoFisher	25-7185-80	SPRCL5	2.5µL
CD153	BV421	BD	740059	RM153	2.5µL
TLR7	FITC	ThermoFisher	PA5-23489	-	0.28µL
Xcl1	-	BD Biosciences	MAB486	80222	0.5µL
anti-rat IgG2a	AF647	Abcam	ab172333	2A 8F4	Dil 1:2000

*For sorting analysis, the volume of antibody was doubled and the quantity was tripled.

8. RNA isolation and Quantitative Real Time PCR

Total RNA from spleens (15-20 mg) and sorted cells ($5x10^4$) was isolated, including DNAse treatment (Qiagen) according to the manufacturer's instructions using RNeasy Mini Kit for spleen tissue and Qiagen RNeasy Micro Kit for sorted cells (Qiagen). The quality (RNA integrity number (RIN)) and concentration was determined using Agilent Bioanalyzer. 50ng of RNA was reverse-transcribed to cDNA using SuperScript III Reverse Transcriptase (ThermoFisher). Quantitative real-time PCR was performed in a total volume of 10µL, 50ng of cDNA, 300nM of forward and reverse primers and 5ul of SYBR Select Master mix (ThermoFisher). Each reaction was performed in triplicate in a 384 well plate (Sigma-Aldrich) in a Quantstudio 12K Flex Real Time PCR (ThermoFisher) using the housekeeping gene *Gapdh* for normalization of all target genes' expression. The parameters were the following: 2 min 50°C, 95°C 10 min, 40 cycles of 15 sec at 95°C and 60 sec at 60°C. Primers for all genes were designed using the program Primer Express 3.0 (Applied Biosystems). Primer selection parameters were as follows: primer size between 10 and 40 nucleotides; primer melting temperature from 52ºC to 60ºC; GC content between 40% and 60%; and product size between 150 and 250 nucleotides. Primers were ordered from Biomers. Sequences for the primers used can be found in Table M2.

Table M2. Primer sequence

Gene	Strand	Sequence
Gapdh	Forward	5'-CCA GTA TGA CTC CAC TCA CG-3'
	Reverse	5'-GAC TCC ACG ACA TAC TCA GC-3'
Ccr1	Forward	5'-CTC ATG CAG CAT AGG AGG CTT-3'
	Reverse	5'-ACA TGG CAT CAC CAA AAA TCC A-3'
C5ar1	Forward	5'-TAC CAT TAG TGC CGA CCG TTT-3'
	Reverse	5'-CCG GTA CAC GAA GGA TGG AAT-3'
Itgam	Forward	5'-GCA CCA AAA CTG CAA GGA GAA-3'
	Reverse	5'-CCG GAG CCA TCA ATC AAG AA-3'

9. RNA-Seq library preparation and sequencing

Transcriptome analysis by RNA-Seq was performed at the Centre de Regulació Genòmica (CRG-PRBB, Spain). Sequencing libraries were obtained after removing ribosomal RNA by a Ribo-Zero kit (Illumina). cDNA was synthesized and tagged by addition of barcoded Truseq adapters. Libraries were quantified using the KAPA Library Quantification Kit (KapaBiosystems) prior to amplification with Illumina's cBot. Four libraries were pooled and sequenced (paired end, 50nts) on an Illumina HiSeq2000 sequencer to obtain 50-60 million reads per sample.

10. Statistical analysis

Two-tailed t test or one-way ANOVA analyses were performed using GraphPad Prism 6.0 (San Diego, CA, USA). p-values (p) below 0.05 were considered significant and were indicated by asterisks: $*p \leq 0.05$; $**p \leq 0.01$; $***p \leq 0.001$; $****p \leq 0.0001$. Non-significant differences were indicated as "ns". Pearson's correlation was used to measure the degree of similarity between the module eigengene and DCQ inferred cell kinetics. Fisher's exact test was used to quantify the significance of gene overlap between acute-brown module hub genes and genes from $CD8^+$ T cells and monocytes/macrophages cell subsets.

RESULTS

1. Immune cell dynamics during acute and chronic LCMV infection

To obtain a global view of the biological processes that participate in acute and chronic LCMV infection, we created a new computational approach that combines WGCNA-derived gene coexpression networks with DCQ-inferred immune cell kinetics to study the mechanisms of chronicity development and virus control. As input, we used our previously determined RNA-Seq data set (Argilaguet et al. 2018, submitted) that consists of time-resolved splenic transcriptomes from C57BL/6J mice infected with a low-dose ($2x10^2$ PFU; acute infection) or a high-dose ($2x10^6$ PFU; chronic infection) of LCMV strain Docile ($LCMV_{Doc}$) (Figure R1). The time points (days 0, 3, 5, 6, 7, 9 and 31 postinfection (p.i.)) were selected according to the main viral and immunological features, and therefore represent the main states of an acute and chronic infection. 13,971 genes were identified as differentially expressed (DE) when compared to uninfected animals, and were analyzed by WGCNA to obtain modules of highly coexpressed genes (Argilaguet et al. 2018, submitted) (Figure R1).

To link immune cell dynamics during acute and chronic LCMV infection to WGCNA-derived gene coexpression modules, we used the expression kinetics of the DE genes as an input for DCQ (Altboum et al., 2014). The DCQ output consisted of predicted kinetics of 207 different immune cell subsets. Of these, 125 cell subsets had a significant change in their quantity between at least two consecutive time points (robustness score higher/lower than ± 20, see methods). We constructed a comprehensive map of the dynamic changes of these 125 cell subsets during the course of acute and chronic LCMV infection (Figure R2). 68 cell subsets were predicted to increase and 57 were predicted to decrease in both acute and chronic infections (Supplementary Table 1 and 2).

During LCMV infection, effector $CD8^+$ T cells play a critical role. They control virus expansion in acute infection while $CD8^+$ T cell exhaustion is a hallmark of chronic infection (Oldstone, 2006). Therefore, in order to verify that DCQ correctly predicts changes in the dynamics of immune cell subsets with major roles during LCMV infection, we first focused on DCQ-inferred kinetics of effector $CD8^+$ T cells. In concordance with the kinetics of LCMV-specific IFNɣ-producing $CD8^+$ T cells analyzed by flow cytometry (Supplementary

Figure 1A), DCQ predicted an increase of effector $CD8^+$ T cells (OT-I-specific $CD8^+$ T cell that were monitored at days 5, 6 and 8 p.i. with Listeria (LIS) or Vesicular stomatitis virus (VSV)) in both acute and chronic infections. Importantly, DCQ correctly predicted exhaustion of $CD8^+$ T cells in chronic infection, showing a drastic decrease of these effector cells between days 7 and 9 (Figure R2 and Supplementary Figure 1B). Moreover, the kinetics of late effector and memory $CD8^+$ T cells (T.CD8+EFF, OT-I & VSV-15d and T.CD8+MEM, OT-I & LIS-100d) also showed the failure of chronically infected mice to generate a memory T cell response, in contrast to acute infected mice (Figure R2 and Supplementary Figure 1B).

DCQ also correctly predicted the changes in immune cell quantities of several other cell subsets with a specific role in LCMV chronic infection. For example, $CD4^+$ regulatory T cells (T.CD4+FP3+CD25+) only increased late in chronic infection (day 31 p.i.) (Supplementary Figure 2), as previously described (Schmitz et al., 2013) and further validated by flow cytometry (Supplementary Figure 3A). Two conventional dendritic cell (cDC) subsets expressing the marker CD103 and isolated from small intestine also showed an increase from day 9 in chronic infection (cDC.CD103+CD11b-) (Supplementary Figure R2). These $CD103^+$ $CD11b^-$ DCs from intestine are also present in other tissues such as the spleen. They express CD8 and the chemokine receptor XCR1, and are specialized in antigen cross-presentation (Ohta et al., 2016). Thus, these predicted DC kinetics likely represent the appearance of $XCR1^+$ DCs during the chronic infection phase that we have recently described to contribute to the maintenance of an antiviral cytotoxic T cell response and viral control (Argilaguet et al. 2018, submitted). Finally, DCQ also predicted in acute infection a transient increase of two neutrophil subsets (GN.ARTH) that in contrast, remained elevated at day 31 p.i. in chronically infected mice (Supplementary Figure 2). These neutrophils, which were monitored from arthritic mice in the immune cell compendium, likely represent the previously reported appearance of neutrophilic suppressor cells which have an immunomodulatory role during chronic infection (Norris et al., 2013).

Other immune cell subsets kinetics inferred by DCQ showed a similar overall response in acute and chronic infected mice. For example, despite previous reports that attributed different roles to NK cells in both infections outcomes (Robbins et al., 2007; Waggoner et al., 2011b), activated NK cells predicted by DCQ (NK cells monitored in mice infected with murine cytomegalovirus (MCMV)) showed a similar kinetic in acute and chronic infection

(Figure R2 and Supplementary Figure 3B), with an early peak at days 5 and 3 p.i., respectively. Analysis of NK cell kinetics in chronic LCMV infection by flow cytometry showed a total NK cells decrease early after infection. However, increase of activated NK cells predicted by DCQ was validated when analyzing the kinetics of NK cell at different maturation states by staining cells with anti-CD11b and anti-CD27 antibodies. Indeed, only NK cells coexpressing these two surface markers, markers expressed in activated effector NK cells (Chiossone et al., 2009), showed an identical kinetic than activated NK cells predicted by DCQ (Supplementary Figure 3C), therefore demonstrating the ability of DCQ to predict the quantity of immune cell subsets in a particular functional stage. DCQ also predicted differences in the dynamics of two different macrophage (MF) subsets: (i) CD169+ MFs, known to promote an early wave of innate immune responses and in priming cytotoxic T cells (Bernhard et al., 2015; van Dinther et al., 2018), increased early after infection (day 3 p.i.), and (ii) activated MFs (monitored at 5 days post stimulation with thioglycollate), increased at days 7 and 9 p.i. (Figure R2 and Supplementary Figure 4A), when the adaptive T cell response appears (Supplementary Figure 1A). Finally, DCQ-prediction of monocyte kinetics were also validated by FACS, showing a rapid increase of inflammatory Ly6c^{+} monocytes followed by an increase of resident Ly6c^{-} monocytes at later time points in both acute and chronic infection (Supplementary Figure S4-B and C).

By infecting progenitor cells and dendritic cells (DCs), LCMV prevents the maturation and migration of DCs (Sevilla et al., 2003, Sevilla et al., 2004). Accordingly, DCQ also correctly predicted the kinetics of DCs: the number of plasmacytoid DCs (pDC) in the spleen increased early after infection, while most conventional DCs (cDCs) decreased, as described previously (Montoya et al., 2005) (Figure R2). Finally, several other cell subsets showed a decrease in numbers in both acute and chronic infections: undifferentiated T cells, in accordance with the DCQ-derived results obtained by Altboum et al. (Altboum et al., 2014) in lungs from influenza infected mice, and B cells, in agreement with previous literature that reported a Type I IFN- or NK-mediated depletion of B cells in acute and chronic LCMV infections (Cook et al., 2015; Fallet et al., 2016; Rydyznski et al., 2015).

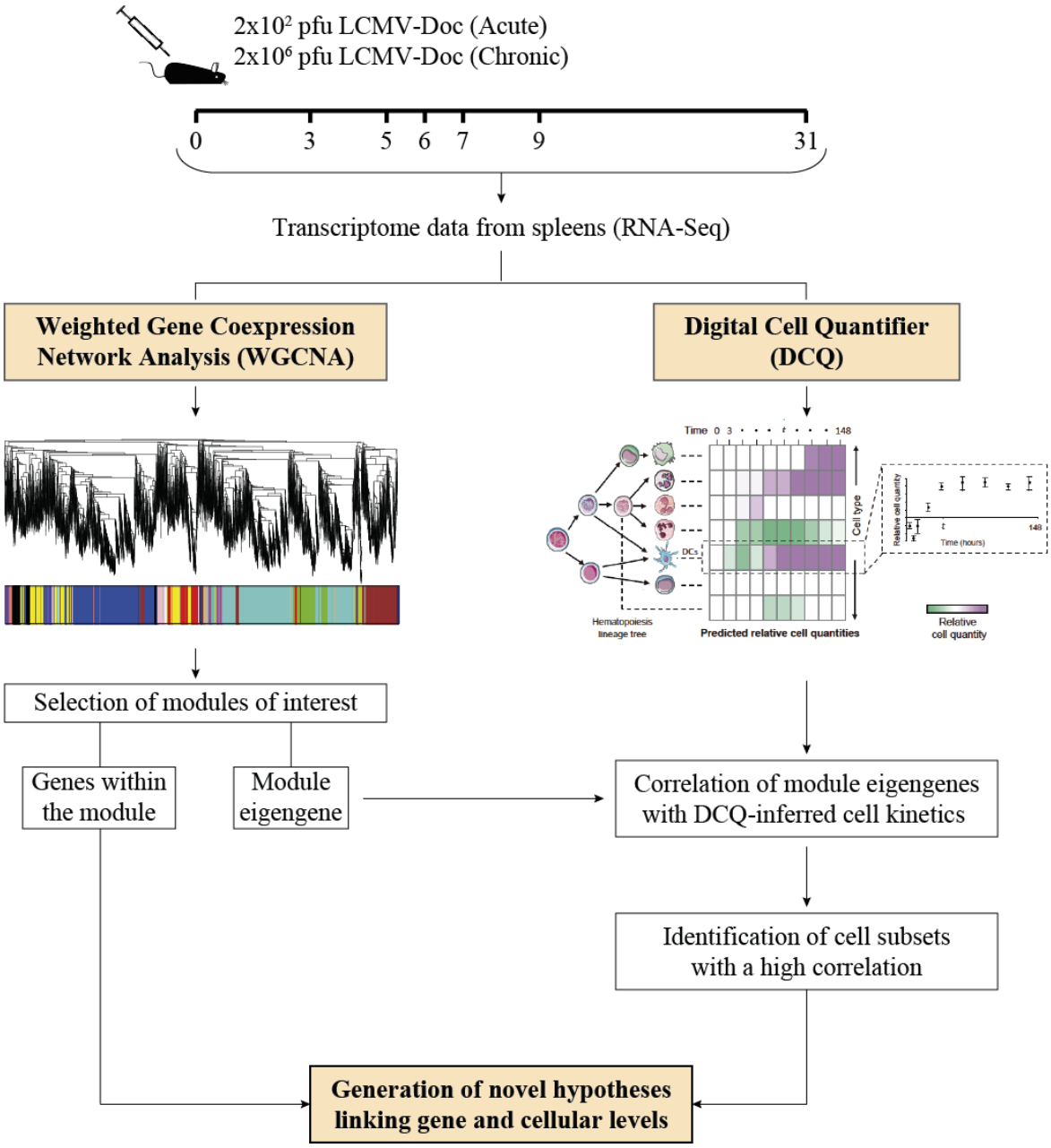

Figure R1. Schematic representation of the experimental design. Mice were infected with either $2x10^2$ or $2x10^6$ PFU of LCMV Docile ($LCMV_{Doc}$), and spleens were collected at the indicated days postinfection to obtain time-resolved transcriptomes in acute and chronic infections, respectively. Differentially expressed (DE) gene kinetics obtained by RNA-Seq were used as input for weighted gene coexpression network analysis (WGCNA) and digital cell quantifier (DCQ) to obtain modules of highly coexpressed genes and predictions of immune cell kinetics in spleen, respectively. To identify the cell subsets expressing a cluster of genes from a particular module, we performed a Pearson's correlation analysis of the module eigengene with DCQ-inferred cell kinetics, and novel hypotheses are generated.

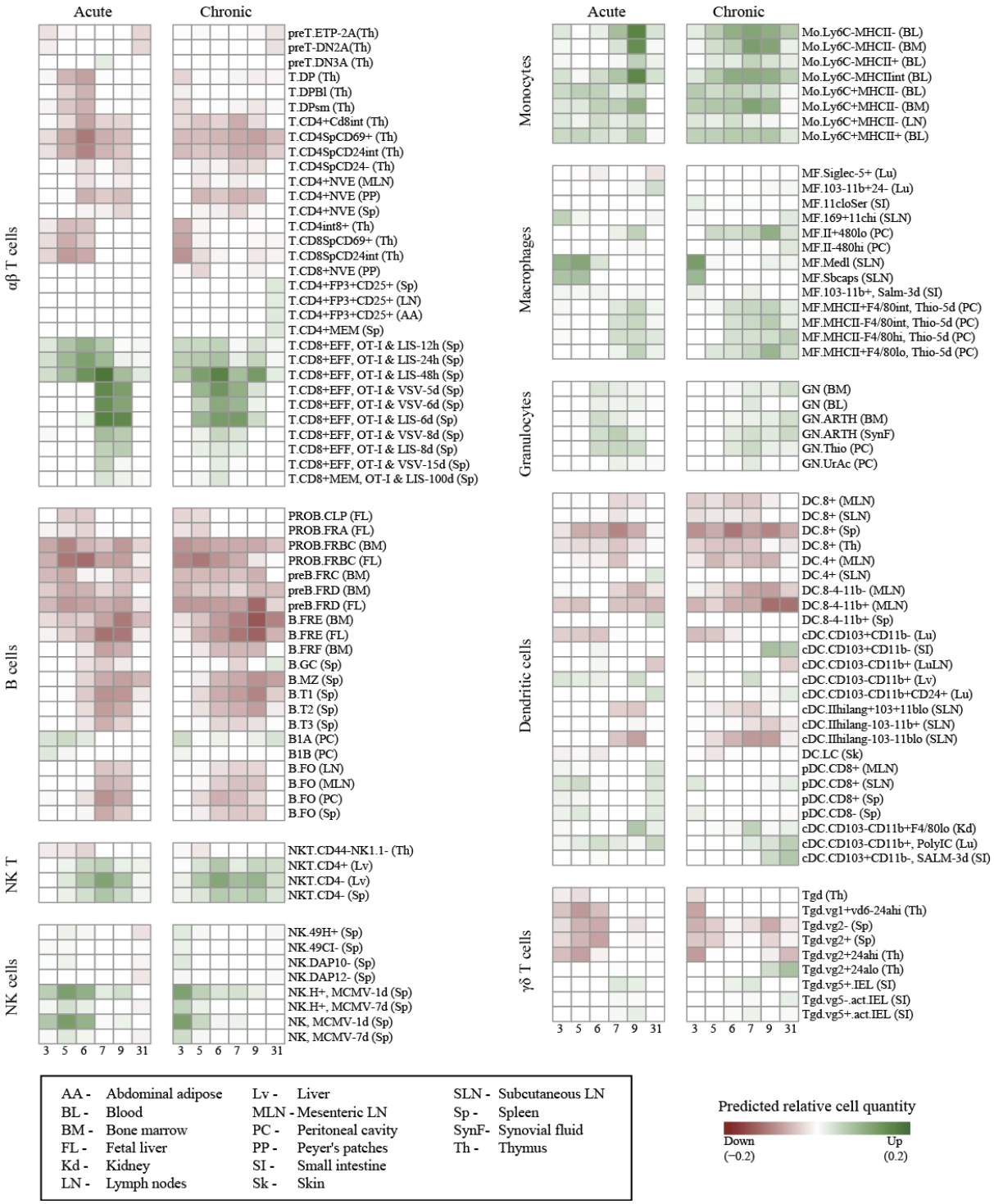

Figure R2. DCQ reconstruction of global immune cell dynamics during acute and chronic LCMV infections. Global dynamics in immune cell quantities (green/increase, red/decrease in relative cell quantities) after acute and chronic LCMV infections, predicted by DCQ at different time points postinfection (columns) for 125 different immune cell types (rows). Each cell type heading is followed by the code of the tissue from which the cell type was isolated in the compendium. The box at the bottom left contains details for these abbreviations.

2. Combining WGCNA and DCQ to link immune cell subsets to gene coexpression networks

Using the same RNA-Seq data set from acute and chronic LCMV infections, our group previously obtained spleen transcriptome-derived coexpression modules by WGCNA (Argilaguet et al. 2018, submitted). This analysis provided relevant information about biological processes playing a major role in response to a virus-induced host perturbation. However, the gene coexpression analysis of total organ RNA lacks information about the cell subsets that participate in the expression of genes within the coexpression modules. In order to decipher which immune cell subsets are involved in spleen-derived gene coexpression modules obtained by WGCNA, we hypothesized that, in some circumstances, changes in the quantity of a particular cell subset will be translated also to changes of the genes expressed by that cell. When this hypothesis is true, the kinetics of a set of coexpressed genes will correlate with the kinetics of the cell subset expressing them. Thus, in order to further explore our time-resolved splenic transcriptome data set from acute and chronic LCMV infections, we performed Pearson's correlation analysis between WGCNA-derived module eigengenes (Argilaguet et al. 2018, submitted) and DCQ-inferred cell kinetics (Figure R1).

In our previous work, we identified the acute-brown module as the representative of the LCMV-specific $CD8^+$ T cell response induced in acute infection (Argilaguet et al. 2018, submitted). Its eigengene expression kinetics highly correlated with the LCMV-specific $CD8^+$ T cell response measured by intracellular staining of IFNɣ after *in vitro* virus-specific stimulation (Figure R3-A). Further analysis of the 315 hub genes within the module revealed an enrichment on T cell activated genes. Therefore, in order to validate our approach, we first analyzed which DCQ-inferred immune cell subset kinetics from acute infection correlated with the acute-brown module eigengene. From the 125 immune cell subsets inferred by DCQ, 23 cells showed a significant positive correlation (p-value<0.05) (Supplementary Table S3). As expected, effector $CD8^+$ T cells (activated at days 5, 6 and 8 p.i. with LIS or VSV) showed correlation scores above 0.9 (Figure R3-A and Supplementary Table S3), thus indicating that our approach correctly predicts the immune cell subsets responsible for the expression of genes within the module of interest. However, similar to effector $CD8^+$ T cells, several monocyte and macrophage cell subsets also showed high correlation scores and thus similar kinetics to acute-brown module eigengene (Figure R3-A and R3-B), suggesting that these cells might express also genes contained in the module. To test this hypothesis, we

performed RNA-Seq analysis of sorted monocytes/macrophages and $CD8^+$ T cells from naive mice and animals infected with a low dose of $LCMV_{Doc}$ (acute infection). A total of 5291 genes were significantly upregulated at day 7 p.i. in activated $CD44^+$ $CD8^+$ T cells compared to $CD44^-$ $CD8^+$ T cells from uninfected naive mice. Monocytes/macrophages showed 3520 genes significantly upregulated at day 7 p.i. compared to uninfected mice. To analyze if the genes within the acute-brown module were significantly enriched for genes from these two cell subsets, we determined the gene overlap between the module hub genes and the genes upregulated in $CD8^+$ T cells and monocytes/macrophages by a Fisher's Exact Test (Figure R4-A). The acute-brown module was highly enriched for genes upregulated in both cell subsets. From the 315 hub genes within the module, 182 overlapped with genes upregulated in activated $CD8^+$ T cells (p-value$<1.6x10^{-16}$) and were enriched for genes involved in the T cell response, TGF-β signaling and leukocyte migration, among others (Figure R4-B and Supplementary Table S4-A). Importantly, 113 hub genes overlapped with genes upregulated in monocytes/macrophages (p-value$<3.6x10^{-7}$) and were enriched for genes involved in TCR signaling pathway, T cell activation and IL-4 production (Figure R4-C and Supplementary Table S4-B), thus indicating that the acute-brown module represents the complex process on the induction of the T cell adaptive response that requires the coordination of monocytes/macrophages and $CD8^+$ T cells. All together, these results demonstrate that the combination of DCQ and WGCNA is a very valuable tool to better characterize the immune cell subsets that participate in a complex biological pathway represented by a gene coexpression module.

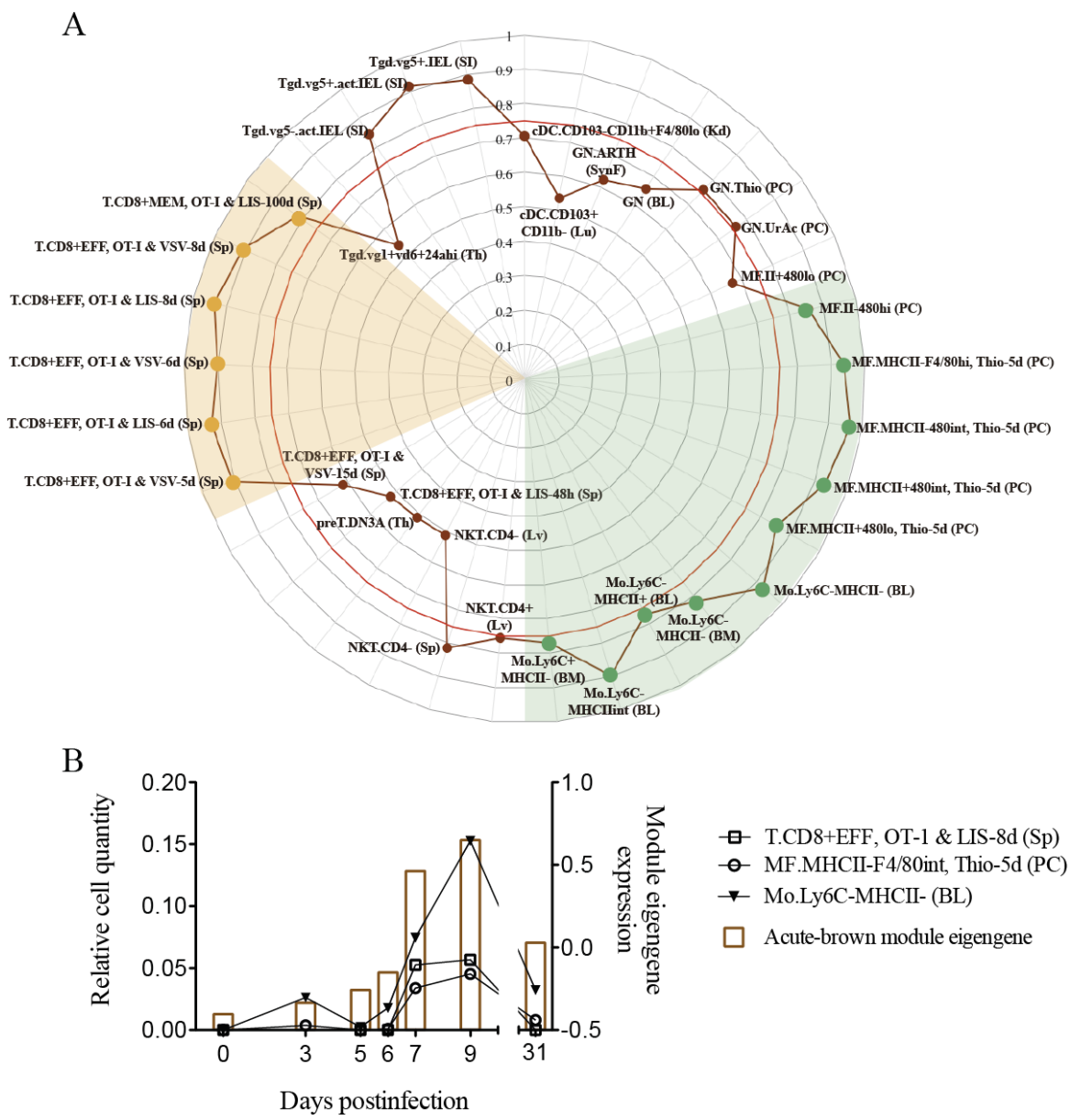

Figure R3. Acute-brown module correlates with effector CD8$^+$ T cells and monocyte/macrophage subsets. (A) Radar chart showing the correlation values of immune cell subsets from acute infection with acute-brown module eigengene kinetics (only shown cell subsets with a correlation >0.5). Red line shows Pearson's correlation score with a p-value= 0.05. (B) Kinetics of acute-brown module eigengene (right axis) and the CD8$^+$ T cell, macrophage and monocyte subsets (left axis) with the highest correlation scores.

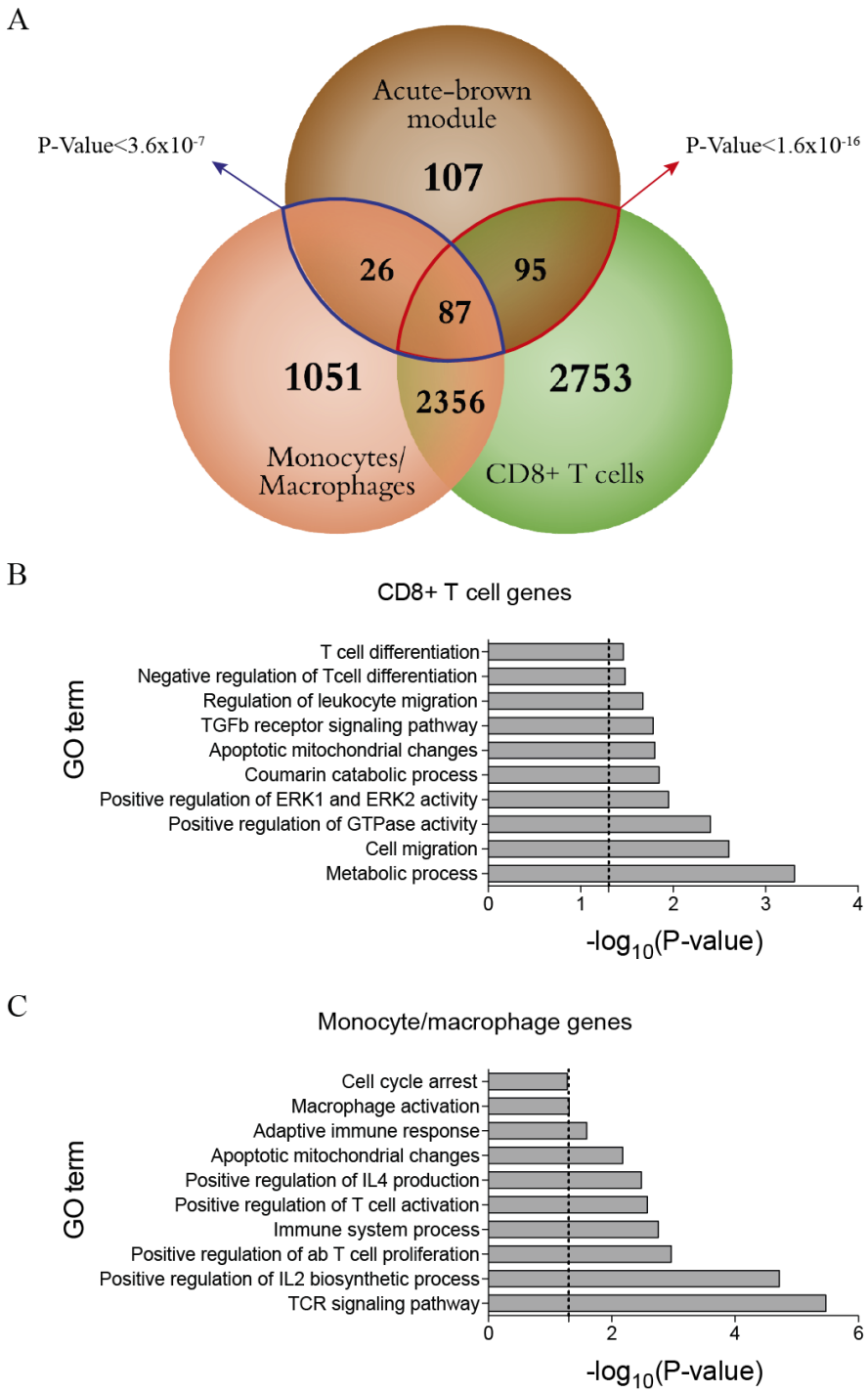

Figure R4. Monocytes/macrophages and CD8$^+$ T cells cooperate in the induction of the T cell response during LCMV acute infection. (A) Venn diagram of overlaps among differentially expressed genes between days 0 and 7 after acute LCMV infection from sorted monocytes/macrophages and CD8$^+$ T cells, and hub genes from acute-brown module (genes with intramodular connectivity (K_{IM})>0.6). The significance of gene overlap between monocytes/macrophages (blue line) and CD8$^+$ T cells (red line) with acute-brown module was calculated by Fisher's Exact Test. (B-C) Ten representative GO terms enriched in genes from CD8$^+$ T cells (B) and monocytes/macrophages (C) (dashed lines mark P-value=0.05).

3. Neutrophil and macrophage migration are altered during chronic infection concomitant with CD8$^+$ T cell exhaustion

Next we aimed to test our novel approach analyzing gene coexpression modules that represent critical features of chronic LCMV infection. Exhaustion of CD8$^+$ T cells is a widely studied hallmark of chronic infections (Wherry, 2011; Zuniga and Hacker, 2012). However, little is known about the behavior of other immune components during its appearance. We therefore analyzed which WGCNA-derived module might represent biological processes that are concomitant to CD8$^+$ T cell exhaustion. Interestingly, the chronic-magenta module eigengene showed an expression kinetics very similar to the one of LCMV-specific CD8$^+$ T cells (Supplementary Figure S1) (Argilaguet et al. 2018, submitted), with a marked downregulation between days 7 and 9 postinfection (Figure R5-B). Therefore, this indicates that this module might represent a biological pathway concomitant with CD8$^+$ T cell exhaustion. Aiming to identify the immune cell subsets responsible for the expression of genes within this module, we analyzed which DCQ-inferred cell kinetics from chronic infection correlated with the chronic-magenta module eigengene. 14 cell subtypes showed a correlation value above 0.7, including effector CD8$^+$ T cells, dendritic cells, Tgd cells, activated neutrophils (GN, GN.Thio and GN.UrAc) and several monocytes/macrophages (Figure R5-A and Supplementary Table S3). Gene ontology (GO) analysis of the chronic-magenta module hub genes showed an enrichment for genes related to neutrophil chemotaxis and/or inflammatory response (*Ccr1*, *C5ar1*, *Itgam*, *Trem1*, *Vav3*, *Itgb2*) (Supplementary Table S7), suggesting that these pathways are altered at the same time when CD8$^+$ T cell exhaustion appears. Therefore, we next focused on the analysis of neutrophils and monocytes/macrophages (Figure R5-B), since they play a major role during inflammation (Kumar et al., 2018). To validate the DCQ-predicted kinetics of these cell subsets, we first analyzed by FACS the percentages of total neutrophils and monocytes/macrophages in the spleen from naive mice and animals at days 7 and 9 p.i. with a high dose of LCMV$_{Doc}$ (chronic infection). Both cell subsets were increased at day 7 postinfection but, surprisingly, none of them showed a significant decrease at 9 days p.i. (Figure R6-A). These results might indicate that these DCQ-predictions represent a particular functional stage of neutrophils and/or monocytes/macrophages, as stated before (Supplementary Figure S4) (Altboum., 2014). Thus, we next focused on the analysis of three hub genes involved in inflammatory responses (*Ccr1*, *C5ar1* and *Itgam*). Their expression kinetics obtained by RNA-Seq showed a peak of expression at day 7 followed by a decrease at day 9 p.i. (Figure R5-C), that we

confirmed in additional animals by qPCR from spleens at these same time points (Supplementary Figure S5). In order to identify cell subsets responsible for the downregulation of these genes, we analyzed their expression levels in sorted neutrophils and monocytes/macrophages from animals at days 7 and 9 p.i.. Interestingly, *Ccr1* and *C5ar1* were significantly downregulated at these time points in both cell subsets, while *Itgam* showed a non-significant tendency to decrease (Figure R6-B). These results suggest that the immune adaptation to a chronic infection is a complex process that involves the immunosuppression of T cells as well as cells from the innate immune system with an important role in inflammation. Further studies are necessary to elucidate the functional implications of such observations and their relevance in the infection outcome. All together, these results demonstrate that combining DCQ with WGCNA allows to better characterize the dynamic cell events occurring in complex tissues, generating hypotheses about the immune cell types that participate in a coordinated way in a particular biological process.

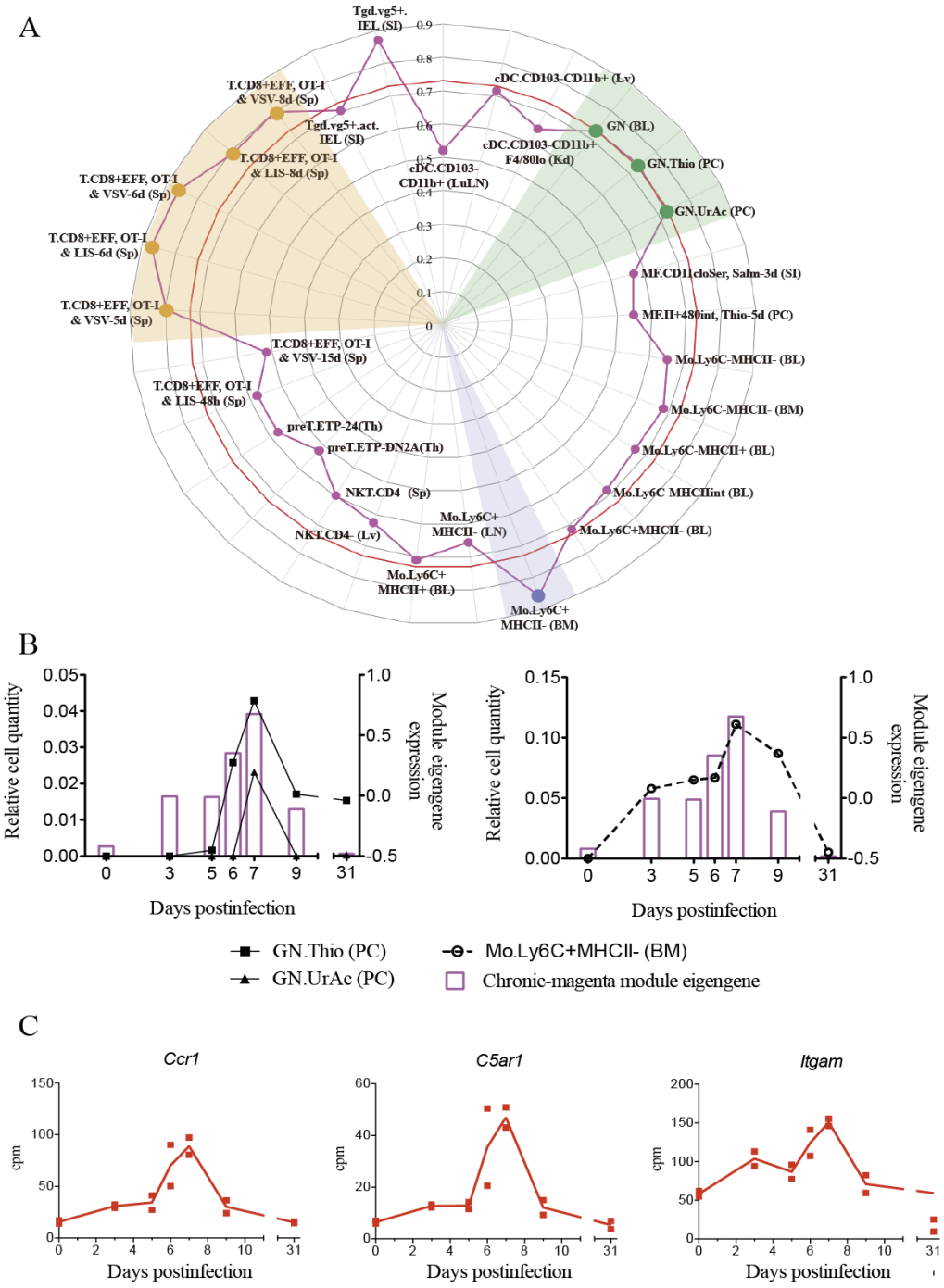

Figure R5. Activated neutrophils and monocytes/macrophages correlate with chronic-magenta module. (A) Radar chart showing the correlation values of immune cell subsets from chronic infection with chronic-magenta module eigengene kinetics (only shown cell subsets with a correlation >0.5). Red line shows the Pearson's correlation score with a p-value = 0.05. (B) Kinetics of chronic-magenta module eigengene (right axis) and activated neutrophils (left) and monocytes (right). (C) Normalized gene expression (cpm) kinetics of the genes *Ccr1*, *C5ar1* and *Itgam*, obtained from the RNA-Seq analysis of the spleens of chronically infected mice.

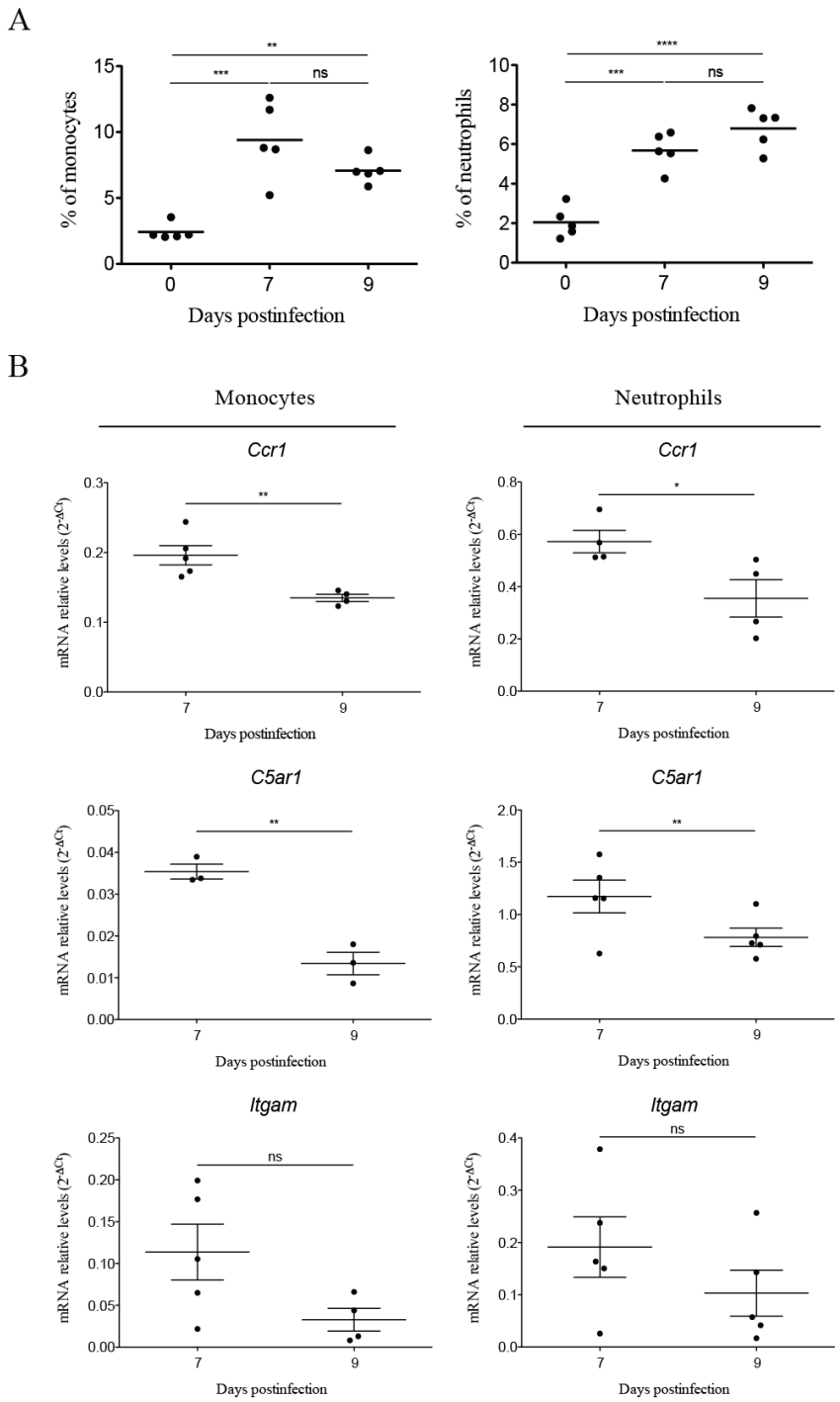

Figure R6. Monocytes and neutrophils downregulate genes involved in inflammatory response during chronic infection. (A) Percentage of monocytes/macrophages and neutrophils in spleen at the indicated days postinfection in chronically infected mice determined by FACS analysis (significance determined using one-way ANOVA). (B) Expression levels of *Ccr1, C5ar1 and Itgam* measured by qPCR from sorted monocytes and neutrophils. Relative gene expression level was normalized by *Gapdh*. Data are shown as mean ± SEM from 4 to 5 mice. Significant differences were determined by an unpaired two-tailed t test. ns, non significant; * $p \leq 0.05$; ** $p \leq 0.01$.

4. XCL1-producing cells during the adaptation phase to a chronic infection present an immature early effector phenotype

Analysis of infection-fate-specific modules in Argilaguet et al. (Argilaguet et al. 2018, submitted) allowed to identify the biological pathways specific of chronic infection. In particular, the chronic-darkturquoise module contains the cytokine XCL1, showing a "two-peak" behavior with an expression peak at day 5 and a second upregulation from day 7 to day 9 p.i., at the time when exhaustion of $CD8^+$ T cells appears (Figure R7-B and Supplementary Figure S1-A). We showed that XCL1 expression resulted in the recruitment of cross-presenting dendritic cells that express its receptor (XCR1), and that these cells contribute to the maintenance of an antiviral cytotoxic T cell response and participates in viral control in the chronic infection phase. Phenotypic analyses allowed us to describe that XCL1 was mainly expressed by LCMV-specific $CD8^+$ T cells expressing the receptor CXCR5, a marker of exhausted $CD8^+$ T cells that retain effector functions (He et al., 2016; Im et al., 2016). However, due to the complexity of effector and exhausted $CD8^+$ T cell subpopulations present during a chronic infection (Bengsch et al., 2018), a detailed phenotypic characterization of XCL1-producing $CD8^+$ T cells was lacking.

In order to better characterize the phenotype and activation state of the XCL1-producing $CD8^+$ T cells in LCMV chronic infection, we used our approach to analyze what DCQ-inferred immune cell subset kinetics from chronic infection correlated with the chronic-darkturquoise module eigengene. Interestingly, only two $CD8^+$ T cell subsets isolated at 12 and 24h post Listeria (LIS) infection (T.CD8+EFF, OT-I & LIS-12h and 24h) showed a significant correlation (Figure R7-A and R7-B), suggesting that XCL1-producing $CD8^+$ T cells have an immature early effector phenotype. Using the "Population Comparison" tool from the Immunological Genome (ImmGen) Project, we next analyzed which genes are upregulated in these two cell subsets compared to late effector $CD8^+$ T cells (OVA-specific T cells at days 5, 6 and 8 postinfection with LisOva or VSVOva). 385 genes showed expression values significantly higher in early versus late effector $CD8^+$ T cells (Supplementary Table S8). To note, within them we found XCL1 and CXCR5, with a mean fold-change of 25.14 and 4.94, respectively, further indicating that XCL1 is produced by $CD8^+$ T cells with a phenotype characteristic of immature early effector $CD8^+$ T cells. To validate this hypothesis, we infected mice with a high dose of $LCMV_{Doc}$ to induce a chronic infection, and analyzed by FACS the level of expression of proteins characteristic of early effector $CD8^+$ T cells by

XCL1-producing cells at day 9 p.i.. Using the "My GeneSet" tool from ImmGen, we selected four proteins with high gene expression values in early effector T cells: TNFSF8, a cytokine that induces proliferation of T cells; TLR7, a receptor selectively upregulated by exhausted CXCR5^{+} CD8^{+} T cells (Im et al., 2016); CCR9, an chemokine receptor that regulates early phases of inflammation (López-Pacheco et al., 2016); and CD83, which is upregulated upon T cell stimulation during virus infection (Ju et al., 2016) (Figure R8-A and Supplementary Table S8). Expression of TNFSF8, TLR7 and CD83 by XCL1- CD8^{+} T cells was similar between naive mice and infected animals at day 9 p.i. (Figure R8-B). By contrast, CCR9 showed higher expression levels in naive mice, in concordance with data obtained from ImmGen dataset, where CCR9 showed a high gene expression value in naive OT1 cells (Figure R8-A). Importantly, TNFSF8, TLR7 and CCR9 were highly expressed by XCL1^{+} CD8^{+} T cells at day 9 p.i., showing mean fluorescence intensities (MFI) significantly higher than in XCL1^{-} cells (Figure R8-B). These results demonstrate that XCL1 produced by CD8^{+} T during the adaptation phase to a chronic infection is produced by CD8^{+} T cells that express markers characteristic of early effector cells. Further experiments are necessary to decipher whether these cells are *de novo* activated naive T cells or exhausted T cells with a phenotype similar to early effector T cells. All together, these results demonstrate that by combining WGCNA with DCQ, it is possible to generate novel hypotheses to characterize the activation and differentiation status of cells that participate in the relevant immune processes.

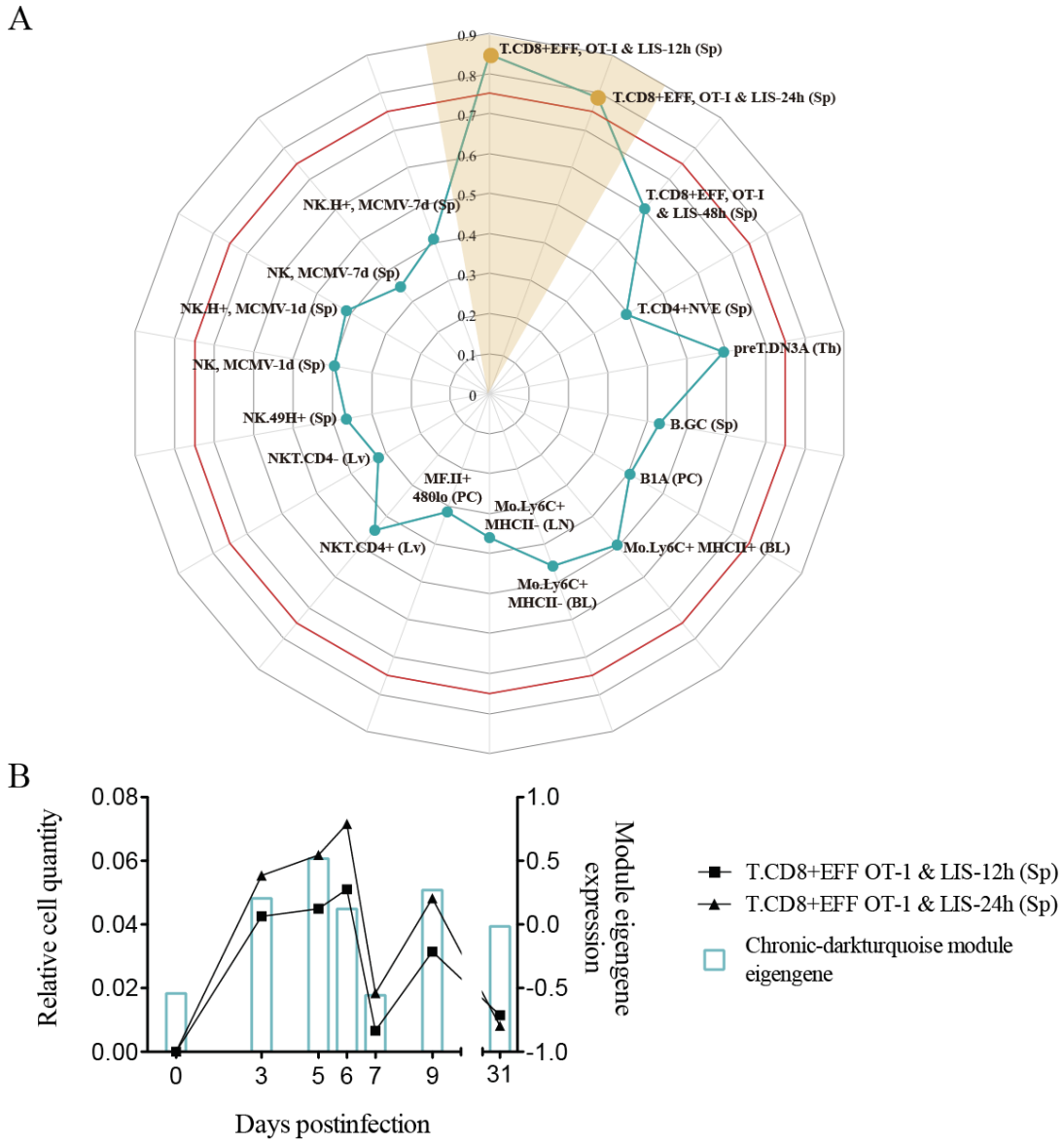

Figure R7. Chronic-darkturquoise module correlates with early effector CD8$^+$ T cells. (A) Radar chart showing the correlation values of immune cell subsets from chronic infection with chronic-darkturquoise module eigengene kinetics (only shown cell subsets with a correlation >0.3). Red line shows the Pearson's correlation score with a p-value = 0.05. (B) Kinetics of early effector CD8$^+$ T cells (left axis) and chronic-darkturquoise module eigengene (right axis).

A

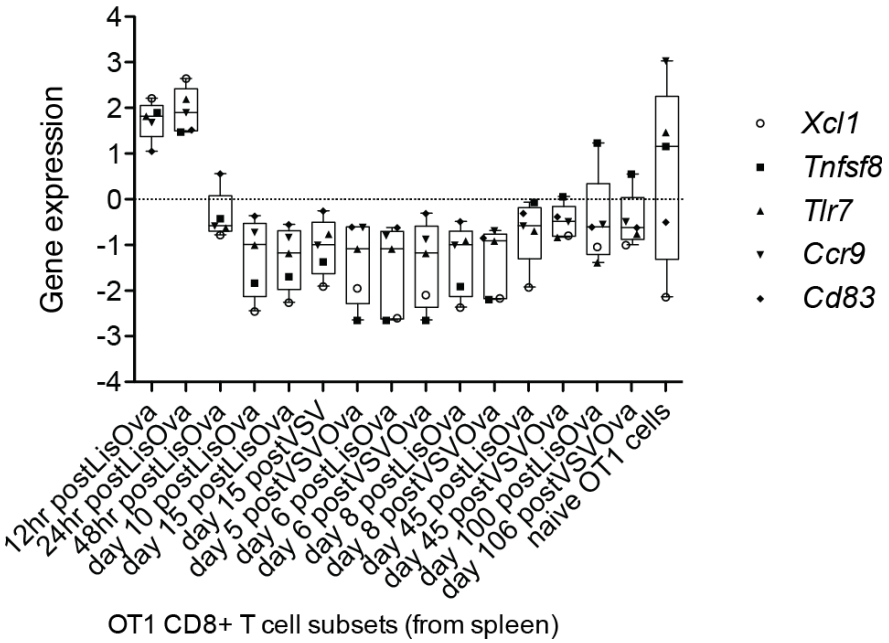

B

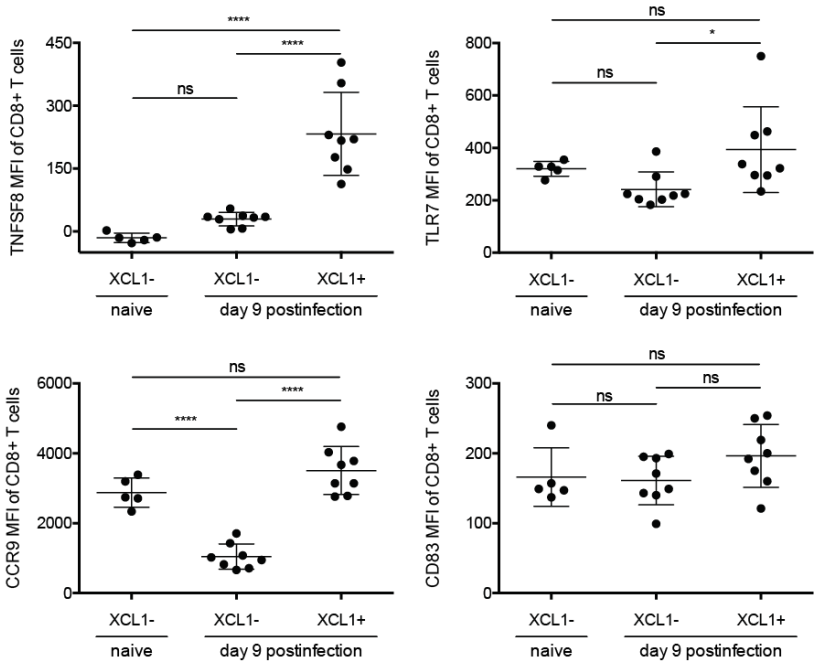

Figure R8. XCL1-producing CD8$^+$ T cells express markers characteristic of early effector CD8$^+$ T cells. (A) Box-plot representation of *Xcl1, Tnfsf8, Tlr7, Ccr9 and Cd83* expression. Mean-normalized expression values (log2) of selected genes in Ova-specific OT1 CD8$^+$ T cells were obtained using "My GeneSet" tool from ImmGen (http://www.immgen.org/). (B) Mean fluorescence intensity (MFI) of *Tnfsf8, Tlr7, Ccr9 and Cd83* in XCL1$^-$ and XCL1$^+$ CD8$^+$ T cells in naive mice and in chronically-infected animals at day 9 p.i.. Significant differences were determined by one-way ANOVA. ns, non significant; * $p \leq 0.05$; ** $p \leq 0.01$.

SUPPLEMENTARY FIGURES AND TABLES

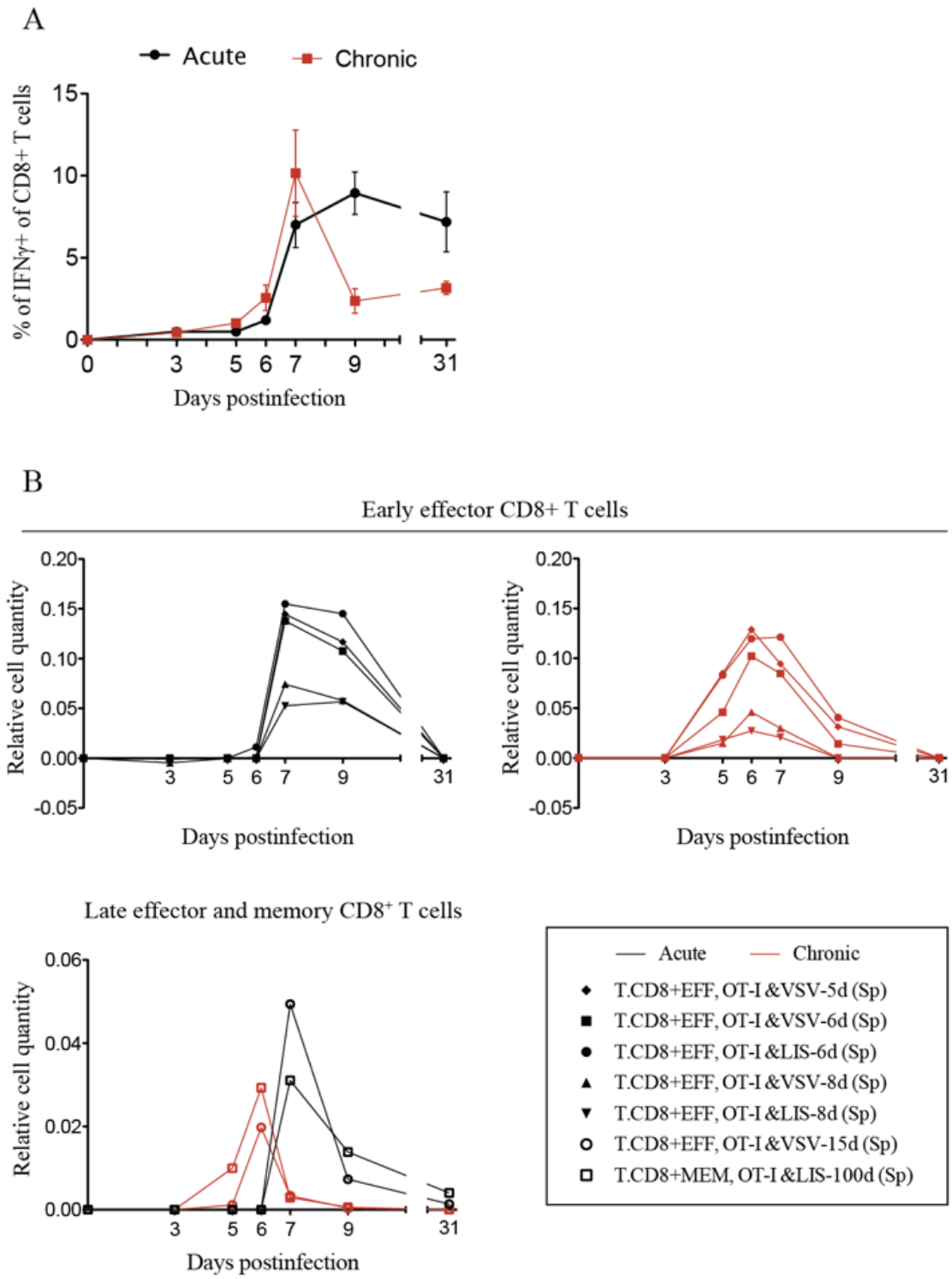

Figure S1. Dynamics of effector CD8$^+$ T cells predicted by DCQ show exhaustion appearance in chronic LCMV infection. (A) Percentages of GP33-specific IFN□-producing CD8$^+$ T cells in spleen. The mean ± SEM is shown. (B) DCQ-inferred cell kinetics of effector CD8$^+$ T cells isolated after VSV or Listeria (LIS) infections at the indicated time points.

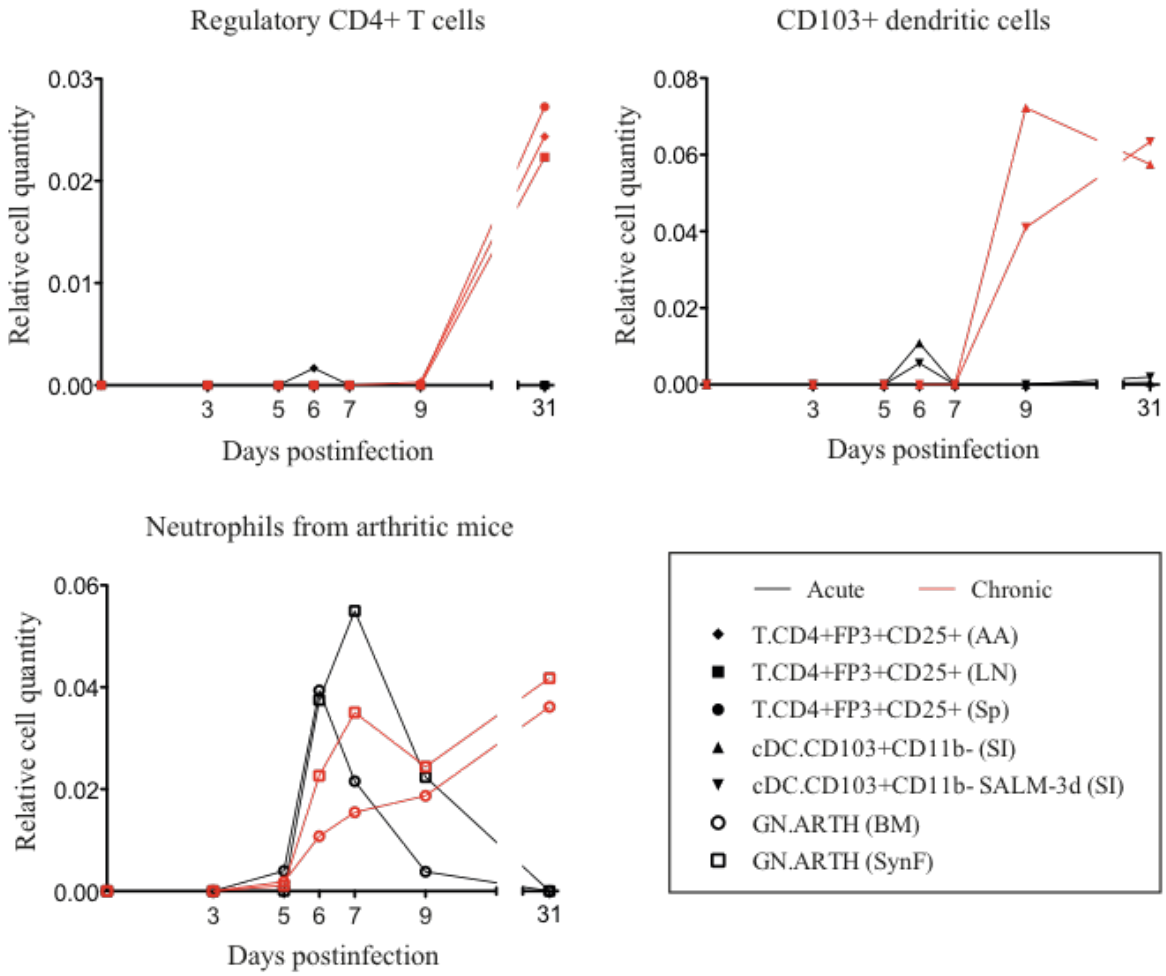

Figure S2. DCQ-predictions of immune cell subsets with specific roles during chronic infection. DCQ cell predictions of regulatory $CD4^+$ $Foxp3^+$ T cells, $CD103^+$ dendritic cell subsets and granulocytes from arthritic mice from acutely or chronically infected mice.

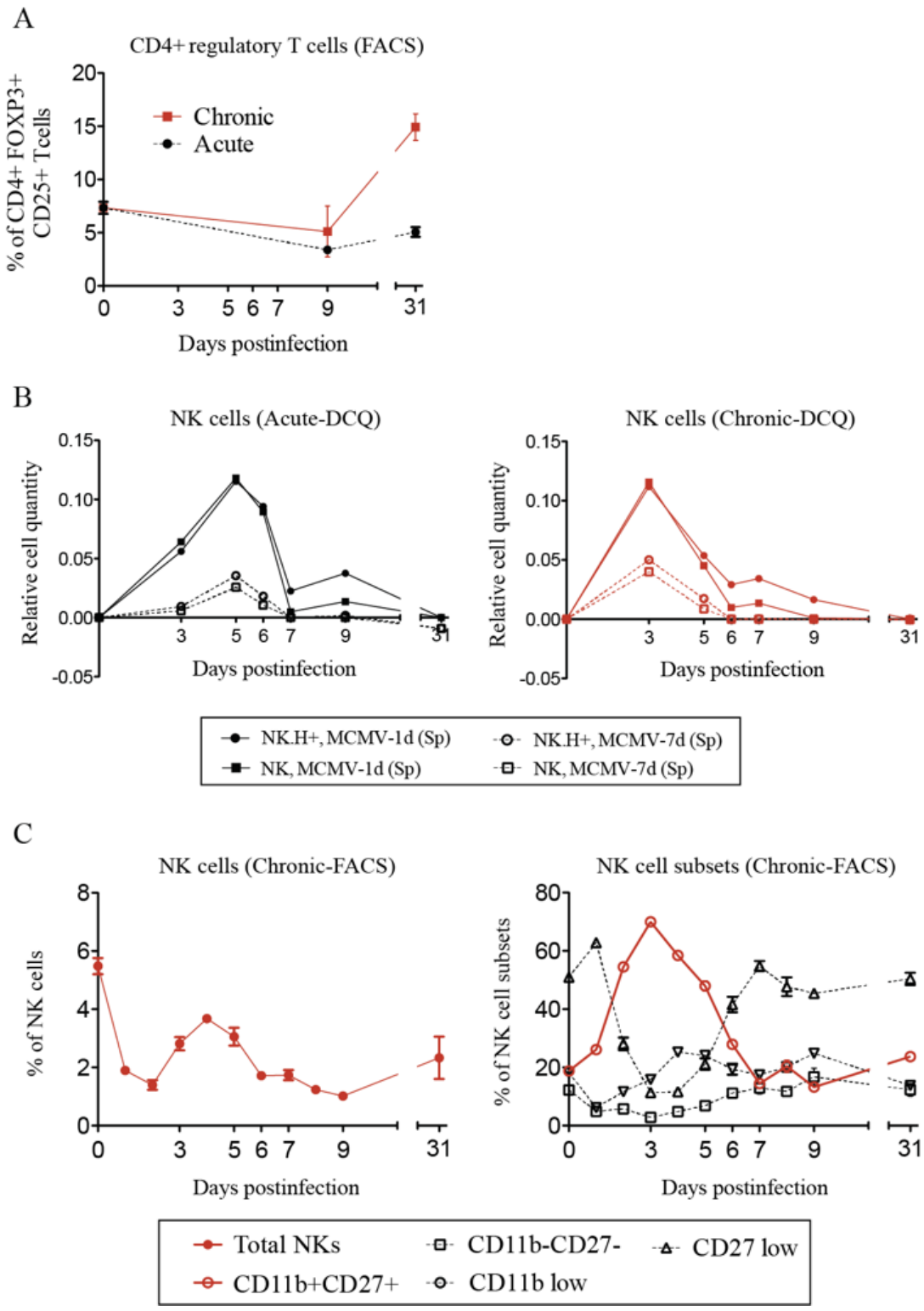

Figure S3. Validation of DCQ-predicted kinetics. Kinetics of of $CD4^+$ regulatory T cells (A) and effector NK cells (B and C) were validated by FACS at the indicated time points.

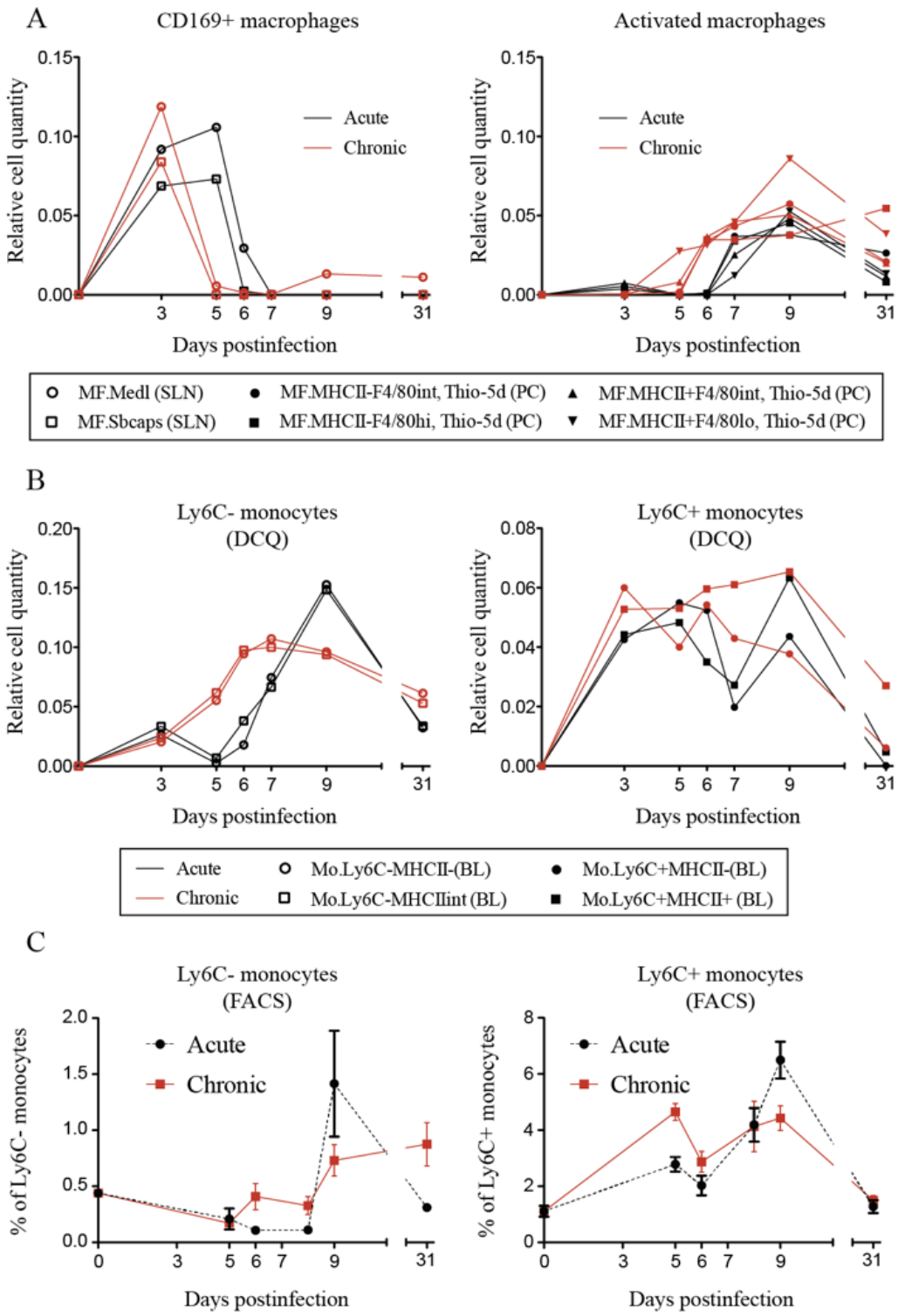

Figure S4. Dynamics of macrophage and monocyte cell subsets. DCQ-predicted cell changes in quantity of (A) macrophages and (B) monocyte cell subsets. (C) Validation by FACS of cell quantity dynamics of Ly6C$^-$ and Ly6C$^+$ monocytes in acute and chronic LCMV infection at the indicated time-points.

A

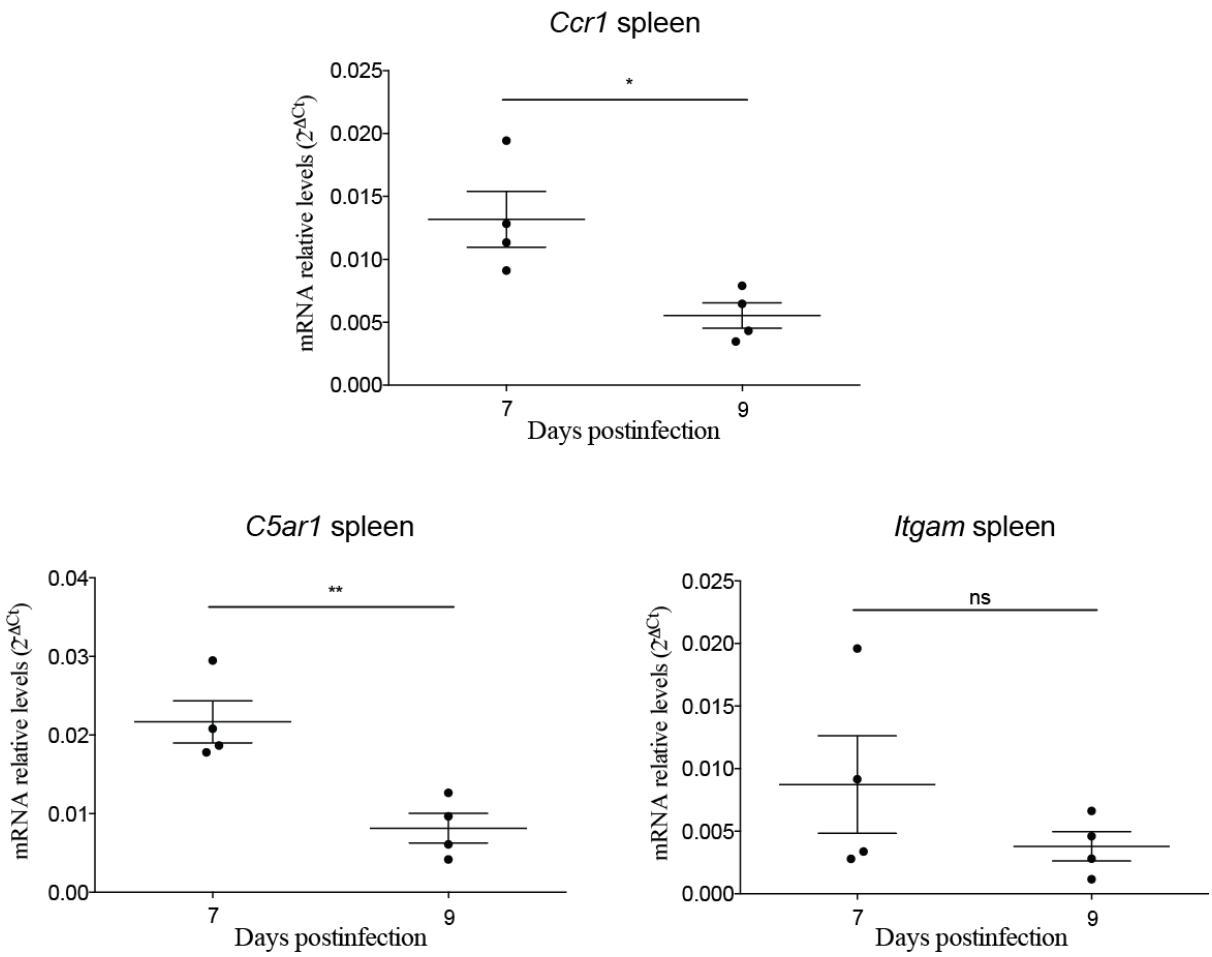

Figure S5. Validation of downregulation of *Ccr1*, *C5ar1* and *Igam* by qPCR from spleens. (A) qPCR of the neutrophil chemotaxis/inflammatory response related genes performed at the indicated days postinfection from spleens of chronic infected mice. Relative gene expression level was normalized by *Gapdh*. Data are shown as mean ± SEM from 4 mice. Significant differences were determined by an unpaired two-tailed t test. ns, non significant; * $p \leq 0.05$; ** $p \leq 0.01$.

Supplementary Table S1. DCQ's predictions of dynamically changing cell types during the course of acute LCMV infection. Shown are predicted cell quantities and the –log10 t-test p-value results, only for those cell types (rows) that are significantly changing based on our robustness evaluation of the DCQ's predictions (see methods). Column 3 indicates whether the cell type is predicted to increase or decrease during infection.

Cell type	Short Name	Kinetics	day 3		day 5		day 6		day 7		day 9		day 31	
			Prediction	P value	Prediction	P value	Prediction	P value	Prediction	P value	Prediction	P value	Prediction	P value
Granulocytes	GN.ARTH (BM)	UP	0.0000	0.0000	0.0040	8.1959	0.0394	40.3107	0.0215	26.0869	0.0038	8.0697	0.0000	0.0000
	GN.ARTH (SynF)		0.0000	0.0000	0.0001	0.7299	0.0375	41.4143	0.0550	55.1896	0.0224	36.4604	0.0000	0.0000
	GN (BL)		0.0000	0.0000	0.0000	0.0000	0.0154	19.7640	0.0122	15.9873	0.0141	24.7887	-0.0018	-3.5320
	GN (BM)		0.0000	0.0000	0.0008	2.2178	0.0295	30.2941	0.0197	23.7849	0.0111	17.2496	0.0000	0.0000
	GN.Thio (PC)		0.0000	0.0000	0.0008	2.9458	0.0406	45.0878	0.0464	46.8694	0.0428	49.7615	0.0000	0.0000
	GN.UrAc (PC)		0.0000	0.0000	0.0000	0.0000	0.0018	2.0330	0.0156	17.2532	0.0086	13.8985	-0.0039	-4.3631
Monocytes	Mo.Ly6C+MHCII- (BL)		0.0264	35.7135	0.0025	38.6032	0.0180	47.1775	0.0746	27.3286	0.1527	33.6662	0.0324	0.6616
	Mo.Ly6C+MHCII- (BM)		0.0095	21.2408	0.0000	20.1222	0.0004	35.5315	0.0314	46.5782	0.1389	41.7320	0.0062	0.0000
	Mo.Ly6C+MHCII- (LN)		0.0082	27.0304	0.0001	11.3739	0.0000	38.1108	0.0076	22.7179	0.0523	24.3120	0.0144	0.0000
	Mo.Ly6C+MHCII+ (BL)		0.0335	31.9864	0.0068	32.3500	0.0381	32.6402	0.0666	27.5800	0.1485	37.2286	0.0338	5.8823
	Mo.Ly6C-MHCII- (BL)		0.0425	37.6342	0.0549	4.5259	0.0524	23.3260	0.0198	55.3052	0.0436	55.6668	0.0001	41.3637
	Mo.Ly6C-MHCII- (BM)		0.0250	11.0132	0.0271	0.0000	0.0525	1.1722	0.0538	24.3032	0.0975	38.8163	0.0000	7.5058
	Mo.Ly6C-MHCII+ (BL)		0.0249	9.9580	0.0116	0.4918	0.0395	0.0000	0.0215	7.5134	0.0344	26.1486	0.0000	17.2491
	Mo.Ly6C-MHCIIint (BL)		0.0442	35.6443	0.0483	9.3747	0.0350	40.2386	0.0272	41.3128	0.0634	42.8773	0.0047	33.6951
Macrophages	MF.103-11b+24- (Lu)		0.0000	0.0000	0.0000	0.0000	0.0003	0.8654	0.0006	1.3507	0.0099	10.3721	0.0380	36.6652
	MF.103-11b+, Salm-3d (SI)		0.0109	23.0754	0.0092	28.9676	0.0110	39.8084	0.0001	1.4688	0.0086	13.4167	-0.0001	-0.6899
	MF.11cloSer (SI)		0.0000	25.7062	0.0000	15.4772	0.0001	26.9768	0.0000	0.7061	0.0048	7.0890	-0.0013	-0.4926
	MF.169+11chi (SLN)		0.0514	31.9757	0.0106	9.2060	0.0000	0.4922	0.0000	0.0000	0.0000	0.0000	0.0098	11.3840
	MF.Il+480lo (PC)		0.0007	0.0000	0.0000	0.0000	0.0000	1.0002	0.0000	16.1027	0.0060	30.0277	0.0001	0.5420
	MF.Il-480hi (PC)		0.0000	2.0300	0.0000	0.0000	0.0003	0.0000	0.0154	0.0000	0.0525	6.5285	0.0005	0.4909
	MF.Medl (SLN)		0.0918	65.1710	0.1057	51.9452	0.0295	33.5255	0.0000	0.0000	0.0001	0.4921	0.0000	0.0000
	MF.Sbcaps (SLN)		0.0687	32.1220	0.0731	28.9826	0.0024	3.0446	0.0000	0.0000	-0.0001	-0.4927	0.0000	0.0000
	MF.Il+480int, Thio-5d (PC)		0.0054	13.3808	0.0000	0.7855	0.0012	0.4927	0.0369	37.6863	0.0378	46.9663	0.0264	28.0575
	MF.Il+480lo, Thio-5d (PC)		0.0037	0.4923	0.0000	0.0000	0.0009	0.0000	0.0340	17.3301	0.0453	39.5304	0.0082	23.3651
	MF.MHCII-F4/80hi, Thio-5d (PC)		0.0075	9.0936	0.0001	0.0000	0.0000	2.3734	0.0252	38.3964	0.0484	32.3173	0.0117	34.2763
	MF.MHCII-F4/80int, Thio-5d (PC)		0.0000	6.9581	0.0000	0.4925	0.0000	2.8107	0.0122	41.8750	0.0527	42.2940	0.0133	18.4096
Dendritic cells	MF.103-11b+, Salm-3d (SI)		0.0300	0.0000	0.0208	0.0000	0.0162	8.3019	0.0000	0.0000	0.0391	0.0000	0.0000	3.4974
	cDC.CD103+CD11b- (SI)		0.0103	0.0000	0.0218	0.0000	0.0360	10.2320	0.0226	0.0000	0.0086	0.0000	0.0468	1.0283
	cDC.CD103-CD11b+ (Lv)		0.0061	27.4995	0.0000	18.7517	0.0000	18.7334	0.0010	0.4914	0.0640	30.3954	0.0168	0.0000
	cDC.CD103-CD11b+, PolyIC (Lu)		-0.0342	18.9054	-0.0387	24.4017	-0.0430	41.1338	-0.0015	28.0587	-0.0003	10.1597	0.0000	33.2813
	cDC.CD103-CD11b+CD24+ (Lu)		0.0000	0.0000	0.0000	0.0000	0.0056	0.0000	0.0000	0.4913	0.0000	0.0000	0.0020	24.9531
	cDC.CD103-CD11b+F4/80lo (Kd)		0.0000	9.2358	0.0000	0.7492	0.0108	0.0000	0.0000	1.7727	0.0000	31.7589	0.0006	19.7206
	DC.4+ (SLN)		0.0000	0.4921	0.0000	0.0000	0.0000	0.0000	0.0000	0.0000	0.0000	0.0000	0.0272	28.9079
	DC.8-4-11b+ (Sp)		-0.0203	0.0000	-0.0266	0.0000	-0.0240	-2.7615	-0.0419	0.0000	-0.0229	0.0000	-0.0030	28.7535
	pDC.CD8- (Sp)		0.0139	25.0209	0.0268	22.6713	0.0039	5.1954	0.0000	0.0000	0.0000	0.0000	0.0241	35.0888
	pDC.CD8+ (MLN)		0.0110	14.5979	0.0042	5.7001	0.0000	0.0000	0.0000	0.0000	0.0000	0.0000	0.0307	28.0286
	pDC.CD8+ (SLN)		0.0284	30.7158	0.0409	30.0228	0.0040	5.0944	0.0000	0.0000	0.0000	0.0000	0.0295	31.3990
	pDC.CD8+ (Sp)		0.0133	22.8002	0.0090	9.3840	0.0002	1.0638	0.0000	0.0000	0.0000	0.0000	0.0202	26.9690
NKT cells	NKT.CD4- (Lv)		0.0001	0.4972	0.0269	17.5595	0.0699	35.6404	0.1101	48.0255	0.0696	43.7266	0.0101	14.7894
	NKT.CD4- (Sp)		0.0005	0.8038	0.0157	8.7419	0.0358	19.6878	0.0663	30.7936	0.0422	28.9262	0.0113	14.3346
	NKT.CD4+ (Lv)		0.0000	0.0000	0.0122	8.3542	0.0449	25.3433	0.0531	27.7382	0.0169	14.0009	0.0141	23.5862
NK cells	NK.49CI- (Sp)		0.0046	9.4702	0.0066	18.2656	0.0000	5.4509	0.0000	0.0000	0.0000	0.0000	-0.0007	-2.2312
	NK.DAP10- (Sp)		0.0030	4.5177	0.0120	10.0719	0.0020	3.0298	0.0000	0.0000	0.0000	0.0000	-0.0075	-15.5214
	NK.H+, MCMV-1d (Sp)		0.0560	33.5541	0.1153	46.6853	0.0940	42.5631	0.0224	31.0806	0.0375	40.6278	0.0000	0.0000
	NK.H+, MCMV-7d (Sp)		0.0095	13.6147	0.0355	25.9037	0.0181	14.4191	0.0000	0.0000	0.0018	3.5669	-0.0090	-21.4115
	NK, MCMV-1d (Sp)		0.0641	40.9716	0.1182	48.6276	0.0894	39.6875	0.0050	7.3946	0.0136	16.6208	0.0000	0.0000
	NK, MCMV-7d (Sp)		0.0059	9.2887	0.0257	20.2262	0.0106	9.1497	0.0000	0.0000	0.0000	0.0000	-0.0093	-19.5736
B cells	B1A (PC)		0.0317	28.4979	0.0414	18.3525	0.0234	19.0259	0.0000	0.0000	0.0000	0.0000	0.0000	0.0000
	B1B (PC)		0.0249	22.4180	0.0083	4.3655	0.0003	0.8814	0.0000	0.0000	0.0000	0.0000	0.0000	0.0000
αβ T cells	preT.DN3A (Th)		-0.0009	-2.8351	0.0000	-0.4921	0.0002	0.7881	0.0204	24.9897	0.0000	0.0000	0.0000	0.0000
	T.CD4+FP3+CD25+ (AA)		0.0000	0.0000	0.0000	0.0000	0.0017	2.7787	0.0000	0.0000	0.0000	0.0000	0.0000	0.0000
	T.CD4+FP3+CD25+ (LN)		0.0000	0.0000	0.0000	0.0000	0.0000	0.0000	0.0000	0.0000	0.0000	0.0000	0.0000	0.0000
	T.CD4+FP3+CD25+ (Sp)		0.0000	0.0000	0.0000	0.0000	0.0000	0.0000	0.0000	0.0000	0.0000	-0.4923	0.0000	0.4923
	T.CD4+MEM (Sp)		0.0000	0.0000	0.0000	0.0000	0.0000	0.0000	0.0000	0.0000	0.0000	0.0000	0.0012	4.5141
Tcell activation	T.CD8+EFF, OT-I & LIS-12h (Sp)		0.0272	21.3925	0.0662	24.1383	0.0947	32.3110	0.0602	23.1514	0.0040	2.9038	0.0089	18.0820
	T.CD8+EFF, OT-I & LIS-24h (Sp)		0.0350	28.6116	0.0803	31.3956	0.1141	39.8081	0.0810	33.9431	0.0134	10.2383	0.0082	15.1040
	T.CD8+EFF, OT-I & LIS-48h (Sp)		0.0371	30.7387	0.0755	29.9779	0.1309	41.9556	0.1700	51.0473	0.0755	36.2991	0.0234	34.6254
	T.CD8+EFF, OT-I & VSV-15d (Sp)		0.0000	0.0000	0.0000	0.0000	0.0000	0.0000	0.0095	24.7271	0.0025	4.2937	0.0000	3.2795
	T.CD8+EFF, OT-I & VSV-5d (Sp)		0.0000	0.0000	0.0000	0.0000	0.0009	1.4548	0.1446	44.5341	0.1167	43.2165	0.0000	0.0000
	T.CD8+EFF, OT-I & LIS-6d (Sp)		0.0000	0.0000	0.0000	0.0000	0.0112	4.7763	0.1550	40.9593	0.1451	40.8648	0.0000	0.0000
	T.CD8+EFF, OT-I & VSV-6d (Sp)		0.0000	0.0000	0.0000	0.0000	0.0000	0.0000	0.1379	42.3737	0.1077	37.6299	0.0000	0.0000
	T.CD8+EFF, OT-I & LIS-8d (Sp)		-0.0008	-1.8266	0.0000	0.0000	0.0000	0.0000	0.0527	24.6318	0.0568	27.1651	0.0000	0.0000
	T.CD8+EFF, OT-I & VSV-8d (Sp)		-0.0047	-4.8510	-0.0003	-0.7969	0.0000	0.0000	0.0742	29.4941	0.0580	25.1407	0.0000	0.0000
	T.CD8+MEM, OT-I & LIS-100d (Sp)		0.0000	0.0000	0.0000	0.0000	0.0000	0.0000	0.0311	21.1267	0.0138	11.5253	0.0040	9.8554
γδ T cells	Tgd.vg2+24alo (Th)		0.0000	0.0000	0.0000	0.0000	0.0002	0.8499	0.0036	3.6453	0.0000	0.0000	0.0000	0.0000
	Tgd.vg5-.act.IEL (SI)		0.0000	0.0000	0.0000	0.0000	0.0000	0.0000	0.0077	11.4235	0.0044	4.4770	0.0000	0.0000
	Tgd.vg5+.act.IEL (SI)		0.0000	0.0000	0.0000	0.0000	0.0000	0.0000	0.0088	11.9751	0.0177	21.9685	0.0000	0.0000
	Tgd.vg5+.IEL (SI)		0.0000	0.0000	0.0000	0.0000	0.0000	0.0000	0.0253	36.9737	0.0179	23.8012	0.0000	0.0000

Cell type	Short Name	Kinetics	day 3		day 5		day 6		day 7		day 9		day 31	
			Prediction	P value	Prediction	P value	Prediction	P value	Prediction	P value	Prediction	P value	Prediction	P value
Macrophages	MF.Siglec-5+ (Lu)		-0.0001	-0.4920	-0.0024	-2.2441	-0.0117	-14.8414	0.0000	0.0000	0.0000	0.0000	-0.0202	-25.9726
	cDC.CD103+CD11b- (Lu)		0.0000	-34.6841	0.0000	-26.4384	0.0086	-31.8349	0.0000	-3.5783	0.0000	-0.8818	-0.0390	0.0000
	cDC.CD103-CD11b+ (LuLN)		0.0000	0.0000	0.0000	0.0000	0.0000	8.7649	0.0000	0.0000	0.0000	0.0000	0.0345	-28.3181
	DC.4+ (MLN)		0.0000	0.0000	-0.0084	-4.9864	-0.0098	-7.0429	-0.0457	-29.4350	-0.0052	-5.2924	0.0000	0.0000
	DC.8+ (MLN)		-0.0047	-1.5499	-0.0014	-1.7470	0.0000	0.0000	-0.0307	-22.3148	-0.0531	-18.9600	-0.0188	0.0000
	DC.8+ (SLN)		-0.0369	-0.4926	-0.0463	-1.5448	-0.0004	-3.2932	-0.0448	-20.4461	-0.0447	-4.3911	-0.0527	0.0000
	DC.8+ (Sp)		0.0000	-16.5330	0.0000	-26.3596	-0.0014	-31.6692	0.0000	-47.6563	0.0000	-30.7410	0.0319	-7.4763
Dendritic cells	DC.8+ (Th)		-0.0010	-19.8103	-0.0015	-19.0449	0.0000	-23.5274	-0.0286	-35.7104	-0.0216	-24.0294	0.0000	-5.3398
	DC.8-4-11b- (MLN)		0.0000	-4.8694	-0.0005	-1.3131	-0.0031	0.0000	-0.0199	-29.2032	-0.0035	-38.0881	0.0000	-16.4539
	DC.8-4-11b+ (MLN)		-0.0198	-30.7456	-0.0604	-27.3060	-0.0576	-0.5960	-0.0916	-40.5973	-0.0614	-41.4285	-0.0065	-39.0646
	cDC.IIhilang+103+11blo (SLN)		-0.0002	0.0000	0.0000	0.0000	0.0000	0.0000	0.0000	-25.9499	-0.0066	-23.9693	-0.0018	0.0000
	cDC.IIhilang-103-11b+ (SLN)		0.0000	-0.5236	0.0000	0.0000	0.0000	0.0000	-0.0430	0.0000	-0.0706	-7.7363	0.0000	-2.9534
	cDC.IIhilang-103-11blo (SLN)		0.0000	-0.7925	0.0000	-0.4916	0.0000	0.0000	-0.0340	-34.7994	-0.0409	-40.4091	0.0000	-0.4916
	DC.LC (Sk)		-0.0094	-25.0312	-0.0038	-6.1795	-0.0159	-35.9691	-0.0002	-1.2297	0.0000	0.0000	0.0000	0.0000
NK cells	NK.49H+ (Sp)		0.0009	1.6497	0.0140	8.8567	0.0074	5.5351	0.0000	0.0000	0.0000	0.0000	-0.0217	-31.1745
	NK.DAP12- (Sp)		0.0001	0.7581	0.0024	2.7910	0.0001	0.5376	0.0000	0.0000	0.0000	0.0000	-0.0177	-34.3357
NKT cells	NKT.CD44-NK1.1- (Th)		-0.0144	-16.3338	-0.0180	-13.1654	-0.0312	-25.6054	0.0000	0.0000	-0.0002	-0.4909	0.0000	0.0000
	B.FO (LN)		0.0000	0.7890	0.0000	0.0000	-0.0002	-0.6316	-0.0414	-24.9347	-0.0346	-24.7419	-0.0004	-0.9664
	B.FO (MLN)		0.0000	0.0000	0.0000	0.0000	-0.0017	-1.7771	-0.0552	-26.7018	-0.0473	-29.1038	-0.0006	-1.9036
	B.FO (PC)		0.0045	6.1468	0.0000	0.0000	-0.0212	-28.3147	-0.0819	-41.3166	-0.0621	-36.8519	0.0000	0.0000
	B.FO (Sp)		0.0002	0.8779	0.0000	0.0000	-0.0057	-9.4430	-0.0628	-38.9385	-0.0395	-29.7178	-0.0001	-0.4937
	B.FRE (BM)		-0.0256	-27.1802	-0.0430	-30.0802	-0.0342	-27.2762	-0.0686	-33.3624	-0.1021	-45.0809	-0.0494	-34.7708
	B.FRE (FL)		-0.0086	-7.6650	-0.0304	-16.6331	-0.0552	-31.8777	-0.1084	-40.7649	-0.1043	-39.8439	-0.0120	-9.5186
	B.FRF (BM)		0.0000	0.0000	0.0000	0.0000	-0.0192	-22.9189	-0.0696	-32.1114	-0.0594	-31.9354	-0.0009	-2.0870
	B.GC (Sp)		0.0000	0.4928	0.0000	0.0000	-0.0219	-34.9410	-0.0347	-31.8427	-0.0138	-15.5515	0.0022	3.4207
	B.MZ (Sp)		0.0000	0.0000	-0.0016	-2.3025	-0.0313	-40.4296	-0.0620	-40.0349	-0.0711	-44.0276	-0.0537	-39.6092
B cells	B.T1 (Sp)		0.0000	0.0000	-0.0004	-1.1615	-0.0385	-39.9598	-0.0814	-36.0994	-0.0787	-35.8803	-0.0159	-15.2891
	B.T2 (Sp)		0.0000	0.0000	0.0000	0.0000	-0.0255	-36.0615	-0.0739	-40.2096	-0.0606	-37.2236	-0.0058	-6.9322
	B.T3 (Sp)	**DOWN**	0.0000	0.0000	0.0000	0.0000	-0.0176	-29.2793	-0.0585	-37.1725	-0.0327	-25.6258	-0.0001	-0.9595
	preB.FRC (BM)		-0.0368	-32.8685	-0.0618	-34.5061	-0.0565	-36.4742	-0.0293	-30.3766	-0.0478	-35.9683	-0.0012	-1.7054
	preB.FRD (BM)		-0.0515	-31.3355	-0.0643	-32.9359	-0.0089	-6.5252	-0.0074	-5.9608	-0.0382	-22.6098	-0.0297	-32.0715
	preB.FRD (FL)		-0.0518	-32.3835	-0.0777	-30.6929	-0.0696	-32.9972	-0.0601	-41.0601	-0.0709	-39.1464	-0.0170	-23.2145
	PROB.CLP (FL)		-0.0143	-20.6354	-0.0380	-26.2779	-0.0370	-26.9767	0.0000	-0.4921	0.0000	0.0000	0.0000	0.0000
	PROB.FRA (FL)		-0.0080	-13.5359	-0.0196	-18.4414	-0.0307	-28.0671	-0.0029	-4.7684	0.0000	0.0000	0.0000	0.0000
	PROB.FRBC (BM)		-0.0657	-41.6595	-0.0926	-39.8697	-0.0537	-29.4373	-0.0440	-31.2596	-0.0763	-39.8156	-0.0324	-36.7958
	PROB.FRBC (FL)		-0.0593	-30.9748	-0.1046	-36.0063	-0.1133	-42.0799	-0.0670	-34.9796	-0.0718	-30.3420	-0.0097	-7.9958
	preT.DN2A(Th)		-0.0121	-19.4261	-0.0003	-1.2022	0.0000	0.0000	0.0000	0.0000	0.0000	0.0000	-0.0290	-34.1735
	preT.ETP-DN2A(Th)		-0.0217	-26.6013	-0.0048	-5.0051	0.0000	0.0000	0.0000	0.0000	0.0000	0.0000	-0.0306	-27.8953
	T.CD4+Cd8int (Th)		-0.0016	-2.9846	-0.0256	-17.2509	-0.0686	-33.6010	-0.0321	-22.1283	-0.0304	-28.3192	0.0000	0.0000
	T.CD4int8+ (Th)		-0.0148	-16.1835	-0.0486	-23.6658	-0.0449	-21.1756	0.0000	0.0000	0.0000	0.0000	0.0000	0.0000
	T.CD4+NVE (MLN)		0.0000	0.0000	0.0000	0.0000	-0.0219	-18.0533	-0.0033	-3.5932	-0.0123	-10.0160	0.0000	0.0000
	T.CD4+NVE (PP)		0.0000	0.0000	-0.0012	-0.8852	-0.0587	-28.0651	-0.0379	-22.6299	-0.0477	-26.0045	0.0000	0.0000
	T.CD4+NVE (Sp)		0.0000	0.0000	0.0000	0.0000	-0.0089	-9.1805	-0.0103	-11.8326	-0.0308	-27.5373	0.0000	0.0000
αβ T cells	T.CD4SpCD24- (Th)		-0.0001	-0.9406	-0.0055	-5.1839	-0.0276	-23.5317	-0.0022	-3.3095	-0.0274	-29.2058	0.0000	0.0000
	T.CD4SpCD24int (Th)		-0.0209	-30.7738	-0.0603	-38.5058	-0.0944	-50.4648	-0.0544	-41.1507	-0.0423	-41.5975	0.0000	0.0000
	T.CD4SpCD69+ (Th)		-0.0255	-38.0255	-0.0643	-46.1452	-0.1022	-58.8654	-0.0598	-45.5970	-0.0471	-42.0061	0.0000	0.0000
	T.CD8+NVE (PP)		0.0000	0.0000	0.0000	0.0000	-0.0004	-1.5371	0.0000	0.0000	0.0000	0.0000	0.0000	0.0000
	T.CD8SpCD24int (Th)		-0.0295	-35.2934	-0.0742	-41.4465	-0.0640	-38.5909	0.0000	0.0000	0.0000	0.0000	0.0000	0.0000
	T.CD8SpCD69+ (Th)		-0.0242	-22.9651	-0.0605	-28.0062	-0.0388	-20.6506	0.0000	0.0000	0.0000	0.0000	0.0000	0.0000
	T.DP (Th)		-0.0056	-11.1300	-0.0537	-29.7029	-0.0708	-30.0987	-0.0013	-3.1090	0.0000	0.0000	0.0000	0.0000
	T.DPBl (Th)		0.0000	0.0000	-0.0322	-21.7033	-0.0568	-30.5897	0.0000	0.0000	0.0000	0.0000	0.0041	8.0209
	T.DPsm (Th)		-0.0076	-13.6121	-0.0428	-27.8072	-0.0568	-30.0431	-0.0012	-3.2538	0.0000	0.0000	0.0000	0.0000
	Tgd (Th)		-0.0132	-20.4374	-0.0238	-21.9564	0.0000	0.0000	0.0000	0.0000	0.0000	0.0000	0.0000	0.0000
γδ T cells	Tgd.vg1+vd6-24ahi (Th)		-0.0438	-38.2888	-0.0759	-40.1933	-0.0472	-31.9886	0.0000	0.0000	0.0000	0.0000	-0.0011	-1.7499
	Tgd.vg2- (Sp)		-0.0238	-24.3018	-0.0556	-29.7063	-0.0626	-39.8752	0.0000	0.0000	-0.0212	-12.3212	-0.0003	-1.0472
	Tgd.vg2+ (Sp)		-0.0276	-27.0656	-0.0534	-30.1933	-0.0695	-44.1288	0.0000	0.0000	-0.0045	-2.6330	-0.0031	-2.8184
	Tgd.vg2+24ahi (Th)		-0.0470	-53.1498	-0.0716	-47.6360	-0.0098	-9.6710	0.0000	0.0000	0.0000	0.0000	-0.0004	-1.4176

Supplementary Table S2. DCQ's predictions of dynamically changing cell types during the course of chronic LCMV infection. Shown are predicted cell quantities and the –log10 t-test p-value results, only for those cell types (rows) that are significantly changing based on our robustness evaluation of the DCQ's predictions (see methods). Column 3 indicates whether the cell type is predicted to increase or decrease during infection.

Cell type	Short Name	Kinetics	day 3		day 5		day 6		day 7		day 9		day 31	
			Prediction	P value	Prediction	P value	Prediction	P value	Prediction	P value	Prediction	P value	Prediction	P value
Granulocytes	GN.ARTH (BM)	UP	0.0000	0.0000	0.0018	4.7589	0.0108	17.4189	0.0155	21.0867	0.0187	29.7298	0.0362	37.4644
	GN.ARTH (SynF)		0.0000	0.0000	0.0011	5.7353	0.0226	40.2761	0.0350	42.3291	0.0244	37.3368	0.0418	49.3783
	GN (BL)		0.0000	0.0000	0.0000	0.0000	0.0001	0.4928	0.0245	33.9717	0.0002	0.6350	0.0003	0.7022
	GN (BM)		0.0000	0.0000	0.0001	1.0586	0.0082	16.2146	0.0218	25.8239	0.0165	26.4427	0.0355	39.6585
	GN.Thio (PC)		0.0000	0.0000	0.0016	4.7471	0.0258	41.5530	0.0429	47.2094	0.0171	25.7017	0.0153	21.1209
	GN.UrAc (PC)		0.0000	0.0000	0.0000	0.0000	0.0000	0.0000	0.0232	26.2603	0.0000	0.0000	0.0003	1.5023
Monocytes	Mo.Ly6C+MHCII- (BL)		0.0205	37.1945	0.0554	39.9810	0.0945	43.2831	0.1072	34.4111	0.0962	29.8854	0.0613	8.5721
	Mo.Ly6C+MHCII- (BM)		0.0081	34.1673	0.0371	46.5956	0.0587	43.6081	0.1162	51.6741	0.1077	43.4152	0.0175	7.6661
	Mo.Ly6C+MHCII- (LN)		0.0018	24.1748	0.0242	16.7926	0.0209	28.4965	0.0499	11.9608	0.0330	5.8874	0.0184	0.0000
	Mo.Ly6C+MHCII+ (BL)		0.0239	34.1689	0.0618	45.7067	0.0976	40.1027	0.1001	39.6992	0.0939	39.1811	0.0530	30.4393
	Mo.Ly6C-MHCII- (BL)		0.0600	25.6285	0.0400	44.0903	0.0542	52.0798	0.0429	49.6208	0.0377	46.6159	0.0061	50.9216
	Mo.Ly6C-MHCII- (BM)		0.0579	7.4300	0.0650	26.8074	0.0669	30.1785	0.1110	44.2503	0.0869	41.1417	0.0052	14.4895
	Mo.Ly6C-MHCII+ (BL)		0.0286	2.3911	0.0161	23.0280	0.0360	15.1371	0.0157	28.6777	0.0082	19.9248	0.0000	18.8710
	Mo.Ly6C-MHCIIint (BL)		0.0527	29.3569	0.0531	42.2449	0.0596	43.4533	0.0610	38.6385	0.0653	38.2965	0.0270	39.1969
Macrophages	MF.103-11b+24- (Lu)		0.0000	0.0000	0.0000	0.0000	0.0015	2.1694	0.0015	1.8450	0.0050	4.5482	0.0070	9.3212
	MF.103-11b+, Salm-3d (SI)		0.0163	25.5568	0.0000	1.0140	0.0001	4.0655	0.0154	34.7489	0.0000	19.7495	0.0000	0.0000
	MF.11cloSer (SI)		0.0177	22.5050	0.0014	3.0991	0.0029	4.0081	0.0031	4.2519	0.0010	1.6771	0.0000	0.0000
	MF.169+11chi (SLN)		0.0048	4.4128	0.0000	0.0000	0.0000	0.0000	0.0000	0.0000	0.0024	2.0823	0.0239	21.6214
	MF.II+480lo (PC)		0.0000	0.0000	0.0000	34.0040	0.0050	28.1897	0.0016	30.8517	0.0029	37.7079	0.0266	24.5574
	MF.II-480hi (PC)		0.0000	0.0000	0.0418	0.0000	0.0365	5.4573	0.0473	2.5403	0.0956	2.7621	0.0299	25.7360
	MF.Medl (SLN)		0.1187	55.5908	0.0056	7.1507	0.0014	2.2861	0.0003	0.9843	0.0132	11.3512	0.0111	16.5999
	MF.Sbcaps (SLN)		0.0838	31.0897	0.0000	0.0000	0.0000	0.0000	0.0000	0.0000	0.0000	0.0000	0.0000	0.0000
	MF.II+480int, Thio-5d (PC)		0.0000	1.4714	0.0001	16.4581	0.0347	42.8989	0.0347	48.6711	0.0376	41.3088	0.0545	33.5158
	MF.II+480lo, Thio-5d (PC)		0.0002	0.0000	0.0018	33.7063	0.0340	33.4071	0.0432	39.4108	0.0573	43.9871	0.0209	40.4852
	MF.MHCII-F4/80hi, Thio-5d (PC)		0.0004	0.4914	0.0081	0.6767	0.0366	35.1588	0.0462	31.7780	0.0504	27.7465	0.0201	42.6606
	MF.MHCII-F4/80int, Thio-5d (PC)		0.0000	1.1639	0.0276	3.4695	0.0314	37.5575	0.0459	42.5595	0.0858	42.7123	0.0385	28.9280
Dendritic cells	MF.103-11b+, Salm-3d (SI)		0.0167	0.0000	0.0001	0.0000	0.0005	0.0000	0.0369	0.0000	0.0000	36.9457	0.0000	46.3878
	cDC.CD103+CD11b- (SI)		0.0010	0.0000	0.0000	0.0000	0.0013	0.0000	0.0236	0.8693	0.0314	32.7032	0.0551	25.4266
	cDC.CD103-CD11b+ (Lv)		0.0006	13.4394	0.0054	0.4914	0.0071	0.9206	0.0519	31.1914	0.0060	0.0000	0.0169	0.0000
	cDC.CD103-CD11b+, PolyIC (Lu)		-0.0476	2.2577	-0.0411	0.0000	-0.0134	3.9503	0.0000	28.0849	0.0000	31.4852	0.0000	38.4045
	cDC.CD103-CD11b+CD24+ (Lu)		0.0000	0.0000	0.0000	0.0000	0.0000	0.0000	0.0000	0.0000	0.0411	4.3884	0.0634	15.5642
	cDC.CD103-CD11b+F4/80lo (Kd)		0.0000	1.3027	0.0000	6.3264	0.0000	6.0203	0.0001	32.0447	0.0723	4.7704	0.0575	18.9614
	DC.4+ (SLN)		0.0000	0.0000	0.0000	0.0000	0.0000	0.0000	0.0000	0.0000	0.0000	0.0000	0.0036	3.6424
	DC.8-4-11b+ (Sp)		-0.0329	-0.4928	-0.0436	-0.4928	-0.0464	0.0000	-0.0418	0.0000	-0.0049	-0.7719	-0.0174	0.0000
	pDC.CD8- (Sp)		0.0165	15.1546	0.0000	0.4929	0.0000	0.0000	0.0000	0.0000	0.0000	0.0000	0.0041	8.0566
	pDC.CD8+ (MLN)		0.0004	1.0811	0.0000	0.0000	0.0000	0.0000	0.0000	0.0000	0.0000	0.0000	0.0027	3.7849
	pDC.CD8+ (SLN)		0.0269	21.2535	0.0006	1.6906	0.0002	1.1099	0.0001	0.7683	0.0084	12.3037	0.0190	25.0348
	pDC.CD8+ (Sp)		0.0024	3.4042	0.0000	0.0000	0.0000	0.0000	0.0000	0.0000	0.0000	0.0000	0.0001	0.5733
NK cells	NK.49CI- (Sp)		0.0149	27.0043	0.0000	5.4628	0.0000	0.0000	0.0000	0.0000	0.0000	0.0000	-0.0005	0.0000
	NK.DAP10- (Sp)		0.0242	20.4405	0.0011	2.7357	0.0000	0.0000	0.0000	0.0000	0.0000	0.0000	-0.0016	-3.6066
	NK.H+, MCMV-1d (Sp)		0.1118	48.5597	0.0537	45.0934	0.0291	37.0206	0.0343	39.0238	0.0164	23.6449	0.0000	0.0000
	NK.H+, MCMV-7d (Sp)		0.0501	35.2256	0.0174	24.7223	0.0000	0.0000	0.0004	1.3406	0.0000	0.0000	0.0000	0.0000
	NK, MCMV-1d (Sp)		0.1156	51.6251	0.0452	39.5870	0.0099	12.7756	0.0135	16.2933	0.0011	1.7213	0.0000	0.0000
	NK, MCMV-7d (Sp)		0.0400	31.1556	0.0087	12.8380	0.0000	0.0000	0.0000	0.0000	0.0000	0.0000	-0.0004	-0.8622
NKT cells	NKT.CD4- (Lv)		0.0158	11.2494	0.0658	42.6918	0.1064	46.4454	0.0766	44.7413	0.0885	44.7963	0.0385	31.0821
	NKT.CD4- (Sp)		0.0125	7.9358	0.0291	22.8102	0.0609	28.6337	0.0514	30.5298	0.0608	33.0034	0.0294	23.5701
	NKT.CD4+ (Lv)		0.0031	2.5022	0.0314	25.5642	0.0639	30.6616	0.0206	14.0451	0.0462	25.1323	0.0370	27.3690
B cells	B1A (PC)		0.0398	17.3431	0.0035	5.9789	0.0151	14.5750	0.0000	0.4909	0.0157	12.9286	0.0316	21.1550
	B1B (PC)		0.0119	6.0804	0.0000	0.0000	0.0000	0.0000	0.0000	0.0000	0.0000	0.0000	0.0004	1.0875
αβ T cells	T.CD4+FP3+CD25+ (AA)		0.0000	0.0000	0.0000	0.0000	0.0000	0.0000	0.0000	0.0000	0.0003	0.9851	0.0243	32.2372
	T.CD4+FP3+CD25+ (LN)		0.0000	0.0000	0.0000	0.0000	0.0000	0.0000	0.0000	0.0000	0.0000	0.0000	0.0223	26.2121
	T.CD4+FP3+CD25+ (Sp)		0.0000	0.0000	0.0000	0.0000	0.0000	0.0000	0.0000	0.0000	0.0000	0.0000	0.0272	36.0603
	T.CD4+MEM (Sp)		0.0000	0.0000	0.0000	0.0000	0.0000	0.0000	0.0000	0.0000	0.0000	0.0000	0.0251	24.8943
	preT.DN3A (Th)		0.0000	0.0000	0.0013	2.4727	0.0007	1.7959	0.0000	0.0000	0.0000	0.0000	-0.0001	-0.4921
T cell activation	T.CD8+EFF, OT-I & LIS-12h (Sp)		0.0425	19.5225	0.0449	24.0214	0.0510	21.3578	0.0066	5.6579	0.0314	19.1082	0.0115	12.6217
	T.CD8+EFF, OT-I & LIS-24h (Sp)		0.0553	27.4301	0.0618	34.0931	0.0716	31.7867	0.0184	15.1186	0.0482	28.9570	0.0082	9.6767
	T.CD8+EFF, OT-I & LIS-48h (Sp)		0.0596	28.2813	0.1171	49.5432	0.1520	50.2596	0.0747	38.9118	0.1226	54.1085	0.0210	22.3604
	T.CD8+EFF, OT-I & VSV-15d (Sp)		0.0000	0.0000	0.0011	1.4631	0.0198	12.1995	0.0034	2.4711	0.0004	1.0515	0.0000	0.0000
	T.CD8+EFF, OT-I & VSV-5d (Sp)		0.0000	0.0000	0.0849	44.1327	0.1288	46.4932	0.0945	42.5357	0.0314	24.3164	0.0000	0.0000
	T.CD8+EFF, OT-I & LIS-6d (Sp)		0.0000	0.0000	0.0832	35.2950	0.1198	36.9410	0.1213	42.0509	0.0406	24.4671	0.0000	0.0000
	T.CD8+EFF, OT-I & VSV-6d (Sp)		0.0000	0.0000	0.0460	29.6906	0.1023	37.7486	0.0848	35.2730	0.0142	10.7335	0.0000	0.0000
	T.CD8+EFF, OT-I & LIS-8d (Sp)		0.0000	0.0000	0.0184	14.4684	0.0274	15.7099	0.0209	12.3440	0.0000	0.0000	0.0000	0.0000
	T.CD8+EFF, OT-I & VSV-8d (Sp)		0.0000	0.0000	0.0149	13.0084	0.0461	23.2270	0.0299	16.1087	0.0000	0.0000	0.0000	0.0000
	T.CD8+MEM, OT-I & LIS-100d (Sp)		0.0000	0.0000	0.0100	9.6418	0.0293	19.8527	0.0029	2.8624	0.0006	1.0978	0.0000	0.0000
γδ T cells	Tgd.vg2+24alo (Th)		0.0000	0.0000	0.0000	0.0000	0.0000	0.0000	0.0001	0.4904	0.0386	19.3357	0.0711	31.4650
	Tgd.vg5-.act.IEL (SI)		-0.0002	-0.4918	0.0000	0.0000	0.0032	5.0505	0.0045	5.8279	0.0000	0.0000	0.0178	31.5537
	Tgd.vg5+.act.IEL (SI)		0.0000	0.0000	0.0000	0.0000	0.0056	8.8017	0.0146	18.0325	0.0000	0.0000	0.0050	8.1525
	Tgd.vg5+.IEL (SI)		0.0000	0.0000	0.0000	0.0000	0.0144	24.4286	0.0261	33.9039	0.0005	1.2799	0.0015	3.0956

Cell type	Short Name	Kinetics	day 3		day 5		day 6		day 7		day 9		day 31	
			Prediction	P value	Prediction	P value	Prediction	P value	Prediction	P value	Prediction	P value	Prediction	P value
Macrophages	MF.Siglec-5+ (Lu)		-0.0001	-0.4920	0.0000	0.0000	0.0000	0.0000	0.0000	0.0000	0.0000	0.0000	0.0000	0.0000
Dendritic cells	cDC.CD103+CD11b- (Lu)		0.0000	-33.2204	0.0000	-42.0189	0.0000	-19.9106	0.0000	0.0000	-0.0002	0.0000	-0.0340	0.0000
	cDC.CD103-CD11b+ (LuLN)		0.0000	0.0000	0.0000	0.0000	0.0000	0.0000	0.0000	0.0000	0.0047	-0.7347	0.0199	-21.7700
	DC.4+ (MLN)		-0.0163	-11.0276	-0.0521	-36.2175	-0.0335	-19.4546	-0.0517	-30.2343	-0.0551	-25.2079	-0.0041	-3.0963
	DC.8+ (MLN)		-0.0071	-24.2617	-0.0201	-19.8190	-0.0422	-24.1313	-0.0676	-26.6580	-0.0708	-6.8643	-0.0347	0.0000
	DC.8+ (SLN)		-0.0542	-17.7242	-0.0319	-16.7636	-0.0604	-12.2089	-0.0645	-22.7267	-0.1114	0.0000	-0.1084	0.0000
	DC.8+ (Sp)		-0.0001	-33.8731	-0.0001	-38.5890	0.0000	-46.8392	0.0000	-38.3733	-0.0001	-38.2931	0.0000	-30.3190
	DC.8+ (Th)		-0.0357	-23.3084	-0.0224	-40.6291	-0.0386	-36.9581	-0.0399	-33.9500	-0.0113	-6.1168	0.0000	-16.1492
	DC.8-4-11b- (MLN)		-0.0234	-5.4662	-0.0169	-25.3445	-0.0145	-29.6575	-0.0241	-39.2273	0.0000	-28.9842	0.0000	-19.4221
	DC.8-4-11b+ (MLN)		-0.0831	-31.3060	-0.0623	-35.9198	-0.1044	-43.6757	-0.0743	-44.0317	-0.0919	-49.7294	-0.0583	-49.9844
	cDC.IIhilang+103+11blo (SLN)		-0.0005	-0.5675	0.0000	-14.1716	-0.0017	-17.9650	-0.0232	-21.5901	-0.0364	-3.2569	-0.0144	0.0000
	cDC.IIhilang-103-11b+ (SLN)		-0.0008	-0.4914	-0.0248	-0.4914	-0.0549	-1.7537	-0.0758	-18.7111	-0.0739	-20.9850	-0.0109	-9.8452
	cDC.IIhilang-103-11blo (SLN)		-0.0003	-1.9039	-0.0132	-29.5531	-0.0243	-37.6455	-0.0372	-43.5022	-0.0046	-36.2095	0.0000	-9.3965
	DC.LC (Sk)		-0.0020	-4.6073	-0.0187	-40.2558	-0.0005	-1.9113	0.0000	0.0000	0.0000	0.0000	-0.0019	-5.2887
NK cells	NK.49H+ (Sp)		0.0234	15.5045	0.0070	8.4141	0.0000	0.0000	0.0000	0.0000	0.0000	0.0000	-0.0058	-7.1071
	NK.DAP12- (Sp)		0.0081	7.6730	0.0001	0.4930	0.0000	0.0000	0.0000	0.0000	0.0000	0.0000	-0.0050	-8.3952
NKT cells	NKT.CD44-NK1.1- (Th)		-0.0047	-4.0214	-0.0177	-23.0738	0.0000	0.0000	-0.0001	-0.4909	0.0000	0.0000	0.0000	0.0000
B cells	B.FO (LN)		0.0000	0.0000	-0.0037	-7.7208	-0.0232	-20.7147	-0.0313	-22.8090	-0.0288	-17.9405	-0.0001	-0.4916
	B.FO (MLN)		0.0000	0.0000	-0.0058	-10.7497	-0.0345	-24.2304	-0.0461	-28.6835	-0.0444	-24.3588	-0.0003	-0.7361
	B.FO (PC)		0.0000	0.0000	-0.0272	-38.9267	-0.0577	-40.2313	-0.0487	-30.9231	-0.0282	-16.9611	-0.0001	-0.5530
	B.FO (Sp)		0.0000	0.0000	-0.0120	-25.9103	-0.0357	-32.1927	-0.0406	-31.0325	-0.0357	-24.7465	0.0000	-0.4921
	B.FRE (BM)		-0.0217	-19.1983	-0.0445	-33.5026	-0.0754	-39.5760	-0.0973	-43.4569	-0.1311	-45.0332	-0.0938	-44.0732
	B.FRE (FL)		-0.0098	-6.8050	-0.0557	-34.5363	-0.0783	-35.5979	-0.1057	-39.8358	-0.1222	-36.8080	-0.0549	-26.7370
	B.FRF (BM)		0.0000	0.0000	-0.0181	-30.0656	-0.0503	-32.8181	-0.0536	-30.5710	-0.0522	-26.4957	-0.0015	-2.5795
	B.GC (Sp)		0.0000	0.0000	-0.0007	-1.7066	-0.0014	-2.1435	-0.0312	-33.7959	0.0000	-0.4928	0.0225	21.3739
	B.MZ (Sp)		0.0000	0.0000	-0.0118	-22.4497	-0.0528	-42.2232	-0.0634	-43.2480	-0.0821	-45.7416	-0.0711	-43.0306
	B.T1 (Sp)		0.0000	0.0000	-0.0277	-34.4108	-0.0617	-35.9348	-0.0741	-36.7681	-0.0923	-37.6060	-0.0363	-24.1628
	B.T2 (Sp)		0.0000	0.0000	-0.0216	-36.8107	-0.0497	-38.6071	-0.0574	-37.0874	-0.0728	-39.1778	-0.0133	-11.1083
	B.T3 (Sp)	**DOWN**	0.0000	0.0000	-0.0038	-9.2358	-0.0290	-27.2678	-0.0304	-24.8488	-0.0216	-14.4811	-0.0010	-2.0033
	preB.FRC (BM)		-0.0508	-32.7238	-0.0508	-31.7650	-0.0511	-37.4503	-0.0448	-36.0935	-0.0580	-31.3590	-0.0003	-0.7499
	preB.FRD (BM)		-0.0549	-28.6062	-0.0382	-22.8439	-0.0390	-23.1687	-0.0272	-18.3639	-0.0490	-23.7325	-0.0471	-31.6077
	preB.FRD (FL)		-0.0766	-33.1178	-0.0766	-38.4785	-0.0738	-39.5690	-0.0709	-43.0886	-0.1169	-49.7696	-0.0304	-27.0845
	PROB.CLP (FL)		-0.0301	-23.7196	-0.0266	-22.4479	-0.0001	-0.7961	0.0000	0.0000	0.0000	0.0000	-0.0004	-0.9587
	PROB.FRA (FL)		-0.0205	-20.5699	-0.0323	-30.2881	-0.0004	-0.6875	0.0000	0.0000	0.0000	0.0000	-0.0006	-0.9286
	PROB.FRBC (BM)		-0.0809	-39.1761	-0.0712	-36.4463	-0.0641	-35.9341	-0.0628	-37.5587	-0.0635	-31.4780	-0.0442	-31.9047
	PROB.FRBC (FL)		-0.0904	-34.0861	-0.1038	-40.1630	-0.0804	-33.4649	-0.0610	-29.3984	-0.0175	-6.7201	-0.0015	-1.7324
αβ T cells	preT.DN2A(Th)		0.0000	0.0000	0.0000	0.0000	0.0000	0.0000	0.0000	0.0000	0.0000	0.0000	-0.0224	-27.7650
	preT.ETP-DN2A(Th)		-0.0011	-1.1985	-0.0035	-5.4002	-0.0001	-0.7593	0.0000	0.0000	-0.0049	-7.4942	-0.0200	-20.1879
	T.CD4+Cd8int (Th)		-0.0277	-23.1562	-0.0428	-36.0264	-0.0322	-24.7868	-0.0612	-40.6634	-0.0263	-25.4764	0.0000	0.0000
	T.CD4int8+ (Th)		-0.0596	-28.9805	-0.0076	-7.6098	0.0000	0.0000	0.0000	0.0000	-0.0027	-3.0406	-0.0003	-0.4904
	T.CD4+NVE (MLN)		0.0000	0.0000	-0.0183	-21.9712	-0.0038	-4.8161	-0.0130	-11.5885	-0.0029	-4.1440	0.0000	0.0000
	T.CD4+NVE (PP)		-0.0003	-0.4911	-0.0529	-36.4002	-0.0405	-26.2259	-0.0550	-30.4139	-0.0479	-28.6744	0.0000	0.0000
	T.CD4+NVE (Sp)		0.0000	0.0000	-0.0078	-12.0522	-0.0109	-13.9526	-0.0314	-30.5879	-0.0046	-7.4699	0.0000	0.0000
	T.CD4SpCD24- (Th)		-0.0004	-0.9097	-0.0133	-17.0542	-0.0077	-9.9807	-0.0300	-28.1067	-0.0241	-25.0222	0.0000	0.0000
	T.CD4SpCD24int (Th)		-0.0480	-37.2289	-0.0415	-41.8270	-0.0448	-39.2722	-0.0624	-46.8549	-0.0596	-48.0267	-0.0342	-37.1315
	T.CD4SpCD69+ (Th)		-0.0483	-45.1834	-0.0484	-48.9994	-0.0529	-46.8802	-0.0642	-45.8845	-0.0714	-56.4113	-0.0479	-43.6319
	T.CD8+NVE (PP)		-0.0049	-4.8608	-0.0296	-36.4132	0.0000	0.0000	-0.0015	-3.1650	-0.0093	-11.7055	0.0000	0.0000
	T.CD8SpCD24int (Th)		-0.0813	-44.7384	-0.0247	-26.8152	-0.0073	-9.6057	-0.0003	-0.8163	-0.0159	-18.9435	-0.0082	-8.6479
	T.CD8SpCD69+ (Th)		-0.0690	-31.6308	-0.0077	-6.9764	-0.0001	-0.5366	0.0000	0.0000	-0.0048	-4.7973	-0.0061	-5.5212
	T.DP (Th)		-0.0315	-27.7973	-0.0016	-2.0373	-0.0012	-2.1489	-0.0074	-6.6067	-0.0111	-9.6926	-0.0062	-7.5694
	T.DPBl (Th)		-0.0108	-11.4079	0.0000	0.0000	0.0000	0.0000	0.0000	0.0000	0.0000	0.0000	0.0000	0.0000
	T.DPsm (Th)		-0.0250	-22.6613	-0.0002	-0.8445	-0.0004	-1.7922	-0.0075	-7.0421	-0.0177	-18.1851	-0.0041	-5.3147
γδ T cells	Tgd (Th)		0.0000	-23.0946	0.0000	0.0000	0.0000	0.0000	0.0000	0.0000	0.0000	0.0000	-0.0004	0.0000
	Tgd.vg1+vd6-24ahi (Th)		-0.0680	-37.5383	0.0000	0.0000	0.0000	0.0000	0.0000	0.0000	-0.0002	-0.7501	-0.0003	-0.7421
	Tgd.vg2- (Sp)		-0.0578	-29.5715	-0.0370	-37.1378	-0.0090	-10.8318	-0.0248	-18.8700	-0.0626	-40.3297	-0.0183	-15.3177
	Tgd.vg2+ (Sp)		-0.0409	-26.0901	-0.0343	-37.8346	-0.0079	-8.5423	-0.0017	-1.6564	-0.0303	-27.9054	-0.0074	-7.6933
	Tgd.vg2+24ahi (Th)		-0.0737	-50.0144	-0.0007	-1.6010	0.0000	0.0000	0.0000	0.0000	-0.0112	-12.4934	-0.0504	-40.2375

Supplementary Table S3. List of DCQ-predicted cell subsets that correlates in their kinetics with the module eigengenes of acute-brown (cells with a Pearson's correlation higher than 0.5 are shown), chronic-magenta (cells with a Pearson's correlation higher than 0.5 are shown) or chronic-darkturquoise (cells with a Pearson's correlation higher than 0.3 are shown).

Acute-brown		
Cell type name	Correlation	P-Value
MF.MHCII-480int, Thio-5d (PC)	0.966783231	0.000379381
MF.MHCII-F4/80hi, Thio-5d (PC)	0.937977375	0.00177928
T.CD8+EFF, OT-I & LIS-8d (Sp)	0.937830579	0.001789683
MF.MHCII+480int, Thio-5d (PC)	0.931023531	0.002311887
T.CD8+EFF, OT-I & LIS-6d (Sp)	0.928552963	0.002521075
Mo.Ly6C-MHCII- (BL)	0.926568132	0.00269689
Tgd.vg5+.act.IEL (SI)	0.914805761	0.003884765
T.CD8+EFF, OT-I & VSV-8d (Sp)	0.908634269	0.004611234
T.CD8+EFF, OT-I & VSV-5d (Sp)	0.90782203	0.004712285
T.CD8+EFF, OT-I & VSV-6d (Sp)	0.902677979	0.005382138
Mo.Ly6C-MHCIIint (BL)	0.897831569	0.006061102
Tgd.vg5+.IEL (SI)	0.886084287	0.007904626
MF.II-480hi (PC)	0.856819361	0.013772492
MF.MHCII+480lo, Thio-5d (PC)	0.853635008	0.014524981
Tgd.vg5-.act.IEL (SI)	0.845892637	0.016450632
Mo.Ly6C-MHCII- (BM)	0.819508242	0.02405794
T.CD8+MEM, OT-I & LIS-100d (Sp)	0.815285034	0.025428607
NKT.CD4- (Sp)	0.813368066	0.026064908
Mo.Ly6C+MHCII- (BM)	0.769622338	0.04302666
Mo.Ly6C-MHCII+ (BL)	0.769395845	0.043126813
GN, UrAc (PC)	0.761464004	0.046715296
GN, Thio (PC)	0.760697637	0.04707038
NKT.CD4+ (Lv)	0.756495711	0.04904354
cDC.CD103-CD11b+F4/80lo (Kd)	0.704711667	0.077031696
MF.II-480hi (PC)	0.671095607	0.098850874
GN (BL)	0.655406095	0.110015639
GN.ARTH (SynF)	0.622623933	0.135341488
T.CD8+EFF, OT-I & VSV-15d (Sp)	0.616636819	0.140256197
Tgd.vg1+vd6+24ahi (Th)	0.536723785	0.214186823
cDC.CD103+CD11b- (Lu)	0.534415066	0.216547329
T.CD8+EFF, OT-I & LIS-48h (Sp)	0.521076706	0.230423939
preT.DN3A (Th)	0.511293561	0.240858399
NKT.CD4+ (Lv)	0.510167409	0.242073322

Chronic-magenta		
Cell type name	Correlation	P-Value
Tgd.vg5+.IEL (SI)	0.870989519	0.01069846
T.CD8+EFF, OT-I & LIS-6d (Sp)	0.870016371	0.01089541
T.CD8+EFF, OT-I & VSV-6d (Sp)	0.860620028	0.012904217
Mo.Ly6C+MHCII- (BM)	0.857777602	0.013550525
T.CD8+EFF, OT-I & VSV-8d (Sp)	0.799032067	0.031105521
T.CD8+EFF, OT-I & VSV-5d (Sp)	0.79786288	0.031538694
T.CD8+EFF, OT-I & LIS-8d (Sp)	0.790498561	0.034344228
GN, Thio (PC)	0.735879493	0.059370603
GN (BL)	0.727251109	0.064012505
GN, UrAc (PC)	0.724278618	0.065655463
Mo.Ly6C+MHCII- (BL)	0.716487168	0.070068636
cDC.CD103-CD11b+ (Lv)	0.715481821	0.070649331
Mo.Ly6C+MHCII+ (BL)	0.709537634	0.074135317
Tgd.vg5+.act.IEL (SI)	0.703916796	0.077514439
Mo.Ly6C-MHCIIint (BL)	0.68365578	0.09036233
Mo.Ly6C-MHCII- (BM)	0.680411153	0.092516786
Mo.Ly6C-MHCII+ (BL)	0.665641272	0.102661637
Mo.Ly6C+MHCII- (LN)	0.656967562	0.108876624
Mo.Ly6C-MHCII- (BL)	0.651935913	0.112568974
cDC.CD103-CD11b+F4/80lo (Kd)	0.644743274	0.117957761
NKT.CD4- (Lv)	0.626309057	0.132360641
NKT.CD4- (Sp)	0.598470516	0.155709534
T.CD8+EFF, OT-I & LIS-48h (Sp)	0.575435135	0.176461962
preT.ETP-24 (Th)	0.575228346	0.176654053
MF.CD11cloSer, Salm-3d (SI)	0.567603814	0.183808075
MF.II+480int, Thio-5d (PC)	0.54794129	0.202893245
cDC.CD103-CD11b+ (LuLN)	0.521020687	0.230483073
preT.ETP-DN2A(Th)	0.519735573	0.231841593
T.CD8+EFF, OT-I & VSV-15d (Sp)	0.516048692	0.235759779

Chronic-darkturquoise		
Cell type name	Correlation	P-Value
T.CD8+EFF, OT-I & LIS-12h (Sp)	0.84830022	0.015837164
T.CD8+EFF, OT-I & LIS-24h (Sp)	0.78726087	0.035619939
T.CD8+EFF, OT-I & LIS-48h (Sp)	0.60294946	0.151824222
preT.DN3A (Th)	0.59328221	0.160271408
Mo.Ly6C+MHCII+ (BL)	0.4954048	0.258260167
Mo.Ly6C+MHCII- (BL)	0.45896418	0.300240276
NKT.CD4+ (Lv)	0.44641834	0.31533931
B.GC (Sp)	0.43138034	0.333859018
NK, H+.MCMV-1d (Sp)	0.41514504	0.354356011
NK, H+.MCMV-7d (Sp)	0.41012101	0.360802277
B1A (PC)	0.40542733	0.366868134
NK, MCMV-1d (Sp)	0.39506045	0.380412498
T.CD4+NVE (Sp)	0.39446956	0.38119052
NK.49H+ (Sp)	0.36496012	0.420848909
Mo.Ly6C-MHCII+ (BL)	0.35985309	0.42786817
NK, MCMV-7d (Sp)	0.3469985	0.445732119
NKT.CD4+ (Lv)	0.32212676	0.481065996
MF.II+480lo (PC)	0.31402714	0.492783199

Supplementary Table S4. List of hub genes from acute-brown module that overlap with genes that are upregulated in CD8^{+} T cells (A) and monocytes/macrophages (B) at day 7 post-infection versus non-infected mice. For each gene the adjusted P-value (false discovery rate) and the Log2 Fold-Change are shown.

A. Genes overlapping between acute-brown module and CD8+ T cells

EnsemblGeneID	Gene Symbol	Log Fold Change	Adjusted P-Value
ENSMUSG00000002190	*Clgn*	10.33131561	1.54827E-10
ENSMUSG00000002274	*Metrn*	1.510903517	4.52767E-05
ENSMUSG00000002778	*Kdelr1*	0.390551659	0.023751182
ENSMUSG00000002957	*Ap2a2*	0.760584482	2.89946E-05
ENSMUSG00000003644	*Rps6ka1*	0.619144998	5.79489E-12
ENSMUSG00000003948	*Mmd*	1.535157595	5.17478E-09
ENSMUSG00000004610	*Etfb*	2.431855874	1.76012E-13
ENSMUSG00000004814	*Ccl24*	4.645194458	0.01186634
ENSMUSG00000006179	*Prss16*	6.10339407	3.68675E-32
ENSMUSG00000006313	*Upk1a*	3.170132753	6.70456E-05
ENSMUSG00000006378	*Gcat*	3.948127561	1.96601E-08
ENSMUSG00000007021	*Syngr3*	9.971823141	4.07302E-08
ENSMUSG00000009092	*Derl3*	2.885476803	3.74062E-05
ENSMUSG00000009563	*Tor2a*	0.431021068	0.04250966
ENSMUSG00000016427	*Ndufa1*	1.234972133	1.96297E-08
ENSMUSG00000016541	*Atxn10*	0.839720029	6.45458E-05
ENSMUSG00000018548	*Trim37*	1.779763349	2.35242E-41
ENSMUSG00000018927	*Ccl6*	1.111585271	0.002236513
ENSMUSG00000019312	*Grb7*	5.030877198	3.76978E-19
ENSMUSG00000019889	*Ptprk*	2.790963446	6.83605E-10
ENSMUSG00000019987	*Arg1*	7.109833368	1.41433E-05
ENSMUSG00000019988	*Nedd1*	0.998388199	2.39636E-12
ENSMUSG00000020020	*Usp44*	8.229778457	1.28537E-06
ENSMUSG00000020399	*Havcr2*	7.659080476	4.0335E-236
ENSMUSG00000020592	*Sdc1*	3.944876333	1.21725E-08
ENSMUSG00000021065	*Fut8*	1.704605201	5.27214E-46
ENSMUSG00000021108	*Prkch*	0.329510817	0.049477394
ENSMUSG00000021629	*Slc30a5*	0.464876245	0.017704357
ENSMUSG00000021676	*Iqgap2*	0.821652651	0.016832526
ENSMUSG00000021785	*Ngly1*	0.735017433	2.89845E-05
ENSMUSG00000021866	*Anxa11*	0.837211101	4.74622E-14
ENSMUSG00000022106	*Rcbtb2*	0.460704599	0.016034609
ENSMUSG00000022186	*Oxct1*	0.470716223	0.000228526
ENSMUSG00000022498	*Txndc11*	0.442112805	0.00991759
ENSMUSG00000022533	*Atp13a3*	0.728925618	0.008223305
ENSMUSG00000022723	*Crybg3*	3.998222603	6.81721E-29
ENSMUSG00000022803	*Popdc2*	7.124124534	7.64267E-25
ENSMUSG00000023830	*Igf2r*	1.543566811	1.25813E-26
ENSMUSG00000023909	*Paqr4*	4.569787573	4.38695E-27
ENSMUSG00000024033	*Rsph1*	5.625878979	0.000742745
ENSMUSG00000024556	*Me2*	1.508862922	3.14032E-38
ENSMUSG00000024725	*Ostf1*	0.882685127	1.88802E-12
ENSMUSG00000024870	*Rab1b*	0.751334549	8.82201E-10
ENSMUSG00000025068	*Gsto1*	2.206065697	5.60996E-18
ENSMUSG00000025154	*Arhgap19*	4.781642951	1.91713E-62
ENSMUSG00000025227	*Tmem180*	4.14257938	3.58387E-17
ENSMUSG00000025381	*Cnpy2*	0.951393195	2.83152E-07
ENSMUSG00000025465	*Echs1*	0.859928042	1.65152E-09
ENSMUSG00000025474	*Tubgcp2*	1.512942348	1.23753E-09
ENSMUSG00000025534	*Gusb*	0.409165747	0.014083618
ENSMUSG00000025786	*Zdhhc3*	0.681190339	7.16766E-10
ENSMUSG00000025809	*Itgb1*	2.957840426	1.5916E-48
ENSMUSG00000025810	*Nrp1*	4.70186339	5.45145E-18
ENSMUSG00000025968	*Ndufs1*	0.664337768	5.26677E-10
ENSMUSG00000026012	*Cd28*	1.292843643	9.79992E-14
ENSMUSG00000026014	*Raph1*	5.460201436	7.06138E-36
ENSMUSG00000026070	*Il18r1*	2.793569006	2.63174E-23
ENSMUSG00000026155	*Smap1*	1.260996272	2.87945E-19
ENSMUSG00000026427	*Eif2d*	0.891576704	0.00030286
ENSMUSG00000026687	*Aldh9a1*	1.06442044	8.29044E-08
ENSMUSG00000027009	*Itga4*	1.887962611	1.10168E-13
ENSMUSG00000027456	*Sdcbp2*	3.5290499	9.3924E-13
ENSMUSG00000027544	*Nfatc2*	0.482410036	0.018670179
ENSMUSG00000027809	*Etfdh*	0.972227047	1.37043E-05
ENSMUSG00000027843	*Ptpn22*	0.675731308	7.03031E-05
ENSMUSG00000028218	*Fam92a*	1.844083889	0.000173636
ENSMUSG00000028251	*Tstd3*	1.938363071	6.7746E-32
ENSMUSG00000028551	*Cdkn2c*	4.351502867	3.44398E-32
ENSMUSG00000028931	*Kcnab2*	1.053685139	6.24143E-19
ENSMUSG00000029026	*Trp73*	10.94807699	1.73859E-10
ENSMUSG00000029119	*Man2b2*	0.718985959	4.70569E-07
ENSMUSG00000029121	*Crmp1*	5.147106705	7.68502E-34
ENSMUSG00000029171	*Pgm1*	1.197093119	1.03342E-18
ENSMUSG00000029253	*Cenpc1*	1.137243627	2.14879E-05
ENSMUSG00000029276	*Glmn*	1.562276966	2.73752E-05
ENSMUSG00000029463	*Fam216a*	0.980783938	0.010676889
ENSMUSG00000029658	*Wdr95*	4.11081717	4.2052E-11
ENSMUSG00000029759	*Pon3*	1.863744388	0.006827911
ENSMUSG00000030064	*Frmd4b*	3.405479903	4.93079E-49
ENSMUSG00000030148	*Clec4a2*	1.389368637	0.000276029
ENSMUSG00000030616	*Sytl2*	3.120751528	3.08721E-38
ENSMUSG00000031479	*Vps36*	0.848461505	2.17734E-14
ENSMUSG00000031556	*Tm2d2*	0.489984661	0.001396325
ENSMUSG00000031871	*Cdh5*	4.841989557	1.80916E-06
ENSMUSG00000032020	*Ubash3b*	1.979332551	3.22844E-24
ENSMUSG00000032046	*Abhd12*	0.444541041	0.026287388
ENSMUSG00000032135	*Mcam*	2.531017936	0.001879708
ENSMUSG00000032281	*Acsbg1*	1.68157326	1.94775E-05
ENSMUSG00000032336	*Nptn*	1.442835875	7.43306E-12
ENSMUSG00000033107	*Rnf125*	0.946263554	0.001252208
ENSMUSG00000033147	*Slc22a15*	3.652423249	3.03899E-55

EnsemblGeneID	*Gene Symbol*	Log Fold Change	Adjusted P-Value
ENSMUSG00000033530	*Ttc7b*	0.557073762	0.003360297
ENSMUSG00000034573	*Ptpn13*	5.757844636	2.93565E-21
ENSMUSG00000034777	*Vax2*	8.717929829	2.64937E-06
ENSMUSG00000034792	*Gna15*	3.194305762	1.828E-88
ENSMUSG00000034898	*Filip1*	7.183835611	2.1646E-21
ENSMUSG00000036932	*Aifm1*	1.09084245	2.10355E-14
ENSMUSG00000037465	*Klf10*	2.355911794	3.6358E-26
ENSMUSG00000039131	*Gipc2*	9.273447783	1.20239E-07
ENSMUSG00000039153	*Runx2*	5.117394674	3.67259E-78
ENSMUSG00000039234	*Sec24d*	2.105947162	1.73507E-12
ENSMUSG00000039449	*Prpf18*	0.751523881	5.19289E-13
ENSMUSG00000039621	*Prex1*	1.179373956	2.1735E-07
ENSMUSG00000040274	*Cdk6*	1.3529711	2.1077E-06
ENSMUSG00000040680	*Kremen2*	2.296187861	0.000338365
ENSMUSG00000041959	*S100a10*	2.327102372	2.89022E-22
ENSMUSG00000042213	*Zfand4*	6.301733003	3.60814E-32
ENSMUSG00000042312	*S100a13*	1.609259835	3.08093E-12
ENSMUSG00000042671	*Rgs8*	10.04777678	6.16484E-10
ENSMUSG00000042705	*Commd10*	1.104660569	4.97184E-06
ENSMUSG00000042784	*Muc1*	5.870299096	8.5905E-08
ENSMUSG00000044258	*Ctla2a*	5.60517226	9.30505E-29
ENSMUSG00000045679	*Pqlc3*	2.483833121	1.8015E-119
ENSMUSG00000046186	*Cd109*	9.558262897	4.67377E-09
ENSMUSG00000046324	*Ermp1*	1.084614311	0.000302538
ENSMUSG00000046410	*Kcnk6*	2.897052949	1.09346E-22
ENSMUSG00000046876	*Atxn1*	2.38911161	1.8411E-29
ENSMUSG00000047592	*Nxpe5*	2.793931241	0.001693893
ENSMUSG00000048416	*Mlf1*	4.407873449	0.004555927
ENSMUSG00000050232	*Cxcr3*	5.812506386	5.5152E-53
ENSMUSG00000051234	*Rnf7*	0.909976003	7.03031E-05
ENSMUSG00000051359	*Ncald*	9.66410274	2.94995E-14
ENSMUSG00000051457	*Spn*	1.291295397	1.62036E-17
ENSMUSG00000051864	*Tbc1d22a*	0.719249952	2.51254E-09
ENSMUSG00000052102	*Gnpda1*	2.171714794	5.94866E-74
ENSMUSG00000052117	*RP23-334A5.4*	3.5973157	3.26045E-10
ENSMUSG00000052428	*Tmco1*	1.520459513	8.35709E-23
ENSMUSG00000052906	*Ubxn8*	1.62903916	1.90408E-11
ENSMUSG00000053063	*Clec12a*	1.240744326	0.008621092
ENSMUSG00000053219	*Raet1e*	4.304095414	0.01872083
ENSMUSG00000053253	*Ndfip2*	0.804926845	9.72591E-09
ENSMUSG00000053898	*Ech1*	1.334432035	2.80484E-09
ENSMUSG00000054408	*Spcs3*	1.41971861	5.58677E-22
ENSMUSG00000054889	*Dsp*	6.067057863	1.70314E-17
ENSMUSG00000055435	*Maf*	4.200633445	5.3388E-25
ENSMUSG00000056888	*Glipr1*	1.548971455	8.18589E-22
ENSMUSG00000058216	*RP23-41B18.5*	1.060942026	0.030368636
ENSMUSG00000058997	*Vwa8*	0.72680251	1.0221E-05
ENSMUSG00000059316	*Slc27a4*	1.116571146	3.69541E-10
ENSMUSG00000062963	*Ufc1*	1.304907652	6.89169E-10
ENSMUSG00000065979	*Cpped1*	2.560386566	1.91837E-18
ENSMUSG00000067878	*Map7d3*	3.397798453	4.08486E-09
ENSMUSG00000071648	*Rom1*	3.049216285	3.208E-16
ENSMUSG00000074622	*Mafb*	2.782282752	1.31333E-11
ENSMUSG00000076474	*Trbv17*	1.177348398	0.012615779
ENSMUSG00000076475	*Trbv19*	0.869855461	0.012299104
ENSMUSG00000076508	*Igkv17-127*	4.47942012	2.32804E-09
ENSMUSG00000076534	*Igkv12-89*	7.031516368	0.00569144
ENSMUSG00000076540	*Igkv4-80*	7.03291675	0.008180973
ENSMUSG00000076550	*Igkv4-63*	5.605808747	0.009343255
ENSMUSG00000076556	*Igkv4-57*	2.713703729	0.009794989
ENSMUSG00000076577	*Igkv8-30*	3.243924241	0.000119491
ENSMUSG00000076609	*Igkc*	4.048970231	9.25576E-10
ENSMUSG00000076612	*Ighg2c*	13.34125426	2.71626E-10
ENSMUSG00000076613	*Ighg2b*	7.238941134	3.64353E-05
ENSMUSG00000076615	*Ighg3*	10.57515793	6.18427E-08
ENSMUSG00000076731	*Ighv8-12*	8.571374293	0.017296505
ENSMUSG00000076934	*Iglv1*	4.621146509	0.014357146
ENSMUSG00000079173	*Zan*	3.168321529	5.73807E-09
ENSMUSG00000081534	*Slc48a1*	1.08572337	4.99793E-12
ENSMUSG00000084817	*AC121575.1*	3.816295804	0.00122345
ENSMUSG00000085133	*RP24-84B10.1*	5.350506948	1.1858E-25
ENSMUSG00000090124	*Ugt1a7c*	1.426023272	0.001440297
ENSMUSG00000092329	*AC114005.5*	0.28933164	0.025578625
ENSMUSG00000092486	*RP23-3M10.7*	1.799715245	1.62122E-06
ENSMUSG00000093896	*Ighv1-76*	5.377857729	0.001008269
ENSMUSG00000094006	*Igkv4-59*	7.531734662	0.000804925
ENSMUSG00000094088	*Ighv1-64*	3.401245881	8.9335E-05
ENSMUSG00000094102	*Ighv9-2*	6.091625578	0.038779631
ENSMUSG00000094194	*Ighv5-16*	8.21964294	0.000675862
ENSMUSG00000094335	*Igkv1-117*	4.88534451	1.07654E-09
ENSMUSG00000094420	*Igkv10-96*	4.952792056	4.98694E-17
ENSMUSG00000094502	*Ighv1-69*	8.058714455	1.20703E-05
ENSMUSG00000094509	*Ighv14-1*	5.775273341	0.019976015
ENSMUSG00000094787	*Ighv1-54*	2.857759583	0.02924301
ENSMUSG00000094951	*Ighv5-6*	6.243397507	0.024002751
ENSMUSG00000095335	*Igkv3-5*	6.638897425	0.000192315
ENSMUSG00000096255	*Dynlt1b*	1.098091305	5.05241E-06
ENSMUSG00000096459	*Ighv9-3*	6.446087371	0.027977317
ENSMUSG00000096464	*Ighv2-2*	6.43611972	0.000820871
ENSMUSG00000096515	*Igkv14-100*	7.519938438	0.027872922
ENSMUSG00000098428	*Anxa11-ps1*	0.834038018	0.034557881

B. Genes overlapping between acute-brown module and Monocytes/Macrophages

EnsemblGeneID	Gene Symbol	Log Fold Change	Adjusted P-Value
ENSMUSG00000001105	*Ift20*	0.567426081	0.012748094
ENSMUSG00000002014	*Ssr4*	0.799204306	0.002594551
ENSMUSG00000002190	*Clgn*	4.668157113	3.04878E-05
ENSMUSG00000002274	*Metrn*	1.05501784	0.009409296
ENSMUSG00000003948	*Mmd*	0.729429356	0.013168812
ENSMUSG00000004610	*Etfb*	1.378824596	9.54235E-05
ENSMUSG00000004814	*Ccl24*	2.145664348	0.01384617
ENSMUSG00000005763	*Cd247*	1.100199783	0.00560093
ENSMUSG00000006179	*Prss16*	2.513418237	1.19677E-06
ENSMUSG00000006313	*Upk1a*	3.110061863	0.000380463
ENSMUSG00000006378	*Gcat*	2.337141168	0.002092992
ENSMUSG00000007021	*Syngr3*	6.102732329	0.001925608
ENSMUSG00000009563	*Tor2a*	0.476508804	0.03424002
ENSMUSG00000016024	*Lbp*	2.156629669	2.20983E-05
ENSMUSG00000016427	*Ndufa1*	0.67780564	0.004724359
ENSMUSG00000016541	*Atxn10*	0.88251901	4.96831E-05
ENSMUSG00000018548	*Trim37*	0.522246885	0.000532949
ENSMUSG00000019312	*Grb7*	4.207844137	4.85167E-12
ENSMUSG00000019802	*Sec63*	0.604732306	0.002654904
ENSMUSG00000019889	*Ptprk*	4.41964451	3.80308E-16
ENSMUSG00000019987	*Arg1*	7.891998343	1.30489E-14
ENSMUSG00000020020	*Usp44*	9.147945419	1.40243E-07
ENSMUSG00000020401	*Fam71b*	2.837998992	4.46744E-12
ENSMUSG00000021866	*Anxa11*	0.489790469	3.61585E-05
ENSMUSG00000022338	*Eny2*	0.854236145	0.000157268
ENSMUSG00000022667	*Cd200r1*	0.738358157	0.028295027
ENSMUSG00000022803	*Popdc2*	5.742403581	3.59471E-13
ENSMUSG00000023830	*Igf2r*	1.771246692	2.3525E-32
ENSMUSG00000023909	*Paqr4*	2.594966612	5.50999E-09
ENSMUSG00000024033	*Rsph1*	4.470791282	0.012168263
ENSMUSG00000025154	*Arhgap19*	1.343706754	1.21302E-05
ENSMUSG00000025968	*Ndufs1*	0.258068784	0.034476694
ENSMUSG00000026012	*Cd28*	1.01655151	4.78435E-08
ENSMUSG00000026070	*Il18r1*	3.520685624	3.80701E-34
ENSMUSG00000026117	*Zap70*	1.48353414	9.3071E-05
ENSMUSG00000026427	*Eif2d*	1.154545816	5.10719E-06
ENSMUSG00000026778	*Prkcq*	0.920833287	0.00115757
ENSMUSG00000027006	*Dnajc10*	0.481925518	0.044904405
ENSMUSG00000027456	*Sdcbp2*	3.068435414	9.57661E-09
ENSMUSG00000028218	*Fam92a*	2.114895841	5.37339E-05
ENSMUSG00000028551	*Cdkn2c*	0.947985558	0.023023167
ENSMUSG00000029026	*Trp73*	4.882173682	1.48537E-05
ENSMUSG00000029121	*Crmp1*	3.874009277	9.51995E-17
ENSMUSG00000029153	*Ociad2*	5.960063712	0.003060276
ENSMUSG00000029253	*Cenpc1*	0.63571419	0.034519244
ENSMUSG00000029276	*Glmn*	1.465765164	0.000294138
ENSMUSG00000029463	*Fam216a*	1.602908924	6.11489E-05
ENSMUSG00000029658	*Wdr95*	6.200629862	6.00987E-14
ENSMUSG00000030064	*Frmd4b*	1.046782531	1.19804E-05
ENSMUSG00000030616	*Sytl2*	2.347535861	3.37401E-19
ENSMUSG00000031871	*Cdh5*	1.84178932	0.010909044
ENSMUSG00000032011	*Thy1*	2.070418074	8.01214E-08
ENSMUSG00000032020	*Ubash3b*	0.840734288	6.10637E-05
ENSMUSG00000032093	*Cd3e*	1.11933856	0.002105982
ENSMUSG00000032094	*Cd3d*	1.449654695	0.001207855
ENSMUSG00000032135	*Mcam*	2.884045254	0.000481852
ENSMUSG00000032281	*Acsbg1*	3.288718086	4.45253E-16

EnsemblGeneID	Gene Symbol	Log Fold Change	Adjusted P-Value
ENSMUSG00000033107	*Rnf125*	0.767369808	0.024095806
ENSMUSG00000033318	*Gstt2*	1.190896324	0.007171036
ENSMUSG00000034573	*Ptpn13*	3.97370952	1.24817E-09
ENSMUSG00000034777	*Vax2*	6.865726911	0.000525172
ENSMUSG00000034792	*Gna15*	0.842110287	2.19907E-07
ENSMUSG00000034898	*Filip1*	2.669223021	1.89196E-05
ENSMUSG00000036932	*Aifm1*	0.529423071	0.000668781
ENSMUSG00000039131	*Gipc2*	6.985040885	0.000183665
ENSMUSG00000039234	*Sec24d*	0.912983597	0.005348374
ENSMUSG00000040274	*Cdk6*	0.91863495	0.002958196
ENSMUSG00000040680	*Kremen2*	3.267970305	3.73957E-06
ENSMUSG00000041959	*S100a10*	1.806558982	2.61125E-13
ENSMUSG00000042312	*S100a13*	0.8708762	0.00046382
ENSMUSG00000042671	*Rgs8*	7.373731677	1.86553E-05
ENSMUSG00000042784	*Muc1*	2.081706833	0.006157109
ENSMUSG00000044258	*Ctla2a*	3.084745062	5.73095E-09
ENSMUSG00000046876	*Atxn1*	1.840276837	1.30127E-16
ENSMUSG00000048416	*Mlf1*	7.01333989	0.001993542
ENSMUSG00000049109	*Themis*	1.931478523	3.69563E-15
ENSMUSG00000050232	*Cxcr3*	3.601203292	3.45812E-20
ENSMUSG00000051234	*Rnf7*	0.7057059	0.004069063
ENSMUSG00000051359	*Ncald*	7.630547733	1.44311E-08
ENSMUSG00000051735	*Rinl*	0.491485721	4.60641E-05
ENSMUSG00000053044	*Cd8b1*	2.044746371	6.70441E-09
ENSMUSG00000053219	*Raet1e*	2.526984014	0.000396923
ENSMUSG00000053898	*Ech1*	0.654129046	0.008339269
ENSMUSG00000054342	*Kcnn4*	1.558517419	2.43928E-08
ENSMUSG00000054889	*Dsp*	3.778959294	4.58217E-06
ENSMUSG00000055435	*Maf*	1.869088715	8.16325E-07
ENSMUSG00000058216	*RP23-41B18.5*	1.451838871	0.004547059
ENSMUSG00000062963	*Ufc1*	0.689587233	0.002737905
ENSMUSG00000064080	*Fbln2*	6.400637274	1.34967E-05
ENSMUSG00000071648	*Rom1*	2.207921393	2.13608E-08
ENSMUSG00000074622	*Mafb*	0.799263695	0.044596235
ENSMUSG00000076471	*Trbv14*	1.54901288	0.000348848
ENSMUSG00000076473	*Trbv16*	1.848008265	0.000833288
ENSMUSG00000076474	*Trbv17*	2.165071638	3.68968E-05
ENSMUSG00000076475	*Trbv19*	1.890866372	3.33099E-07
ENSMUSG00000076480	*Trbv29*	2.168959224	2.03365E-07
ENSMUSG00000076490	*Trbc1*	1.270959028	0.001761164
ENSMUSG00000076498	*Trbc2*	1.444285005	0.001659883
ENSMUSG00000076508	*Igkv17-127*	1.285136046	0.039293477
ENSMUSG00000076540	*Igkv4-80*	8.676766138	0.001540512
ENSMUSG00000076550	*Igkv4-63*	8.56062214	6.66453E-05
ENSMUSG00000076612	*Ighg2c*	6.850431207	1.23863E-05
ENSMUSG00000076615	*Ighg3*	6.395280235	1.187E-06
ENSMUSG00000079173	*Zan*	8.458944209	3.13924E-07
ENSMUSG00000085133	*RP24-84B10.1*	4.595322022	1.71774E-11
ENSMUSG00000092329	*AC114005.5*	0.76267402	1.57657E-09
ENSMUSG00000092486	*RP23-3M10.7*	2.213672224	9.27825E-09
ENSMUSG00000094194	*Ighv5-16*	8.877923212	0.000407203
ENSMUSG00000094502	*Ighv1-69*	5.321039243	5.9665E-05
ENSMUSG00000094509	*Ighv14-1*	8.169768911	0.003571991
ENSMUSG00000095335	*Igkv3-5*	9.876003899	2.44431E-08
ENSMUSG00000096255	*Dynlt1b*	0.709306864	0.006444076
ENSMUSG00000096464	*Ighv2-2*	2.674359267	0.042390718

Supplementary Table S5. Gene ontology (GO) enriched terms from 182 genes overlapping between CD8$^+$ T cells and acute-brown module hub genes (A), and from 113 genes overlapping between monocytes/macrophages and acute-brown module hub genes (B). Enrichment analysis was performed using DAVID (http://david.ncifcrf.gov/).

A. Gene ontology analysis of genes overlapping between acute-brown module and CD8+ T cells			
Annotation Term (Biological Process)	Genes	P-Value	FDR
GO:0008152~metabolic process	*Acsbg1, Echs1, Aldh9a1, Me2, RP23-41B18.5, Gusb, Oxct1, Slc27a4, Man2b2, Ech1, Ugt1a7c, Gsto1*	4.86E-04	0.747546555
GO:0016477~cell migration	*Ptprk, Nrp1, Itgb2, Itga4, Sdc1, Nfatc2, Fut8*	0.002496227	3.782282899
GO:0043547~positive regulation of GTPase activity	*Ccl24, Itgb1, Prex1, Ccl6, S100a10, Rgs8*	0.003958426	5.93523213
GO:0070374~positive regulation of ERK1 and ERK2 cascade	*Ccl24, Nrp1, Ptpn22, Havcr2, Ccl6, Nptn*	0.011247546	16.01194793
GO:0046226~coumarin catabolic process	*Pon3, Ugt1a7c*	0.014217829	19.82097822
GO:0008637~apoptotic mitochondrial changes	*Ndufs1, Aifm1, Rnf7*	0.01577658	21.75464995
GO:0007179~transforming growth factor beta receptor signaling pathway	*Ptprk, Itgb1, Cdh5, Fut8*	0.016495955	22.63226705
GO:0002685~regulation of leukocyte migration	*Cxcr3, Ptpn22*	0.021251341	28.20616774
GO:1902036~regulation of hematopoietic stem cell differentiation	*Cdk6, Ap2a2*	0.021251341	28.20616774
GO:0042130~negative regulation of T cell proliferation	*Spn, Glmn, Havcr2*	0.033018539	40.42689876
GO:0030217~T cell differentiation	*Runx2, Ptpn22, Prex1*	0.034552697	41.86838962
GO:0019439~aromatic compound catabolic process	*Pon3, Ugt1a7c*	0.042054489	48.45930098
GO:0045589~regulation of regulatory T cell differentiation	*Cd28, Ctla2a*	0.055678899	58.67821276
GO:0030335~positive regulation of cell migration	*Grb7, Mcam, Ccl24, Itgb1, Prex1*	0.057611193	59.9635194
GO:0007155~cell adhesion	*Mcam, Ptprk, Itgb1, Cdh5, Rom1, Itga4, Zan, Nptn*	0.058998063	60.86287235
GO:0006517~protein deglycosylation	*Ngly1, Man2b2*	0.069111016	66.87184634
GO:0008542~visual learning	*Itgb1, Atxn1, Nptn*	0.074434581	69.67695109
GO:0042102~positive regulation of T cell proliferation	*Spn,Cd28, Havcr2*	0.076488309	70.69846361
GO:0045086~positive regulation of interleukin-2 biosynthetic process	*Cd28, Glmn*	0.082353534	73.44142887
GO:0030593~neutrophil chemotaxis	*Ccl24, Prex1, Ccl6*	0.087018304	75.44949669
GO:0003073~regulation of systemic arterial blood pressure	*Ncald, Kcnk6*	0.088904524	76.2204055
GO:0060252~positive regulation of glial cell proliferation	*Prkch, Atxn1*	0.095409107	78.70873247
GO:0045060~negative thymic T cell selection	*Spn, Cd28*	0.095409107	78.70873247
GO:0043508~negative regulation of JUN kinase activity	*Trp73, Ptpn22*	0.095409107	78.70873247
GO:0010839~negative regulation of keratinocyte proliferation	*Ptprk, Cd109*	0.095409107	78.70873247

B. Gene ontology analysis of genes overlapping between acute-brown module and Monocytes/Macrophages			
Annotation Term (Biological Process)	Genes	P-Value	FDR
GO:0050852~T cell receptor signaling pathway	*Themis, Cd3e, Cd28, Thy1, Zap70, Cd247*	3.38E-06	0.004908745
GO:0045086~positive regulation of interleukin-2 biosynthetic process	*Cd3e, Cd28, Glmn, Prkcq*	1.92E-05	0.027872996
GO:0046641~positive regulation of alpha-beta T cell proliferation	*Cd3e, Cd28, Zap70*	0.00108808	1.568148567
GO:0002376~immune system process	*Themis, Cd3e, Cd8b1, Kcnn4, Rnf125, Zap70, Prkcq, Lbp*	0.001761696	2.527461194
GO:0045060~negative thymic T cell selection	*Cd3e, Cd28, Zap70*	0.001784446	2.559706259
GO:0050870~positive regulation of T cell activation	*Cd3e, Thy1, Prkcq*	0.002643433	3.770010421
GO:0007166~cell surface receptor signaling pathway	*Cd3e, Cd3d, Cxcr3, Glmn, Upk1a, Cd247*	0.003190543	4.533568992
GO:0032753~positive regulation of interleukin-4 production	*Cd3e, Cd28, Prkcq*	0.003304249	4.691549623
GO:0008637~apoptotic mitochondrial changes	*Ndufs1, Aifm1, Rnf7*	0.006625056	9.199462942
GO:0033077~T cell differentiation in thymus	*Cd3e, Mafb, Cdk6*	0.013503959	17.91305194
GO:0002250~adaptive immune response	*Themis, Cd8b1, Rnf125, Zap70*	0.025334494	31.10280719
GO:0090330~regulation of platelet aggregation	*Zap70, Prkcq*	0.026906437	32.6985839
GO:0043547~positive regulation of GTPase activity	*Ccl24, S100a10, Thy1, Rgs8*	0.028738537	34.51501005
GO:0042102~positive regulation of T cell proliferation	*Cd3e, Cd28, Prkcq*	0.03416539	39.63115357
GO:0045589~regulation of regulatory T cell differentiation	*Cd28, Ctla2a*	0.035715342	41.0225186
GO:0002281~macrophage activation involved in immune response	*Zap70, Lbp*	0.048781207	51.61983693
GO:0007050~cell cycle arrest	*Trp73, Mlf1, Cdkn2c*	0.052281381	54.14113502
GO:0045059~positive thymic T cell selection	*Cd3e, Zap70*	0.053097512	54.71116151
GO:0007049~cell cycle	*Cdk6, Usp44, Cenpc1, Trp73, Mlf1, Anxa11, Cdkn2c*	0.060035156	59.29716474
GO:0001889~liver development	*Sec63, Arg1, Igf2r*	0.069212572	64.70115914
GO:0007155~cell adhesion	*Mcam, Ptprk, Cdh5, Rom1, Zan, Thy1*	0.069339007	64.77070887
GO:0006954~inflammatory response	*Ccl24, Cxcr3, Trp73, Zap70, Prkcq*	0.071115866	65.73473067
GO:0042326~negative regulation of phosphorylation	*Atxn1, Cdkn2c*	0.078592014	69.52800401
GO:0042346~positive regulation of NF-kappaB import into nucleus	*Il18r1, Prkcq*	0.082774667	71.47579037
GO:0016337~single organismal cell-cell adhesion	*Dsp, Cdh5, Thy1*	0.08630341	73.02823613
GO:0051301~cell division	*Cdk6, Usp44, Dynlt1b, Cenpc1, Anxa11*	0.090109526	74.61429544
GO:0045671~negative regulation of osteoclast differentiation	*Mafb, Ubash3b*	0.095210422	76.60396733
GO:0048041~focal adhesion assembly	*Ptprk, Thy1*	0.099318548	78.09977545

Supplementary Table S6. List of genes from chronic-magenta module with their corresponding intramodular connectivity (K_{IM}) value. Genes selected for qPCR analysis are marked in bold.

Ensembl Gene ID	Gene Symbol	KIM
ENSMUSG00000025804	***Ccr1***	**1**
ENSMUSG00000074874	*Ctla2b*	0.993454148
ENSMUSG00000024936	*Kcnk7*	0.992217146
ENSMUSG00000060131	*Atp8b4*	0.954965462
ENSMUSG00000097634	*Gm26827*	0.944108053
ENSMUSG00000044816	*D630023F18Rik*	0.933315827
ENSMUSG00000071356	*Reg3b*	0.917417566
ENSMUSG00000025161	*Slc16a3*	0.913435028
ENSMUSG00000024725	*Ostf1*	0.899752411
ENSMUSG00000031443	*F7*	0.890835402
ENSMUSG00000048163	*Selplg*	0.888419897
ENSMUSG00000049130	***C5ar1***	**0.887456546**
ENSMUSG00000000290	*Itgb2*	0.863925448
ENSMUSG00000048807	*Slc35e4*	0.863655294
ENSMUSG00000059248	*Septt9*	0.859690568
ENSMUSG00000005514	*Por*	0.853141015
ENSMUSG00000034271	*Jdp2*	0.84727159
ENSMUSG00000026177	*Slc11a1*	0.846593036
ENSMUSG00000032577	*Mapkapk3*	0.842828014
ENSMUSG00000002699	*Lcp2*	0.842583391
ENSMUSG00000054855	*Rnd1*	0.833300169
ENSMUSG00000059343	*Aldoart1*	0.827130517
ENSMUSG00000038366	*Lasp1*	0.825052138
ENSMUSG00000030786	***Itgam***	**0.822860117**
ENSMUSG00000046949	*Nqo2*	0.821065925
ENSMUSG00000029484	*Anxa3*	0.804566255
ENSMUSG00000042265	*Trem1*	0.799623715
ENSMUSG00000029135	*Fosl2*	0.796607636
ENSMUSG00000093973	*Mrgpra2a*	0.796181204
ENSMUSG00000062075	*Lmnb2*	0.783537599
ENSMUSG00000020277	*Pfkl*	0.780394129
ENSMUSG00000032640	*Chsy1*	0.777863042
ENSMUSG00000016946	*Kctd5*	0.76962157
ENSMUSG00000096719	*Mrgpra2b*	0.764197404
ENSMUSG00000018500	*Adora2b*	0.764125194
ENSMUSG00000082632	*Gm13365*	0.759018733
ENSMUSG00000021250	*Fos*	0.753484025
ENSMUSG00000026547	*Tagln2*	0.749781891
ENSMUSG00000079516	*Reg3a*	0.749481674
ENSMUSG00000003038	*Hmgn2*	0.747618648
ENSMUSG00000071343	*Gm10327*	0.745175391
ENSMUSG00000028771	*Ptpn12*	0.745060968
ENSMUSG00000045917	*6330416G13Rik*	0.744255108
ENSMUSG00000022102	*Dok2*	0.743821559
ENSMUSG00000026796	*Fam129b*	0.739886466
ENSMUSG00000015247	*Nipsnap3b*	0.738563008
ENSMUSG00000036894	*Rap2b*	0.738215946
ENSMUSG00000021728	*Emb*	0.731832682
ENSMUSG00000050147	*F2rl3*	0.730863893
ENSMUSG00000068587	*Mgam*	0.72796146
ENSMUSG00000030616	*Sytl2*	0.727739951
ENSMUSG00000032786	*Alas1*	0.721228537
ENSMUSG00000023140	*Reg2*	0.717316157
ENSMUSG00000032504	*Pdcd6ip*	0.715620676
ENSMUSG00000043004	*Gng2*	0.714719537
ENSMUSG00000033161	*Atp1a1*	0.708224853
ENSMUSG00000028494	*Plin2*	0.70728487
ENSMUSG00000035863	*Palm*	0.696417421
ENSMUSG00000039693	*Msantd3*	0.690763509
ENSMUSG00000095203	*Gm13810*	0.68985163
ENSMUSG00000094873	*Gm13812*	0.68985163
ENSMUSG00000025429	*Pstpip2*	0.686711275
ENSMUSG00000027712	*Anxa5*	0.681161834
ENSMUSG00000031584	*Gsr*	0.680933129
ENSMUSG00000043421	*Hilpda*	0.678866011
ENSMUSG00000096957	*E230013L22Rik*	0.677382799
ENSMUSG00000027360	*Hdc*	0.677253732
ENSMUSG00000033721	*Vav3*	0.676635928
ENSMUSG00000026970	*Rbms1*	0.67403783
ENSMUSG00000071648	*Rom1*	0.670296932
ENSMUSG00000000078	*Klf6*	0.664854566
ENSMUSG00000032109	*Nlrx1*	0.659792208
ENSMUSG00000032294	*Pkm*	0.658622312
ENSMUSG00000063193	*Cd300lb*	0.658059403
ENSMUSG00000041926	*Rnpep*	0.657049144
ENSMUSG00000039813	*Tbc1d2*	0.657003457
ENSMUSG00000022893	*Adamts1*	0.656705732
ENSMUSG00000034570	*Inpp5j*	0.642336635
ENSMUSG00000081251	*Gm12164*	0.6415054
ENSMUSG00000022180	*Slc7a8*	0.625101574
ENSMUSG00000098609	*RP24-530J21.3*	0.624967632
ENSMUSG00000058542	*Gm15590*	0.62492143
ENSMUSG00000083997	*Gm12920*	0.622560999
ENSMUSG00000050029	*Rap2c*	0.619978938
ENSMUSG00000026509	*Capn2*	0.618737359
ENSMUSG00000034226	*Rhov*	0.61704399
ENSMUSG00000026600	*Soat1*	0.615573214

Ensembl Gene ID	Gene Symbol	KIM
ENSMUSG00000030017	*Reg3g*	0.60984345
ENSMUSG00000041959	*S100a10*	0.608076158
ENSMUSG00000047045	*Tmem164*	0.606181513
ENSMUSG00000022372	*Sla*	0.587790087
ENSMUSG00000038546	*Ranbp9*	0.58677231
ENSMUSG00000025355	*Mmp19*	0.585926086
ENSMUSG00000028961	*Pgd*	0.58264574
ENSMUSG00000036599	*Chst12*	0.581624926
ENSMUSG00000041754	*Trem3*	0.581506481
ENSMUSG00000078795	*Ceacam15*	0.578313551
ENSMUSG00000073529	*F830208F22Rik*	0.577667298
ENSMUSG00000097680	*Gm26642*	0.572899856
ENSMUSG00000037752	*Xkr8*	0.571312347
ENSMUSG00000031504	*Rab20*	0.569573268
ENSMUSG00000022894	*Adamts5*	0.568176749
ENSMUSG00000043192	*Gm1840*	0.564738747
ENSMUSG00000049999	*Ppp1r3d*	0.563926764
ENSMUSG00000032691	*Nlrp3*	0.555142928
ENSMUSG00000020038	*Cry1*	0.553118446
ENSMUSG00000038059	*Smim3*	0.552525219
ENSMUSG00000086693	*A730081D07Rik*	0.547033233
ENSMUSG00000022221	*Ripk3*	0.537194474
ENSMUSG00000044103	*Il1f9*	0.53554163
ENSMUSG00000029175	*Slc35f6*	0.535500622
ENSMUSG00000019845	*Tube1*	0.534618132
ENSMUSG00000026829	*Gbgt1*	0.533881326
ENSMUSG00000098369	*RP23-100J17.7*	0.529843773
ENSMUSG00000056458	*Stk30*	0.529738781
ENSMUSG00000037960	*1110007C09Rik*	0.52875436
ENSMUSG00000092283	*Gm20412*	0.527369468
ENSMUSG00000098428	*RP24-222L21.1*	0.520100809
ENSMUSG00000038807	*Rap1gap2*	0.520076972
ENSMUSG00000030413	*Pglyrp1*	0.519540905
ENSMUSG00000028978	*Nos3*	0.518017282
ENSMUSG00000036427	*Gpi1*	0.515859015
ENSMUSG00000068341	*Reg3d*	0.515781131
ENSMUSG00000069830	*Nlrp1a*	0.512661266
ENSMUSG00000017670	*Elmo2*	0.512200287
ENSMUSG00000005656	*Snx6*	0.511461162
ENSMUSG00000061981	*Flot2*	0.505457321
ENSMUSG00000051615	*Rap2a*	0.499582016
ENSMUSG00000021794	*Glud1*	0.499555238
ENSMUSG00000052821	*Cysltr1*	0.498086686
ENSMUSG00000033589	*Reep4*	0.497547747
ENSMUSG00000028194	*Ddah1*	0.496732555
ENSMUSG00000083892	*Gm1848*	0.496170269
ENSMUSG00000018341	*Il12rb2*	0.495539025
ENSMUSG00000047777	*Phf13*	0.491116485
ENSMUSG00000000555	*Itga5*	0.4909768
ENSMUSG00000026068	*Il18rap*	0.487559893
ENSMUSG00000022871	*Fetub*	0.486509467
ENSMUSG00000097660	*Gm26762*	0.486342004
ENSMUSG00000023000	*Dhh*	0.482136842
ENSMUSG00000027907	*S100a11*	0.478251394
ENSMUSG00000037035	*Inhbb*	0.477358105
ENSMUSG00000024985	*Tcf7l2*	0.473374301
ENSMUSG00000064246	*Chi3l1*	0.466742753
ENSMUSG00000060063	*Alox5ap*	0.463974428
ENSMUSG00000021360	*Gcnt2*	0.463126274
ENSMUSG00000038383	*Pigu*	0.462543633
ENSMUSG00000030650	*Tmc5*	0.455807422
ENSMUSG00000024913	*Lrp5*	0.451898633
ENSMUSG00000097954	*Gm4217*	0.451834485
ENSMUSG00000040152	*Thbs1*	0.446002465
ENSMUSG00000021125	*Arg2*	0.445220595
ENSMUSG00000037148	*Arhgap10*	0.445002587
ENSMUSG00000029528	*Pxn*	0.443374699
ENSMUSG00000027435	*Cd93*	0.441665964
ENSMUSG00000038517	*Tbkbp1*	0.436761771
ENSMUSG00000022651	*Retnlg*	0.433551921
ENSMUSG00000033027	*Klrc3*	0.431109949
ENSMUSG00000083391	*Gm1448*	0.428774203
ENSMUSG00000097004	*4731419I09Rik*	0.424088329
ENSMUSG00000083659	*Gm11258*	0.422223347
ENSMUSG00000091942	*Gm17138*	0.421114691
ENSMUSG00000014813	*Stc1*	0.420268451
ENSMUSG00000028403	*Zdhhc21*	0.415847482
ENSMUSG00000018340	*Anxa6*	0.41214814
ENSMUSG00000026784	*Pdss1*	0.409665149
ENSMUSG00000026321	*Tnfrsf11a*	0.409223697
ENSMUSG00000052102	*Gnpda1*	0.408455336
ENSMUSG00000044258	*Ctla2a*	0.407888337
ENSMUSG00000028553	*Angptl3*	0.407586695
ENSMUSG00000020961	*Ston2*	0.403221113
ENSMUSG00000024682	*Gif*	0.399349437
ENSMUSG00000028041	*Adam15*	0.397559372
ENSMUSG00000034765	*Dusp5*	0.397188977

Ensembl Gene ID	Gene Symbol	KIM
ENSMUSG00000045377	*Tmem88*	0.394116085
ENSMUSG00000074417	*Gm14548*	0.390833338
ENSMUSG00000024900	*Cpt1a*	0.390760346
ENSMUSG00000074250	*Gm10653*	0.38936587
ENSMUSG00000098180	*Gm5430*	0.387772117
ENSMUSG00000030530	*Furin*	0.386436098
ENSMUSG00000034684	*Sema3f*	0.382695513
ENSMUSG00000050493	*Fam167b*	0.381893181
ENSMUSG00000024897	*Apba1*	0.380205188
ENSMUSG00000034652	*Cd300a*	0.379723479
ENSMUSG00000021036	*Sptlc2*	0.378821231
ENSMUSG00000086769	*Gm15587*	0.374941907
ENSMUSG00000047821	*Trim16*	0.373855276
ENSMUSG00000090307	*1700071M16Rik*	0.37306601
ENSMUSG00000021256	*Vash1*	0.361926149
ENSMUSG00000026656	*Fcgr2b*	0.359900344
ENSMUSG00000067878	*Mtap7d3*	0.356709747
ENSMUSG00000030095	*Tmem43*	0.355180856
ENSMUSG00000053044	*Cd8b1*	0.354541444
ENSMUSG00000032020	*Ubash3b*	0.353351892
ENSMUSG00000015355	*Cd48*	0.35327608
ENSMUSG00000050966	*Lin28a*	0.350697154
ENSMUSG00000030144	*Clec4d*	0.350210896
ENSMUSG00000032602	*Slc25a20*	0.343036113
ENSMUSG00000015053	*Gata2*	0.342814658
ENSMUSG00000033684	*Qsox1*	0.341754157
ENSMUSG00000090213	*Tmem189*	0.339502064
ENSMUSG00000057409	*Zfp53*	0.333244565
ENSMUSG00000007021	*Syngr3*	0.332405311
ENSMUSG00000076476	*Trbv20*	0.331862814
ENSMUSG00000024912	*Fosl1*	0.331521574
ENSMUSG00000002289	*Angptl4*	0.331273956
ENSMUSG00000040511	*Pvr*	0.330803123
ENSMUSG00000026425	*Srgap2*	0.330503963
ENSMUSG00000006587	*Snai3*	0.327847501
ENSMUSG00000000317	*Bcl6b*	0.327642
ENSMUSG00000033530	*Ttc7b*	0.327602317
ENSMUSG00000029925	*Tbxas1*	0.324913887
ENSMUSG00000026204	*Ptprn*	0.324809569
ENSMUSG00000086773	*Gm16192*	0.323411253
ENSMUSG00000022514	*Il1rap*	0.320196073
ENSMUSG00000052688	*5430435G22Rik*	0.318344652
ENSMUSG00000042082	*Arsb*	0.316608497
ENSMUSG00000019055	*Plod1*	0.313494398
ENSMUSG00000032511	*Scn5a*	0.313238153
ENSMUSG00000048572	*Tmem252*	0.308414168
ENSMUSG00000029345	*Tfip11*	0.296938019
ENSMUSG00000037513	*Samd4b*	0.295619012
ENSMUSG00000030069	*Prok2*	0.294490192
ENSMUSG00000036880	*Acaa2*	0.293508309
ENSMUSG00000025723	*Nmb*	0.292811212
ENSMUSG00000047798	*Cd300lf*	0.29077158
ENSMUSG00000051934	*Spats2*	0.286441681
ENSMUSG00000034659	*Tmem109*	0.282069427
ENSMUSG00000022788	*Fgd4*	0.277030447
ENSMUSG00000083041	*Gm9835*	0.273524201
ENSMUSG00000027068	*Dhrs9*	0.269895041
ENSMUSG00000020357	*Flt4*	0.267526217
ENSMUSG00000051335	*Gfod1*	0.266632393
ENSMUSG00000026121	*Sema4c*	0.265685038
ENSMUSG00000059316	*Slc27a4*	0.265181828
ENSMUSG00000028071	*Sh2d2a*	0.264882688
ENSMUSG00000021866	*Anxa11*	0.26225469
ENSMUSG00000046993	*Gm5637*	0.259396731
ENSMUSG00000038007	*Acer2*	0.258105211
ENSMUSG00000006345	*Ggt1*	0.257509391
ENSMUSG00000032739	*Pram1*	0.255965328
ENSMUSG00000078780	*Gm5150*	0.255811666
ENSMUSG00000091423	*Gm17509*	0.25413833
ENSMUSG00000029757	*Dync1i1*	0.254038325
ENSMUSG00000046139	*Patl1*	0.252324938
ENSMUSG00000044707	*Ccnjl*	0.250186967
ENSMUSG00000050910	*Cdr2l*	0.249119429
ENSMUSG00000051029	*Serpinb1b*	0.246693567
ENSMUSG00000005413	*Hmox1*	0.245409511
ENSMUSG00000029640	*Usp12*	0.243522004
ENSMUSG00000028497	*Ptplad2*	0.243104682
ENSMUSG00000058427	*Cxcl2*	0.242022748
ENSMUSG00000037465	*Klf10*	0.241683143
ENSMUSG00000067377	*Tspan6*	0.238790777
ENSMUSG00000019997	*Ctgf*	0.233442877
ENSMUSG00000028893	*Sesn2*	0.233393848
ENSMUSG00000062300	*Pvrl2*	0.229633581
ENSMUSG00000083046	*Gm14699*	0.228751802
ENSMUSG00000074063	*Osgin1*	0.224880256
ENSMUSG00000042286	*Stab1*	0.223281067
ENSMUSG00000037408	*Cnnm4*	0.221564936

Ensembl Gene ID	Gene Symbol	KIM
ENSMUSG00000003484	*Cyp4f18*	0.219854655
ENSMUSG00000026928	*Card9*	0.219309916
ENSMUSG00000021904	*Sema3g*	0.219027602
ENSMUSG00000024413	*Npc1*	0.216885118
ENSMUSG00000025171	*Ubtd1*	0.216740009
ENSMUSG00000039956	*Mrap*	0.216435566
ENSMUSG00000033508	*Asprv1*	0.213643829
ENSMUSG00000030064	*Frmd4b*	0.21192636
ENSMUSG00000031367	*Ap1s2*	0.211589405
ENSMUSG00000040907	*Atp1a3*	0.210002025
ENSMUSG00000024030	*Abcg1*	0.208870153
ENSMUSG00000028862	*Map3k6*	0.202557467
ENSMUSG00000030352	*Tspan9*	0.201638709
ENSMUSG00000028136	*Snx27*	0.200420638
ENSMUSG00000023473	*Celsr3*	0.199392616
ENSMUSG00000049551	*Fzd9*	0.198546974
ENSMUSG00000022579	*Gpihbp1*	0.197151663
ENSMUSG00000038188	*Scarf1*	0.196956555
ENSMUSG00000037697	*Ddhd1*	0.193979082
ENSMUSG00000082791	*Gm4875*	0.191529882
ENSMUSG00000026107	*Nabp1*	0.191437919
ENSMUSG00000019088	*Dnase1l1*	0.189436816
ENSMUSG00000018574	*Acadvl*	0.188842375
ENSMUSG00000031871	*Cdh5*	0.18672297
ENSMUSG00000022887	*Masp1*	0.184596952
ENSMUSG00000022150	*Dab2*	0.184330276
ENSMUSG00000028463	*Car9*	0.184139042
ENSMUSG00000044469	*Tnfaip8l1*	0.184085253
ENSMUSG00000078817	*Nlrp12*	0.180368475
ENSMUSG00000018761	*Mpdu1*	0.178333915
ENSMUSG00000005824	*Tnfsf14*	0.178160156
ENSMUSG00000045349	*Sh2d5*	0.177993155
ENSMUSG00000026582	*Sele*	0.176638341
ENSMUSG00000073386	*9830107B12Rik*	0.173967601
ENSMUSG00000038024	*Dennd4c*	0.163945107
ENSMUSG00000078566	*Bnip3*	0.163219365
ENSMUSG00000027832	*Ptx3*	0.161592691
ENSMUSG00000025701	*Alox5*	0.159514183
ENSMUSG00000038963	*Slco4a1*	0.154352014
ENSMUSG00000000730	*Dnmt3l*	0.152954014
ENSMUSG00000081169	*Gm12551*	0.152689735
ENSMUSG00000000318	*Clec10a*	0.150755783
ENSMUSG00000032754	*Slc8b1*	0.150596436
ENSMUSG00000074825	*Itpripl1*	0.149818842
ENSMUSG00000071714	*Csf2rb2*	0.146994598
ENSMUSG00000019943	*Atp2b1*	0.145009663
ENSMUSG00000031012	*Cask*	0.144068524
ENSMUSG00000038178	*Slc43a2*	0.142471109
ENSMUSG00000038147	*Cd84*	0.139374521
ENSMUSG00000046908	*Ltb4r1*	0.136444415
ENSMUSG00000066364	*Serpina3b*	0.135366509
ENSMUSG00000032046	*Abhd12*	0.133795823
ENSMUSG00000021069	*Pygl*	0.133632904
ENSMUSG00000042759	*Apobr*	0.129429954
ENSMUSG00000049922	*Slc35c1*	0.127905193
ENSMUSG00000046223	*Plaur*	0.126070289
ENSMUSG00000021068	*Nin*	0.125630874
ENSMUSG00000017760	*Ctsa*	0.113836117
ENSMUSG00000031722	*Hp*	0.113787477
ENSMUSG00000075256	*Cerkl*	0.111510226
ENSMUSG00000072594	*Gm16439*	0.110349795
ENSMUSG00000053846	*Lipg*	0.108619709
ENSMUSG00000026819	*Slc25a25*	0.107673077
ENSMUSG00000053158	*Fes*	0.105094425
ENSMUSG00000034744	*Nagk*	0.104914977
ENSMUSG00000009376	*Met*	0.101220227
ENSMUSG00000024767	*Otub1*	0.096713062
ENSMUSG00000066319	*Rtp3*	0.082512069
ENSMUSG00000009378	*Slc16a12*	0.081715798
ENSMUSG00000023045	*Soat2*	0.081715479
ENSMUSG00000034390	*Cmip*	0.064048061
ENSMUSG00000086862	*Gm13346*	0.063270782
ENSMUSG00000006642	*Tcf23*	0.063067087
ENSMUSG00000032776	*Mctp2*	0.056770178
ENSMUSG00000024730	*Ms4a8a*	0.054571323
ENSMUSG00000001128	*Cfp*	0.054461951
ENSMUSG00000020826	*Nos2*	0.053171077
ENSMUSG00000097855	*A930007I19Rik*	0.04972621
ENSMUSG00000022440	*C1qtnf6*	0.04911162
ENSMUSG00000071657	*Bscl2*	0.047806003
ENSMUSG00000003812	*Dnase2a*	0.046268445
ENSMUSG00000022561	*Gpaa1*	0.044479665
ENSMUSG00000029710	*Ephb4*	0.041953751
ENSMUSG00000028680	*Plk3*	0.040705313
ENSMUSG00000020432	*Tcn2*	0.034597787
ENSMUSG00000081660	*Gm11787*	0.033220833
ENSMUSG00000033249	*Hsf4*	0.021146198

Supplementary Table S7. Gene ontology (GO) enrichment analysis of the hub genes from chronic-magenta module. Enrichment analysis was performed using DAVID (http://david.ncifcrf.gov/).

Annotation Term (Biological Process)	Genes	P-Value	FDR
GO:0030593 neutrophil chemotaxis	*Itgam, C5ar1, Trem1, Vav3, Itgb2*	1.32E-04	0.186527443
GO:0031100 organ regeneration	*Pkm, F7, C5ar1, Anxa3*	0.00122272	1.721293786
GO:0006953 acute-phase response	*Reg3a, Reg3b, Reg3g*	0.007653495	10.32983638
GO:0006096 glycolytic process	*Pfkl, Pkm, Aldoart1*	0.008084152	10.88051921
GO:0006954 inflammatory response	*Reg3a, Reg3b, Reg3g, Slc11a1, C5ar1, Ccr1*	0.00948669	12.65223401
GO:0061097 regulation of protein tyrosine kinase activity	*Rap2b, Rap2c*	0.011240183	14.82122977
GO:0007264 small GTPase mediated signal transduction	*Rhov, Vav3, Rap2b, Rap2c, Rnd1*	0.012006481	15.75329668
GO:0007599 hemostasis	*F7, Anxa5, F2rl3*	0.012964667	16.90542184
GO:0045123 cellular extravasation	*Itgam, Itgb2*	0.014959176	19.25680811
GO:0006909 phagocytosis	*Slc11a1, Anxa3, Itgb2*	0.016371731	20.88453411
GO:0000165 MAPK cascade	*Slc11a1, Dok2, Mapkapk3*	0.027808084	32.98330966
GO:0045617 negative regulation of keratinocyte differentiation	*Reg3a, Reg3g*	0.033348395	38.20414527
GO:0050798 activated T cell proliferation	*Itgam, Itgb2*	0.033348395	38.20414527
GO:0032486 Rap protein signal transduction	*Rap2b, Rap2c*	0.036985439	41.42312937
GO:0010838 positive regulation of keratinocyte proliferation	*Reg3a, Reg3g*	0.036985439	41.42312937
GO:0032496 response to lipopolysaccharide	*Fos, Slc11a1, C5ar1, Mapkapk3*	0.038086133	42.36613856
GO:0042493 response to drug	*Fos, Atp1a1, Por, Vav3, Plin2*	0.03874348	42.92256408
GO:0007596 blood coagulation	*F7, Anxa5, F2rl3*	0.039867233	43.86223881
GO:0035879 plasma membrane lactate transport	*Slc16a3, Emb*	0.040609	44.47459928
GO:0002523 leukocyte migration involved in inflammatory response	*Itgam, Itgb2*	0.047815867	50.10937935
GO:0050830 defense response to Gram-positive bacterium	*Reg3b, Reg3g, C5ar1*	0.047888237	50.16316511
GO:0007229 integrin-mediated signaling pathway	*Itgam, Vav3, Itgb2*	0.047888237	50.16316511
GO:0045824 negative regulation of innate immune response	*Ccr1, Nlrx1*	0.054969386	55.17286757
GO:0098792 xenophagy	*Hilpda, Anxa5, Trem1*	0.057423514	56.79690405
GO:0090303 positive regulation of wound healing	*Reg3a, Reg3g*	0.058526262	57.50869682
GO:0031954 positive regulation of protein autophosphorylation	*Rap2b, Rap2c*	0.065600489	61.82189488
GO:0045766 positive regulation of angiogenesis	*C5ar1, Anxa3, Itgb2*	0.07605794	67.45768865
GO:0002230 positive regulation of defense response to virus by host	*Hilpda, Anxa5, Trem1*	0.077143557	67.99613838
GO:0031668 cellular response to extracellular stimulus	*Fos, Adora2b*	0.079592186	69.18036183
GO:0010575 positive regulation of vascular endothelial growth factor production	*C5ar1, Adora2b*	0.086510418	72.30978161
GO:0007159 leukocyte cell-cell adhesion	*Itgam, Itgb2*	0.086510418	72.30978161
GO:0045672 positive regulation of osteoclast differentiation	*Fos, Ccr1*	0.089950294	73.75335068

Supplementary Table S8. Ranked table of differentially expressed genes between early and late effector CD8$^+$ T cells using the "Population Comparison" tool from ImmGen data set (http://www.immgen.org/). Shown are list of genes always expressed in OVA-specific effector CD8$^+$ T cells 12 and 24 hours postinfection with LisOva (Group A) and never expressed in OVA-specific effector CD8$^+$ T cells at days 5, 6 and 8 postinfection with LisOva or VSVOva (Group B). Genes in bold were selected for protein expression analysis by FACS. Min (minimum expression value), Max (maximum expression value) and Mean (mean expression value).

ProbeSet ID	Gene symbol	Gene description	NCBI ID	Mean Fold Change	Group A			Group B		
					Min	Max	Mean	Min	Max	Mean
10582545	*Mela*	melanoma antigen	17276	92.72	1924	1957	1940	18	26	21
10385918	*Il3*	interleukin 3	16187	43.46	428	1495	800	17	20	18
10497878	*Il2*	interleukin 2	16183	37.94	612	1137	834	18	25	22
10531415	*Cxcl10*	chemokine (C-X-C motif) ligand 10	15945	25.92	1348	1782	1550	50	71	60
10359697	***Xcl1***	**chemokine (C motif) ligand 1**	**16963**	**25.14**	**1266**	**1715**	**1473**	**45**	**72**	**59**
10373918	*Lif*	leukemia inhibitory factor	16878	18.49	629	1005	795	37	51	43
10513729	***Tnfsf8***	**tumor necrosis factor (ligand) superfamily member 8**	**21949**	**16.89**	**803**	**1076**	**930**	**47**	**78**	**55**
10504838	*Nr4a3*	nuclear receptor subfamily 4 group A member 3	18124	16.4	952	1388	1150	65	75	70
10379721	*Ccl4*	chemokine (C-C motif) ligand 4	20303	10.62	839	1063	944	65	113	89
10388784	*Rpl23a*	ribosomal protein L23a	268449	10.28	615	689	651	36	105	63
10539592	*Smyd5*	SET and MYND domain containing 5	232187	10.01	901	905	903	74	115	90
10366796	*Mettl1*	methyltransferase like 1	17299	9.84	671	743	706	51	107	72
10439532	*Qtrtd1*	queuine tRNA-ribosyltransferase domain containing 1	106248	9.78	612	788	695	63	80	71
10450363	*Snord52*	small nucleolar RNA C/D box 52	100217427	9.52	254	378	310	29	36	33
10351039	*Gas5*	growth arrest specific 5	14455	9.52	484	501	492	32	76	52
10446907	*Ttc27*	tetratricopeptide repeat domain 27	74196	9.27	616	631	623	45	111	67
10408666	*Rpp40*	ribonuclease P 40 subunit (human)	208366	8.95	147	206	174	16	22	19
10462623	*Ifit1*	interferon-induced protein with tetratricopeptide repeats 1	15957	8.29	503	568	535	52	76	65
10524621	*Oasl2*	2'-5' oligoadenylate synthetase-like 2	23962	8.24	667	684	675	71	112	82
10607870	***Tlr7***	**toll-like receptor 7**	**170743**	**8.02**	**120**	**155**	**137**	**15**	**19**	**17**
10416950	*Mir18*		NA	7.94	128	150	138	15	20	17
10355037	*Wdr12*	WD repeat domain 12	57750	7.67	522	535	529	50	102	69
10604076	*Snora69*	small nucleolar RNA H/ACA box 69	104369	7.61	380	399	390	31	74	51
10406852	*Cnn3*	calponin 3 acidic	71994	7.44	166	173	170	20	27	23
10461148	*Snhg1*	small nucleolar RNA host gene (non-protein coding) 1	83673	7.19	305	437	365	29	110	51
10355984	*Serpine2*	serine (or cysteine) peptidase inhibitor clade E member 2	20720	7.16	147	425	250	33	38	35
10546346	*Chchd4*	coiled-coil-helix-coiled-coil-helix domain containing 4	72170	7.07	517	604	559	63	112	79
10558580	*Ufl1*	undifferentiated embryonic cell transcription factor 1	22286	7.01	272	339	304	36	46	43
10586591	*Car12*	carbonic anyhydrase 12	76459	7.01	356	374	365	45	57	52
10439651	*Cd200*	CD200 antigen	17470	6.99	275	397	331	34	66	47
10373452	*Gm129*	predicted gene 129	229599	6.69	241	274	257	29	52	38
10462618	*Ifit3*	interferon-induced protein with tetratricopeptide repeats 3	15959	6.45	344	367	355	39	67	55
10445767	*Treml2*	triggering receptor expressed on myeloid cells-like 2	328833	6.43	495	560	526	73	90	82
10516064	*Mfsd2a*	major facilitator superfamily domain containing 2	76574	6.37	491	542	516	68	110	81
10398717	*Trmt61a*	tRNA methyltransferase 61 homolog A (S. cerevisiae)	328162	6.36	578	578	578	78	104	91
10569017	*Ifitm3*	interferon induced transmembrane protein 3	66141	6.28	222	301	258	22	84	41
10541091	*Gemin6*	gem (nuclear organelle) associated protein 6	67242	6.14	235	330	279	29	77	45
10595452	*Ube2cbp*	ubiquitin-conjugating enzyme E2C binding protein	70348	6.02	413	530	468	68	90	78
10590620	***Ccr9***	**chemokine (C-C motif) receptor 9**	**12769**	**5.93**	**213**	**247**	**229**	**34**	**43**	**39**
10350159	*Lad1*	ladinin	16763	5.92	423	593	501	70	102	85
10405211	*Gadd45g*	growth arrest and DNA-damage-inducible 45 gamma	23882	5.79	386	503	441	68	94	76
10399882	*Dus4l*	dihydrouridine synthase 4-like (S. cerevisiae)	71916	5.79	288	327	307	38	78	53
10399710	*Rsad2*	radical S-adenosyl methionine domain containing 2	58185	5.76	322	332	327	50	71	57
10363735	*Egr2*	early growth response 2	13654	5.72	426	485	455	63	96	80
10436662	*Mir155*		NA	5.63	304	423	358	57	78	64
10466818	*Cbwd1*	COBW domain containing 1	226043	5.56	303	317	309	35	94	56
10434441	*Ece2*	endothelin converting enzyme 2	107522	5.55	365	376	370	58	75	67
10353034	*Snord87*	small nucleolar RNA C/D box 87	266793	5.31	271	335	301	38	80	57
10538791	*Tnip3*	TNFAIP3 interacting protein 3	414084	5.29	132	133	132	22	29	25
10508721	*Snora44*	small nucleolar RNA H/ACA box 44	100217418	5.08	350	436	391	68	81	77
10368277	*Rps12*	ribosomal protein S12	20042	5.06	377	403	390	62	98	77
10503643	*Ndufaf4*	NADH dehydrogenase (ubiquinone) 1 alpha subcomplex assembly factor 4	68493	5.05	468	501	484	80	115	96
10455961	*Iigp1*	interferon inducible GTPase 1	60440	4.97	127	181	152	26	33	31
10592888	*Cxcr5*	chemochine (C-X-C motif) receptor 5	12145	4.94	141	145	143	27	35	29
10466104	*Ccdc86*	coiled-coil domain containing 86	108673	4.89	509	514	511	84	119	105
10447097	*Gemin6*	gem (nuclear organelle) associated protein 6	67242	4.84	334	379	356	55	107	74
10495659	*Cnn3*	calponin 3 acidic	71994	4.79	295	308	301	61	66	63
10473363	*Timm10*	translocase of inner mitochondrial membrane 10 homolog (yeast)	30059	4.75	296	377	334	55	81	70
10582020	*Gcsh*	glycine cleavage system protein H (aminomethyl carrier)	68133	4.64	122	122	122	21	33	26
10379034	*Tlcd1*	TLC domain containing 1	68385	4.59	360	365	362	70	94	79
10539702	*Fam136a*	family with sequence similarity 136 member A	66488	4.58	225	245	235	33	82	51
10400383	*2700097O09Rik*	RIKEN cDNA 2700097O09 gene	72658	4.57	195	244	218	34	74	48
10514466	*Jun*	Jun oncogene	16476	4.5	281	315	298	54	81	66
10533198	*Oas2*	2'-5' oligoadenylate synthetase 2	246728	4.48	311	414	359	69	97	80
10500272	*Gm129*	predicted gene 129	229599	4.47	201	247	223	37	60	50
10440077	*2610528E23Rik*	RIKEN cDNA 2610528E23 gene	66497	4.46	325	353	339	62	98	76
10419216	*Gnpnat1*	glucosamine-phosphate N-acetyltransferase 1	54342	4.44	343	431	384	68	116	87
10359689	*Atp1b1*	ATPase Na+/K+ transporting beta 1 polypeptide	11931	4.43	262	333	295	55	91	67
10539933	*Txnrd3*	thioredoxin reductase 3	232223	4.36	142	158	150	29	40	34
10405158	*Pus7*	pseudouridylate synthase 7 homolog (S. cerevisiae)	78697	4.32	148	206	175	34	53	40
10395273	*Gdap10*	ganglioside-induced differentiation-associated-protein 10	14546	4.3	203	257	229	39	64	53
10571984	*Ddx60*	DEAD (Asp-Glu-Ala-Asp) box polypeptide 60	234311	4.28	320	349	334	60	116	78
10451287	*Isg15*	ISG15 ubiquitin-like modifier	100038882	4.25	193	219	205	45	52	48
10546710	*Shq1*	SHQ1 homolog (S. cerevisiae)	72171	4.19	330	404	365	74	107	87
10375975	*Zcchc10*	zinc finger CCHC domain containing 10	67966	4.19	160	164	162	30	61	39
10562096	*Tmem147*	transmembrane protein 147	69804	4.15	313	388	348	62	109	84
10416945	*Mir17hg*	microRNA host gene 1 (non-protein coding)	75957	4.14	169	183	176	33	61	43
10346876	*Snora41*	small nucleolar RNA H/ACA box 41	100217464	4.11	147	164	155	31	47	38
10485624	*Prrg4*	proline rich Gla (G-carboxyglutamic acid) 4 (transmembrane)	228413	4.1	160	220	187	39	55	46
10355464	*Pecr*	peroxisomal trans-2-enoyl-CoA reductase	111175	4.08	139	165	152	29	46	37
10463263	*Lztfl1*	leucine zipper transcription factor-like 1	93730	4.01	173	288	223	40	83	56
10432176	*Snora34*	small nucleolar RNA H/ACA box 34	100217417	4	177	183	180	29	57	45
10552118	*LOC100504758*	similar to SMT3B protein	100044517	4	197	295	241	47	89	60
10416958	*Mir92-1*		NA	3.99	164	226	192	39	62	48
10482772	*Nr4a2*	nuclear receptor subfamily 4 group A member 2	18227	3.92	255	445	336	72	109	86
10497703	*Mrpl47*	mitochondrial ribosomal protein L47	74600	3.88	217	255	235	41	77	61
10472994	*Mtx2*	metaxin 2	53375	3.88	231	290	259	51	99	67
10391985	*Taf1d*	TATA box binding protein (Tbp)-associated factor RNA polymerase I D	75316	3.81	256	259	258	47	108	68
10362896	*Cd24a*	CD24a antigen	12484	3.79	151	164	157	30	70	42
10381096	*Igfbp4*	insulin-like growth factor binding protein 4	16010	3.73	243	408	315	65	110	85
10406865	*Mrps27*	mitochondrial ribosomal protein S27	218506	3.71	209	275	240	55	82	65
10450508	*Lta*	lymphotoxin A	16992	3.71	196	271	231	51	73	62
10400883	*Timm9*	translocase of inner mitochondrial membrane 9 homolog (yeast)	30056	3.69	172	175	174	35	58	47
10434758	*St6gal1*	beta galactoside alpha 26 sialyltransferase 1	20440	3.64	157	208	180	45	57	50
10404840	***Cd83***	**CD83 antigen**	**12522**	**3.63**	**266**	**368**	**313**	**71**	**104**	**86**
10526693	*Zcwpw1*	zinc finger CW type with PWWP domain 1	381678	3.63	214	216	215	42	93	59
10364955	*Thop1*	thimet oligopeptidase 1	50492	3.53	294	300	297	72	109	84

10558134	*Plekha1*	pleckstrin homology domain containing family A (phosphoinositide binding specific) member 1	101476	3.51	265	279	272	68	98	77
10353460	*Kcnq5*	potassium voltage-gated channel subfamily Q member 5	226922	3.49	173	258	211	46	79	60
10390505	*Snora21*	small nucleolar RNA H/ACA box 21	100302498	3.47	196	220	208	44	75	60
10496748	*Syde2*	synapse defective 1 Rho GTPase homolog 2 (C. elegans)	214804	3.39	126	130	128	31	41	38
10474671	*Spred1*	sprouty protein with EVH-1 domain 1 related sequence	114715	3.37	202	233	217	48	87	64
10382838	*1810032O08Rik*	RIKEN cDNA 1810032O08 gene	66293	3.37	232	255	243	64	78	72
10475648	*Dtwd1*	DTW domain containing 1	69185	3.37	279	295	287	80	91	85
10564520	*Snora21*	small nucleolar RNA H/ACA box 21	100302498	3.35	190	220	205	42	80	61
10398693	*Snora28*	eukaryotic translation initiation factor 5	217869	3.32	306	332	319	69	116	96
10416230	*Tnfrsf10b*	tumor necrosis factor receptor superfamily member 10b	21933	3.31	152	217	182	50	65	55
10526345	*Nsun5*	NOL1/NOP2/Sun domain family member 5	100609	3.3	321	326	323	87	108	98
10441813	*Snora20*	t-complex protein 1	21454	3.29	173	203	187	30	76	57
10487021	*Slc30a4*	solute carrier family 30 (zinc transporter) member 4	22785	3.27	187	200	193	37	102	59
10410877	*Polr3g*	polymerase (RNA) III (DNA directed) polypeptide G	67486	3.25	226	233	230	60	83	71
10438726	*Masp1*	mannan-binding lectin serine peptidase 1	17174	3.22	139	147	143	34	57	44
10497209	*Mrps28*	mitochondrial ribosomal protein S28	66230	3.22	220	247	233	59	83	72
10508686	*Mecr*	mitochondrial trans-2-enoyl-CoA reductase	26922	3.22	242	254	248	60	107	77
10387219	*Rangrf*	RAN guanine nucleotide release factor	57785	3.21	199	201	200	54	69	62
10400006	*Ahr*	aryl-hydrocarbon receptor	11622	3.19	279	333	305	82	118	95
10580382	*Neto2*	neuropilin (NRP) and tolloid (TLL)-like 2	74513	3.17	141	151	146	28	102	46
10540911	*Tsen2*	tRNA splicing endonuclease 2 homolog (S. cerevisiae)	381802	3.14	174	186	180	47	77	57
10435489	*Ccdc58*	coiled-coil domain containing 58	381045	3.14	272	272	272	62	118	87
10578964	*1810029B16Rik*	RIKEN cDNA 1810029B16 gene	66282	3.13	175	193	184	51	73	59
10463836	*Gsto1*	glutathione S-transferase omega 1	14873	3.13	230	274	251	62	117	80
10360684	*Ephx1*	epoxide hydrolase 1 microsomal	13849	3.13	287	301	294	84	106	94
10589413	*Nme6*	non-metastatic cells 6 protein expressed in (nucleoside-diphosphate kinase)	54369	3.1	284	295	290	81	117	93
10428066	*1700084J12Rik*	RIKEN cDNA 1700084J12 gene	73486	3.1	248	281	264	66	104	85
10484389	*Tfpi*	tissue factor pathway inhibitor	21788	3.09	132	156	144	43	52	47
10490838	*Fabp5*	fatty acid binding protein 5 epidermal	16592	3.07	127	159	142	41	62	46
10497587	*1600012F09Rik*	RIKEN cDNA 1600012F09 gene	67008	3.06	246	251	249	65	103	81
10452307	*Tnfsf14*	tumor necrosis factor (ligand) superfamily member 14	50930	3.05	260	313	285	82	102	93
10436169	*Ift57*	intraflagellar transport 57 homolog (Chlamydomonas)	73916	3.01	161	190	175	47	77	58
10490894	*E2f5*	E2F transcription factor 5	13559	2.95	160	197	178	46	69	60
10585699	*Fabp5*	fatty acid binding protein 5 epidermal	16592	2.92	180	224	200	59	89	69
10509163	*Id3*	inhibitor of DNA binding 3	15903	2.92	197	243	219	62	102	75
10520800	*Gpn1*	GPN-loop GTPase 1	74254	2.92	252	279	265	71	113	91
10385507	*Gm12185*	predicted gene OTTMUSG00000005523	620913	2.88	165	205	184	54	80	64
10565775	*Dgat2*	diacylglycerol O-acyltransferase 2	67800	2.85	258	266	262	83	104	92
10568553	*Chst15*	carbohydrate (N-acetylgalactosamine 4-sulfate 6-O) sulfotransferase 15	77590	2.84	167	171	169	50	70	59
10472860	*Rapgef4*	Rap guanine nucleotide exchange factor (GEF) 4	56508	2.83	201	277	236	68	97	84
10407057	*Ercc8*	excision repaiross-complementing rodent repair deficiency complementation group 8	71991	2.8	160	160	160	50	66	57
10496015	*Pla2g12a*	phospholipase A2 group XIIA	66350	2.79	217	227	222	77	88	79
10437174	*Wrb*	tryptophan rich basic protein	71446	2.77	222	257	239	75	100	86
10417183	*Pcca*	propionyl-Coenzyme A carboxylase alpha polypeptide	110821	2.77	218	236	227	65	91	82
10403756	*1600012F09Rik*	RIKEN cDNA 1600012F09 gene	67008	2.76	183	190	187	50	91	68
10397346	*Fos*	FBJ osteosarcoma oncogene	14281	2.76	160	224	189	57	84	68
10480921	*Qsox2*	quiescin Q6 sulfhydryl oxidase 2	227638	2.74	168	172	170	53	72	62
10389062	*1700071K01Rik*	RIKEN cDNA 1700071K01 gene	237880	2.74	185	240	210	69	93	77
10491721	*Spry1*	sprouty homolog 1 (Drosophila)	24063	2.71	154	263	201	60	82	74
10386844	*Zswim7*	zinc finger SWIM-type containing 7	69747	2.71	192	256	222	76	101	82
10460585	*Fosl1*	fos-like antigen 1	14283	2.7	127	177	150	46	66	56
10359506	*Mettl13*	methyltransferase like 13	71449	2.67	240	241	240	78	99	90
10607465	*Gm4997*		NA	2.66	123	148	135	37	66	51
10508645	*Snord85*	small nucleolar RNA C/D box 85	100217460	2.65	140	146	143	42	67	54
10550906	*Plaur*	plasminogen activator urokinase receptor	18793	2.65	127	235	173	57	77	65
10454782	*Egr1*	early growth response 1	13653	2.62	185	243	212	72	89	81
10529052	*Slc5a6*	solute carrier family 5 (sodium-dependent vitamin transporter) member 6	330064	2.61	212	226	219	76	96	84
10555011	*Nars2*	asparaginyl-tRNA synthetase 2 (mitochondrial)(putative)	244141	2.61	255	260	258	74	120	99
10570764	*Alg11*	asparagine-linked glycosylation 11 homolog (yeast alpha-12-mannosyltransferase)	207958	2.61	192	234	212	73	94	81
10470905	*Set*	SET translocation	56086	2.6	186	192	189	71	74	73
10532019	*Gbp11*	predicted gene EG634650	634650	2.6	212	219	215	54	107	83
10561831	*Zfp566*	zinc finger protein 566	72556	2.59	164	185	174	55	78	67
10540227	*Kbtbd8*	kelch repeat and BTB (POZ) domain containing 8	243574	2.58	172	185	178	50	112	69
10423293	*Myo10*	myosin X	17909	2.56	147	183	164	57	75	64
10483521	*Fastkd1*	FAST kinase domains 1	320720	2.54	222	232	227	72	114	89
10548815	*E330021D16Rik*	ubiquitin-conjugating enzyme E2Q (putative) 2 pseudogene	243676	2.53	138	154	146	48	70	58
10445241	*Tnfrsf21*	tumor necrosis factor receptor superfamily member 21	94185	2.52	204	222	213	73	104	85
10497773	*Mccc1*	methylcrotonoyl-Coenzyme A carboxylase 1 (alpha)	72039	2.52	208	222	215	77	97	85
10487476	*1500011K16Rik*	RIKEN cDNA 1500011K16 gene	67885	2.51	185	215	199	77	81	79
10515528	*Dph2*	DPH2 homolog (S. cerevisiae)	67728	2.46	232	265	248	90	111	101
10365003	*Snord37*	small nucleolar RNA C/D box 37	100217454	2.45	161	199	179	62	85	73
10576896	*Gm9457*	predicted gene 9457	669393	2.44	163	202	181	50	95	74
10373355	*Spryd4*	SPRY domain containing 4	66701	2.41	180	184	182	58	88	76
10427015	*Acvr1b*	activin A receptor type 1B	11479	2.38	193	195	194	73	87	82
10588836	*Gmppb*	GDP-mannose pyrophosphorylase B	331026	2.38	155	162	158	55	88	67
10428579	*Ext1*	exostoses (multiple) 1	14042	2.38	194	217	205	72	105	86
10469110	*Usp6nl*	USP6 N-terminal like	98910	2.38	152	176	164	47	92	69
10396699	*Fntb*	farnesyltransferase CAAX box beta	110606	2.36	170	190	180	63	99	76
10500434	*Bcl9*	B-cell CLL/lymphoma 9	77578	2.35	132	144	138	53	64	59
10485633	*Gm10796*	predicted gene 10796	100038694	2.35	146	167	156	44	85	66
10396778	*Mpp5*	membrane protein palmitoylated 5 (MAGUK p55 subfamily member 5)	56217	2.34	145	158	151	48	81	65
10518726	*Slc25a33*	solute carrier family 25 member 33	70556	2.34	181	194	188	75	85	80
10406614	*Mtx3*	metaxin 3	382793	2.34	207	229	218	81	106	93
10436865	*Ifngr2*	interferon gamma receptor 2	15980	2.33	164	175	169	55	99	73
10353288	*Ube2w*	ubiquitin-conjugating enzyme E2W (putative)	66799	2.32	151	187	168	51	89	72
10419288	*Gch1*	GTP cyclohydrolase 1	14528	2.32	139	148	143	55	68	62
10389701	*Akap1*	A kinase (PRKA) anchor protein 1	11640	2.31	202	224	213	79	116	92
10496417	*Rg9mtd2*	RNA (guanine-9-) methyltransferase domain containing 2	108943	2.31	200	200	200	69	109	87
10458992	*C330018D20Rik*	RIKEN cDNA C330018D20 gene	77422	2.3	144	157	150	51	85	65
10536794	*2310016C08Rik*	RIKEN cDNA 2310016C08 gene	69573	2.3	132	135	134	53	62	58
10407387	*Gm7120*	predicted gene 7120	633640	2.27	200	251	224	80	112	99
10596465	*Acy1*	aminoacylase 1	109652	2.26	219	236	227	94	110	100
10430113	*Arhgap39*	DNA segment Chr 15 Wayne State University 169 expressed	223666	2.26	182	184	183	51	98	81
10368720	*Slc16a10*	solute carrier family 16 (monocarboxylic acid transporters) member 10	72472	2.26	158	160	159	65	78	70
10576482	*Arv1*	ARV1 homolog (yeast)	68865	2.25	231	254	242	93	116	108
10540215	*Slc25a26*	solute carrier family 25 (mitochondrial carrier phosphate carrier) member 26	67582	2.23	213	230	221	79	109	99
10587534	*Bckdhb*	branched chain ketoacid dehydrogenase E1 beta polypeptide	12040	2.23	136	145	141	56	69	63
10394245	*Dnajc27*	DnaJ (Hsp40) homolog subfamily C member 27	217378	2.21	183	195	189	73	100	85
10401713	*Pomt2*	protein-O-mannosyltransferase 2	217734	2.2	206	235	220	92	110	100
10439542	*Zdhhc23*	zinc finger DHHC domain containing 23	332175	2.19	156	194	174	62	106	80

10558914	*Rplp2*	ribosomal protein large P2	67186	2.18	178	208	192	83	93	88
10375019	*Nsg2*	neuron specific gene family member 2	18197	2.13	185	261	220	85	120	104
10579209	*Armc6*	armadillo repeat containing 6	76813	2.12	205	211	208	83	112	98
10384968	*Bod1*	biorientation of chromosomes in cell division 1	69556	2.12	219	222	221	92	119	104
10496485	*Eif4e*	eukaryotic translation initiation factor 4E	13684	2.11	152	164	158	59	93	75
10577517	*Slc25a15*	solute carrier family 25 (mitochondrial carrier ornithine transporter) member 15	18408	2.09	193	237	214	95	108	102
10585956	*Myo9a*	myosin IXa	270163	2.09	128	135	132	46	75	63
10506058	*Inadl*	InaD-like (Drosophila)	12695	2.09	124	146	134	51	78	64
10434191	*Txnrd2*	thioredoxin reductase 2	26462	2.09	168	168	168	66	94	80
10353750	*Bag2*	BCL2-associated athanogene 2	213539	2.09	139	184	160	72	85	77
10425267	*Pick1*	protein interacting with C kinase 1	18693	2.08	165	177	171	77	92	82
10453792	*Thoc1*	THO complex 1	225160	2.08	134	150	142	58	82	68
10471486	*Eng*	endoglin	13805	2.04	160	204	181	75	106	88
10544497	*Tarbp2*	TAR (HIV) RNA binding protein 2	21357	2.04	142	143	143	59	84	70
10585982	*Myo9a*	myosin IXa	270163	2.04	146	150	148	55	87	73
10362394	*Hddc2*	HD domain containing 2	69692	2.04	128	207	163	59	101	80
10360003	*Dusp12*	dual specificity phosphatase 12	80915	2.04	202	202	202	85	118	99
10554017	*Lins*	lines homolog 2 (Drosophila)	72635	2.03	153	167	160	72	88	79
10403716	*AW209491*	expressed sequence AW209491	105351	2.02	194	218	206	98	106	102
10577025	*Rab20*	RAB20 member RAS oncogene family	19332	2.02	162	193	177	78	102	88
10445558	*BC048355*	cDNA sequence BC048355	381101	2.01	144	201	170	74	110	85
10392701	*Slc39a11*	solute carrier family 39 (metal ion transporter) member 11	69806	2	206	224	215	101	119	108
10448842	*Telo2*	TEL2 telomere maintenance 2 homolog (S. cerevisiae)	71718	1.99	182	188	185	75	102	93
10397561	*Adck1*	aarF domain containing kinase 1	72113	1.98	184	208	196	82	109	99
10365870	*Nr2c1*	nuclear receptor subfamily 2 group C member 1	22025	1.98	136	147	141	68	75	72
10350024	*Klhl12*	kelch-like 12 (Drosophila)	240756	1.98	155	160	158	64	91	79
10541094	*Zfp637*	zinc finger protein 637	232337	1.98	134	162	148	60	90	75
10506781	*2010305A19Rik*	RIKEN cDNA 2010305A19 gene	69893	1.98	150	173	161	68	92	81
10359201	*Ralgps2*	Ral GEF with PH domain and SH3 binding motif 2	78255	1.96	149	162	155	63	92	79
10375667	*Rnf130*	ring finger protein 130	59044	1.96	129	131	130	57	78	67
10489051	*5730471H19Rik*	RIKEN cDNA 5730471H19 gene	632764	1.95	148	165	156	62	90	80
10463448	*Peo1*	progressive external ophthalmoplegia 1 (human)	226153	1.95	170	189	179	74	119	92
10453555	*2610044O15Rik*	RIKEN cDNA 2610044O15 gene	72139	1.95	156	157	157	59	114	80
10430783	*Polr3h*	polymerase (RNA) III (DNA directed) polypeptide H	78929	1.94	125	137	131	56	75	68
10350146	*Phlda3*	pleckstrin homology-like domain family A member 3	27280	1.94	136	241	181	83	119	93
10377938	*Eno3*	enolase 3 beta muscle	13808	1.94	160	199	178	78	102	92
10457357	*Mpp7*	membrane protein palmitoylated 7 (MAGUK p55 subfamily member 7)	75739	1.93	124	133	128	55	109	67
10558961	*Tspan4*	tetraspanin 4	64540	1.92	189	191	190	84	106	99
10367973	*Aig1*	androgen-induced 1	66253	1.91	155	190	172	82	100	90
10371293	*1190007I07Rik*	RIKEN cDNA 1190007I07 gene	544717	1.9	179	189	184	84	119	97
10585986	*Myo9a*	myosin IXa	270163	1.9	145	149	147	63	93	77
10502973	*Tyw3*	tRNA-yW synthesizing protein 3 homolog (S. cerevisiae)	209584	1.89	162	163	162	82	98	86
10492846	*Pet112l*	PET112-like (yeast)	229487	1.89	168	200	183	78	115	97
10471337	*Pomt1*	protein-O-mannosyltransferase 1	99011	1.88	135	137	136	54	89	72
10405013	*Ippk*	inositol 13456-pentakisphosphate 2-kinase	75678	1.88	165	189	176	74	116	94
10557009	*Eef2k*	eukaryotic elongation factor-2 kinase	13631	1.88	131	138	134	64	82	71
10405950	*Fastkd3*	FAST kinase domains 3	69577	1.88	160	181	170	73	112	90
10526520	*Plod3*	procollagen-lysine 2-oxoglutarate 5-dioxygenase 3	26433	1.86	155	173	164	84	94	88
10575609	*Zfp1*	zinc finger protein 1	22640	1.86	163	180	171	80	107	92
10410743	*Ankrd32*	ankyrin repeat domain 32	105377	1.85	122	165	142	56	112	77
10441740	*Agpat4*	1-acylglycerol-3-phosphate O-acyltransferase 4 (lysophosphatidic acid acyltransferase delta)	68262	1.85	179	193	186	92	112	100
10404531	*Psmg4*	proteasome (prosome macropain) assembly chaperone 4	69666	1.85	166	167	166	81	96	90
10472794	*Metap1d*	methionine aminopeptidase-like 1	66559	1.84	156	166	161	81	94	88
10444046	*Cd320*	CD320 antigen	54219	1.83	163	185	174	83	106	95
10440037	*Nit2*	nitrilase family member 2	52633	1.83	160	181	170	73	111	93
10409709	*Mir7-1*		NA	1.83	156	163	159	75	94	87
10579607	*B3gnt3*	UDP-GlcNAc:betaGal beta-13-N-acetylglucosaminyltransferase 3	72297	1.81	155	156	155	70	117	86
10586724	*Narg2*	NMDA receptor-regulated gene 2	93697	1.81	170	178	174	83	116	96
10433963	*Ydjc*	YdjC homolog (bacterial)	69101	1.81	162	171	166	76	108	92
10361091	*Atf3*	activating transcription factor 3	11910	1.81	126	207	161	75	104	89
10584541	*Zfp202*	zinc finger protein 202	80902	1.81	154	160	157	73	109	87
10530145	*Tlr1*	toll-like receptor 1	21897	1.81	171	175	173	76	119	96
10508651	*Sdc3*	syndecan 3	20970	1.81	132	178	153	77	93	85
10526120	*Tpst1*	protein-tyrosine sulfotransferase 1	22021	1.8	151	166	158	67	120	88
10366698	*BC048403*	cDNA sequence BC048403	270802	1.8	180	187	183	85	118	102
10449236	*Nme4*	non-metastatic cells 4 protein expressed in	56520	1.8	121	129	125	62	79	70
10425000	*Lrrc14*	leucine rich repeat containing 14	223664	1.79	182	185	184	88	108	103
10567626	*Gga2*	golgi associated gamma adaptin ear containing ARF binding protein 2	74105	1.79	148	159	154	77	105	86
10550730	*Zfp296*	zinc finger protein 296	63872	1.78	129	135	132	67	85	74
10536541	*St7*	suppression of tumorigenicity 7	64213	1.77	159	159	159	72	112	90
10533462	*Rad9b*	RAD9 homolog B (S. cerevisiae)	231724	1.77	121	121	121	61	78	68
10354792	*1110034B05Rik*	RIKEN cDNA 1110034B05 gene	68736	1.76	149	161	155	66	109	88
10551529	*LOC100503763*		NA	1.76	176	180	178	82	118	101
10585601	*Snupn*	snurportin 1	66069	1.76	123	137	130	60	96	74
10440840	*1110004E09Rik*	RIKEN cDNA 1110004E09 gene	68001	1.76	144	144	144	73	92	82
10431463	*Fam116b*	family with sequence similarity 116 member B	69440	1.75	139	149	144	65	109	82
10487433	*Zfp661*	zinc finger protein 661	72180	1.74	145	161	153	81	95	88
10555293	*Lipt2*	RIKEN cDNA 2610209A20 gene	67164	1.74	127	132	129	64	88	74
10471844	*Nek6*	NIMA (never in mitosis gene a)-related expressed kinase 6	59126	1.74	151	182	166	90	110	95
10527229	*2810453I06Rik*	RIKEN cDNA 2810453I06 gene	67238	1.73	150	153	151	76	97	87
10481383	*Wdr34*	WD repeat domain 34	71820	1.73	168	195	181	88	117	104
10393272	*Rnf157*	ring finger protein 157	217340	1.73	152	176	163	89	102	94
10485429	*Pdhx*	pyruvate dehydrogenase complex component X	27402	1.72	143	163	153	64	119	89
10473356	*Ube2l6*	ubiquitin-conjugating enzyme E2L 6	56791	1.71	122	125	124	67	84	72
10364102	*Chchd10*	coiled-coil-helix-coiled-coil-helix domain containing 10	103172	1.71	141	172	156	83	105	91
10396372	*Mnat1*	menage a trois 1	17420	1.71	145	155	150	61	112	87
10518364	*Rps19-ps3*	ribosomal protein S19 pseudogene	277692	1.71	139	164	151	69	97	88
10529402	*Tnip2*	TNFAIP3 interacting protein 2	231130	1.71	149	154	151	78	101	89
10397216	*Coq6*	coenzyme Q6 homolog (yeast)	217707	1.7	123	137	130	64	100	77
10443201	*Pacsin1*	protein kinase C and casein kinase substrate in neurons 1	23969	1.7	142	142	142	70	90	84
10511975	*Slc35a1*	solute carrier family 35 (CMP-sialic acid transporter) member 1	24060	1.7	160	174	167	87	114	98
10500610	*Fam46c*	family with sequence similarity 46 member C	74645	1.68	127	133	130	67	92	78
10580752	*9330175E14Rik*	RIKEN cDNA 9330175E14 gene	320377	1.68	120	121	120	56	111	72
10546510	*Lrig1*	leucine-rich repeats and immunoglobulin-like domains 1	16206	1.68	120	121	121	58	87	72
10422512	*A2ld1*	AIG2-like domain 1	223267	1.68	167	174	170	93	110	102
10401309	*Cox16*	COX16 cytochrome c oxidase assembly homolog (S. cerevisiae)	66272	1.68	134	169	151	75	108	90
10356771	*Mterfd2*	MTERF domain containing 2	69821	1.68	121	134	127	69	84	76
10584435	*Vwa5a*	von Willebrand factor A domain containing 5A	67776	1.67	134	147	140	62	104	84
10441436	*Snx9*	sorting nexin 9	66616	1.67	123	135	129	60	105	77
10427026	*Grasp*	GRP1 (general receptor for phosphoinositides 1)-associated scaffold protein	56149	1.66	135	158	146	80	100	88

10373000	*Xrcc6bp1*	XRCC6 binding protein 1	68876	1.66	156	171	164	93	108	99
10595664	*Tmed3*	transmembrane emp24 domain containing 3	66111	1.65	130	158	143	73	114	87
10571312	*Dusp4*	dual specificity phosphatase 4	319520	1.64	123	153	137	62	112	84
10533633	*Diablo*	diablo homolog (Drosophila)	66593	1.63	155	157	156	76	112	96
10585823	*1600029O15Rik*	RIKEN cDNA 1600029O15 gene	442832	1.63	161	163	162	80	106	99
10386460	*Pemt*	phosphatidylethanolamine N-methyltransferase	18618	1.62	130	138	134	73	91	83
10597095	*3000002C10Rik*	glyceraldehyde-3-phosphate dehydrogenase pseudogene	378954	1.62	131	133	132	68	105	82
10416753	*Pibf1*	progesterone immunomodulatory binding factor 1	52023	1.62	143	147	145	73	103	89
10387659	*Nlgn2*	neuroligin 2	216856	1.61	149	154	151	84	109	94
10438103	*Ccdc116*	coiled-coil domain containing 116	76872	1.61	127	173	148	79	106	92
10581926	*Adat1*	adenosine deaminase tRNA-specific 1	30947	1.6	123	126	124	66	89	78
10481101	*Snora43*	small nucleolar RNA host gene (non-protein coding) 7	72091	1.6	154	175	164	95	112	102
10542757	*Stk38l*	serine/threonine kinase 38 like	232533	1.6	128	135	131	69	95	82
10590383	*Deb1*	differentially expressed in B16F10 1	26901	1.59	121	138	129	69	93	81
10585970	*Myo9a*	myosin IXa	270163	1.59	146	166	156	80	113	98
10561777	*BC027344*	cDNA sequence BC027344	233057	1.58	136	146	141	84	101	89
10389164	*Pex12*	peroxisomal biogenesis factor 12	103737	1.58	136	142	139	76	99	88
10482172	*Zbtb26*	zinc finger and BTB domain containing 26	320633	1.58	152	154	153	75	113	97
10408610	*Tubb2a*	tubulin beta 2A	22151	1.58	136	141	138	71	105	88
10543725	*Tsga14*	testis specific gene A14	83922	1.57	134	152	143	77	111	91
10488748	*Cdk5rap1*	CDK5 regulatory subunit associated protein 1	66971	1.57	137	149	143	73	104	91
10535184	*Psmg3*	proteasome (prosome macropain) assembly chaperone 3	66506	1.56	128	139	133	71	97	86
10508001	*9930104L06Rik*	RIKEN cDNA 9930104L06 gene	194268	1.56	134	141	137	80	104	88
10395855	*Mipol1*	predicted gene 5081	328099	1.55	143	147	145	87	96	94
10564877	*Rccd1*	RCC1 domain containing 1	269955	1.55	159	168	163	97	119	105
10536061	*Zfp141*	cDNA sequence BC063263	434178	1.55	135	150	143	67	112	92
10394283	*Cenpo*	centromere protein O	52504	1.55	127	154	140	78	116	90
10597413	*Crtap*	cartilage associated protein	56693	1.54	123	127	125	74	87	81
10526098	*Scand3*	SCAN domain containing 3	71970	1.54	122	127	124	64	99	81
10532828	*Mmab*	methylmalonic aciduria (cobalamin deficiency) type B homolog (human)	77697	1.53	133	149	141	77	100	92
10454306	*Zfp35*	zinc finger protein 35	22694	1.53	135	142	138	76	102	91
10527233	*Cyth3*	cytohesin 3	19159	1.51	140	152	146	84	108	96
10482249	*Nr6a1*	nuclear receptor subfamily 6 group A member 1	14536	1.51	128	158	142	85	103	94
10355312	*Ikzf2*	IKAROS family zinc finger 2	22779	1.5	128	139	133	72	119	89
10346544	*Ndufb3*	NADH dehydrogenase (ubiquinone) 1 beta subcomplex 3	66495	1.5	122	149	135	73	115	90
10441864	*Mllt4*	myeloid/lymphoid or mixed-lineage leukemia (trithorax homolog Drosophila)								
10416732	*Snora30*	small nucleolar RNA H/ACA box 30	100217442	1.49	138	148	143	78	114	96
10470950	*Endog*	endonuclease G	13804	1.48	121	125	123	81	84	83
10552458	*Ctu1*	ATP binding domain 3	233189	1.48	151	153	152	94	114	102
10575706	*Wwox*	WW domain-containing oxidoreductase	80707	1.47	151	171	161	103	115	109
10445670	*Mrps10*	mitochondrial ribosomal protein S10	64657	1.47	129	157	143	89	113	97
10584634	*Usp2*	ubiquitin specific peptidase 2	53376	1.47	121	131	126	71	100	86
10521798	*Pacrgl*	PARK2 co-regulated-like	66768	1.46	153	167	160	102	119	110
10428353	*Lrp12*	low density lipoprotein-related protein 12	239393	1.46	128	129	129	74	113	88
10523960	*Pigg*	phosphatidylinositol glycan anchor biosynthesis class G	433931	1.46	143	156	149	93	115	102
10477325	*Dnmt3b*	DNA methyltransferase 3B	13436	1.45	151	159	155	96	116	107
10431170	*5031439G07Rik*	RIKEN cDNA 5031439G07 gene	223739	1.44	130	130	130	80	104	90
10568758	*9430038I01Rik*	RIKEN cDNA 9430038I01 gene	77252	1.44	126	145	135	80	107	94
10404763	*Tmem170b*	transmembrane protein 170B	621976	1.44	141	155	148	90	112	103
10413640	*Nek4*	NIMA (never in mitosis gene a)-related expressed kinase 4	23955	1.43	121	123	122	80	94	86
10465374	*Sac3d1*	SAC3 domain containing 1	66406	1.43	132	145	139	90	113	97
10551483	*Eid2*	EP300 interacting inhibitor of differentiation 2	386655	1.43	131	149	140	87	107	98
10554223	*Mrps11*	mitochondrial ribosomal protein S11	67994	1.42	139	142	141	89	109	99
10605315	*Lage3*	L antigen family member 3	66192	1.41	122	159	139	72	119	98
10463112	*Ccnj*	cyclin J	240665	1.41	130	141	135	83	108	96
10450369	*Hspa1a*	heat shock protein 1A	193740	1.4	123	170	144	84	116	103
10352092	*Zfp238*	zinc finger protein 238	30928	1.4	122	125	123	79	96	88
10508892	*Gpatch3*	G patch domain containing 3	242691	1.4	142	143	143	93	111	102
10425477	*Sgsm3*	small G protein signaling modulator 3	105835	1.4	126	143	134	83	111	96
10425158	*Pdxp*	pyridoxal (pyridoxine vitamin B6) phosphatase	57028	1.4	120	127	124	76	100	88
10441017	*Setd4*	SET domain containing 4	224440	1.4	136	143	140	91	110	100
10535213	*Snx8*	sorting nexin 8	231834	1.39	141	143	142	95	110	102
10443221	*Uhrf1bp1*	UHRF1 (ICBP90) binding protein 1	224648	1.37	125	138	131	86	117	96
10458424	*Taf7*	TAF7 RNA polymerase II TATA box binding protein (TBP)-associated factor	24074	1.37	125	133	129	73	114	94
10545910	*Pcyox1*	prenylcysteine oxidase 1	66881	1.35	136	153	144	93	119	107
10383032	*Engase*	endo-beta-N-acetylglucosaminidase	217364	1.35	121	143	131	87	110	97
10570472	*Cln8*	ceroid-lipofuscinosis neuronal 8	26889	1.35	141	162	151	104	119	112
10581151	*Rrad*	Ras-related associated with diabetes	56437	1.35	127	128	128	83	109	94
10533474	*1500011H22Rik*	RIKEN cDNA 1500011H22 gene	68948	1.34	127	148	137	93	113	103
10360957	*Kctd3*	potassium channel tetramerisation domain containing 3	226823	1.34	138	149	143	94	115	107
10485013	*1110051M20Rik*	RIKEN cDNA 1110051M20 gene	228356	1.32	123	124	123	85	103	93
10404996	*Ninj1*	ninjurin 1	18081	1.31	131	153	141	94	120	108
10381211	*Naglu*	alpha-N-acetylglucosaminidase (Sanfilippo disease IIIB)	27419	1.31	132	138	135	90	115	103
10404815	*Sirt5*	sirtuin 5 (silent mating type information regulation 2 homolog) 5 (S. cerevisiae)	68346	1.3	124	124	124	84	108	95
10518366	*2810408P10Rik*	RIKEN cDNA 2810408P10 gene	242747	1.3	137	139	138	95	117	106
10481210	*Vav2*	vav 2 oncogene	22325	1.29	128	149	138	92	117	107
10579860	*Smad1*	MAD homolog 1 (Drosophila)	17125	1.29	126	126	126	85	109	98
10451081	*Ccdc94*	coiled-coil domain containing 94	72886	1.28	121	128	125	87	107	97
10551314	*BC024978*		NA	1.26	122	125	123	83	117	98
10530787	*Aasdh*	aminoadipate-semialdehyde dehydrogenase	231326	1.23	132	137	134	102	116	109
10568638	*Uros*	uroporphyrinogen III synthase	22276	1.23	120	127	123	83	111	100
10572804	*1700030K09Rik*	RIKEN cDNA 1700030K09 gene	72254	1.21	123	138	130	100	115	107
10384452	*Ublcp1*	ubiquitin-like domain containing CTD phosphatase 1	79560	1.21	127	127	127	94	116	105
10552945	*Gys1*	glycogen synthase 1 muscle	14936	1.19	130	134	132	105	119	111
10372926	*Mirlet7i*		NA	1.18	122	125	123	98	118	104
10440246	*Arl13b*	ADP-ribosylation factor-like 13B	68146	1.16	127	134	131	101	117	112
10559261	*Cd81*	CD81 antigen	12520	1.15	123	129	126	103	119	110
10468881	*Zfp826*	zinc finger protein 826	414758	1.15	126	128	127	99	116	111

The results of this thesis will be soon submitted as a journal article; manuscript in preparation:

Linking cell dynamics with gene coexpression networks to characterize key events in chronic virus infections

Mireia Pedragosa[1,¶], Graciela Riera[1,¶], Anna Esteve-Codina[2,3], Yael Steuerman[4], Celina Seth[1], Gennady Bocharov[5], Simon Heath[2,3], Irit Gat-Viks[4], Jordi Argilaguet[1,*] and Andreas Meyerhans[1,6,*]

[1]Infection Biology Laboratory, Department of Experimental and Health Sciences (DCEXS), Universitat Pompeu Fabra, Barcelona, Spain.

[2]CNAG-CRG, Center for Genomic Regulation (CRG), Barcelona Institute of Science and Technology, Barcelona, Spain.

[3]Universitat Pompeu Fabra, Barcelona, Spain

[4]Cell Research and Immunology Department, Tel Aviv University, Tel Aviv, Israel

[5]Institute of Numerical Mathematics, Russian Academy of Sciences, Moscow, Russia.

[6]Institució Catalana de Recerca i Estudis Avançats (ICREA), Barcelona, Spain.

[¶]These authors contributed equally to this work

*Corresponding authors

Correspondence:

Dr. Andreas Meyerhans (andreas.meyerhans@upf.edu)

Dr. Jordi Argilaguet (jordi.argilaguet@upf.edu)

DISCUSSION

In this thesis we created a new computational approach that combines WGCNA-derived gene coexpression networks with DCQ-inferred immune cell kinetics. This enabled us to generate hypotheses about complex immune functioning after a virus-induced perturbation. We show, first, the ability of DCQ to predict changes of immune cell subsets that play major roles during LCMV infection. Second, we were able to characterize immune cell subsets involved in spleen-derived gene coexpression modules that participate in complex biological pathways. Third, in chronic infection, there is an alteration in neutrophil and macrophage migration concomitant with $CD8^+$ T cell exhaustion. Finally, we predicted and subsequently verified experimentally that virus-specific $CD8^+$ T cells with an early effector transcriptome profile participate in the host adaptation to an overwhelming virus threat. Thus, combining WGCNA and DCQ turns out to be a very powerful approach to analyze immune system perturbations in affected tissues solely based on RNA-Seq data. It may provide data of cell subsets and function to mathematical modelers aiming to quantify perturbations and predict directs for interventions, and if further developed, it may help clinicians to optimize therapeutic decisions in personalized medicine.

The immune system is an extraordinary complex and robust defense system that protects a host against pathogens. It has to react fast and specific since pathogens may expand extremely rapidly. For example, a single virus-infected cell may generate 1000 to 100000 infectious progeny viruses in about 24 hours. In addition, since virus replication is highly error-prone, the newly generated viruses may contain genetic alterations like point mutations that change their antigenic features. To cope with this challenging task, the immune system consists of different layers of control, i.e. the fast reacting innate immune response that recognizes conserved features of pathogens and the slower adaptive immune response that is antigen-specific and provides immune memory to a host. Once an infection is initiated, the race between pathogen expansion and immune-mediated pathogen restriction starts and a highly coordinated scheme of inhibitory mechanism is activated. The final outcome of this race is determined by various components including location of initial infection, pathogen replication rate and developmental stage of the immune system. With respect to virus infections, the most common outcomes are acute infections in which the immunes system efficiently controls and later eliminates the virus, and chronic infections in which the immune system partly loses control and establishes a dynamic equilibrium condition with the virus remaining permanently present in the host. Both types of virus infections are of clinical importance and their therapies present significant financial burdens for health care systems.

A quantitative description and understanding of the complex and coordinated immune response against a virus infection requires the merely impossible task of characterizing thousands of cell subsets and humoral factors that orchestrate the immune response in a dynamic fashion. Until today, most of the attempts of describing infection outcomes focused on following individual immune system components over time and analyzing their importance. We however sought to use a more general systemic approach and analyzed time-resolved transcriptomes from spleens of acutely and chronically LCMV-infected mice by Weighted Gene Coexpression Network Analysis (WGCNA) (Argilaguet et al. 2018, submitted). While this approach captured the dynamics of all RNA transcripts within an important lymphatic tissue, information about cell types were lost. To overcome this disadvantage, the idea for this PhD thesis was to combine our previous transcriptome results with another described tool, the Digital Cell Quantifier (DCQ) (Altboum et al., 2014). This tool enabled us to decompose the immune cell complexity during acute and chronic LCMV infections of mice and predict cell subsets involved in chronic infection fate regulation. Moreover, we were able to combine these results with WGCNA to link gene expression changes to cell kinetics. A key advantage of this approach is its ability to integrate clusters of highly coexpressed genes that represent biological pathways with quantitative information about each of the relevant immune cell subsets, and thus, obtaining a global view of the transcription and cell dynamic changes happening in a specific organ.

Our experimental results demonstrate that DCQ correctly predicts changes in the dynamics of immune cell subsets with a major role during LCMV infection including cytotoxic T lymphocyte expansion and $CD8^+$ T cell exhaustion in acutely- and chronically-infected mice, respectively. Moreover, we demonstrate that DCQ predicts known changes in cell type quantities with high accuracy, as well as, correctly identifies cell subsets in a particular functional stage such as different maturation states of NK cells. When applying our new approach to link these predictions to molecular pathways previously obtained by WGCNA, we demonstrate the applicability of such strategy, overcoming the lack of information about the cell subsets involved in gene coexpression modules. This is exemplified by the analysis of DCQ-inferred cell subsets that correlate with the acute-brown module eigengene. In Argilaguet et al. we showed that some hub genes from this module were involved in the T cell response induced during an acute infection (Argilaguet et al. 2018, submitted). In concordance, DCQ-inferred late effector $CD8^+$ T cell kinetics showed high correlation values with the module eigengene. Moreover, monocytes/macrophages showed high correlation

values with this module, suggesting that these cell subsets participate in a coordinated manner in the same biological pathway. Indeed, we show that several acute-brown hub genes involved in T cell activation are also upregulated by monocytes/macrophages, indicating that they participate in a coordinated manner in the induction of the adaptive immune response during an acute infection. These results demonstrate the ability of our novel approach to characterize complex immune events in which several cell subsets are involved. However, this strategy does not completely decipher the global immune cell interactions. For instance, even though DCQ-inferred dendritic cell (DC) kinetics did not show high correlation values with the module, it is well known that they play a critical role in T cell priming (Ng et al., 2013). This may be due to a failure of DCQ to correctly predict the dynamics of DC subsets participating in this process, or to a lack of correlation between the amount of DCs and transcripts. Regardless, it has been shown that DCs are dispensable as antigen presenting cells for protective immunity against LCMV infection (Hilpert et al., 2016), and therefore our results highlight the potential importance of monocytes/macrophages in the induction of the adaptive immune response.

Our approach was also useful when applied to gene coexpression modules that represent critical features of chronic LCMV infection. The observation that, concomitant with $CD8^+$ T cell exhaustion, neutrophils and monocytes downregulate genes involved in cell migration and inflammation, demonstrate that the immune adaptation to a chronic infection is a multiple-faceted process. The fact that we could not validate the decrease of monocytes and activated neutrophil numbers by FACS analysis indicates that DCQ-predictions likely represent specific cell subsets in a certain functional stage. Further studies are necessary to properly characterize the cell subsets within these cell populations responsible for the downregulation of the chronic-magenta hub genes, and its functional implications: i.e. whether neutrophils and monocytes act as inflammatory cells that are attenuated to avoid immunopathology (Medzhitov et al., 2012), or they are important for $CD8^+$ T cell priming and therefore contribute to exhaustion by an alteration on their migration (Hohl et al., 2009; Iijima et al., 2011; Beauvillain et al., 2007; Di Pilato et al., 2015; Duffy et al., 2012). Interestingly, the decrease of these innate immune cells coincides with the appearance of neutrophilic and monocytic suppressor cells (Norris et al., 2013), suggesting a shift of their functional status during the establishment of a chronic infection.

The combination of WGCNA and DCQ also proved to be valuable for the phenotypic characterization of cells known to play a role in a particular biological pathway. We had previously shown that virus-specific $CXCR5^+$ $CD8^+$ T cells are the main producers of XCL1 in the chronic infection phase (Argilaguet et al. 2018, submitted). However, only when combining the information from WGCNA, DCQ and the Immunological Genome (ImmGen) Project, we were able to better characterize the phenotype of XCL1-producing cells. The observation that these cells have a similar phenotype to early effector T cells is a step forward in our understanding of the immune adaptation process to a chronic infection. However, further studies are necessary to understand the origin of these important cells. At least two of the markers expressed by early effector $CD8^+$ T cells, CXCR5 and TLR7, are also expressed by exhausted T cells (Im et al., 2016). Moreover, DCQ output lacks direct information on exhausted T cell subsets, which may also correlate with the chronic-magenta module. Therefore, we cannot specify whether XCL1-producing cells are exhausted T cells that "recover" a functional stage similar to early effectors, or are "*de novo*" primed naive T cells that are recruited to fight the virus during the chronic phase of the infection.

The novel combination of WGCNA and DCQ for interpreting time-resolved transcriptome data from acute and chronic virus infections is a step forward for our understanding of the complex immune responses against pathogen invasion. However, it is just a tiny part of the overall process that needs to be complemented with other measures like in situ imaging techniques and single cell analyses. Furthermore, computational approaches will be necessary to integrate all available data and generate hypotheses about the underlying regulatory principles that make the highly complex, diverse and dynamic immune system so functionally robust against pathogens. While many of the required technologies are in place, the data integration will require tight collaborations across disciplines engaging biologists, clinicians, physicists and mathematical modelers. With this, one can easily envision predictive frameworks that will help in the rational design of therapies in infectious diseases and cancers. An exciting time lies ahead.

CONCLUSIONS

The main conclusions of the present work are the following:

Digital Cell Quantifier (DCQ) predictions fit well with current knowledge of immune cell dynamics during acute and chronic LCMV-infections.

- DCQ correctly predicts exhaustion of $CD8^+$ T cells in chronic infection by a decrease of late effector $CD8^+$ T cells.

- DCQ correctly predicts changes in immune cell quantities of cell subsets with a specific role during LCMV chronic infection, such as regulatory T cells, cross-presenting dendritic cells and neutrophilic suppressor cells.

- DCQ predicts the quantity of immune cell subsets in a particular functional stage, such as activated effector NK cells.

The combination of Weighted Gene Coexpression Network Analysis (WGCNA) and DCQ to analyze time-resolved tissue transcriptomes is a valuable tool to better characterize the immune cell subsets that participate in a complex biological pathway represented by gene coexpression modules.

- Genes expressed by late effector $CD8^+$ T cells and monocytes/macrophages significantly overlap with genes from acute-brown module, demonstrating that in some circumstances the kinetics of a particular cell subset correlates with the kinetics of the genes expressed by that cell.

- The combination of WGCNA and DCQ allows to better characterize the dynamic cell events occurring in complex tissues such as the induction of the adaptive T cell response which requires the coordination of monocytes/macrophages and $CD8^+$ T cells.

This innovative computational approach enabled to generate novel hypotheses about complex immune functioning after a virus-induced perturbation.

- By combining WGCNA with DCQ, it is possible to generate novel hypotheses to characterize the activation and differentiation status of cells that participate in the relevant immune processes.

- Activated neutrophils and monocytes/macrophage downregulate genes involved in cell migration concomitant with exhaustion of $CD8^+$ T cells, suggesting that the immune adaptation to a chronic infection is a complex process that involves the immunosuppression of T cells as well as inflammatory cells from the innate immune system.

- XCL1-producing $CD8^+$ T cells during the adaptation phase to a chronic infection is produced by $CD8^+$ T cells that express markers characteristic of early effector cells.

ANNEXES

ANNEX 1

List of abbreviations

α-DG	α-dystroglycan
BSA	Bovine serum albumin
CCR9	C-C chemokine receptor type 9
cDC	Conventional Dendritic cell(s)
CL13	Clone 13
CTL	Cytotoxic T cell
CXCR5	Chemokine Receptor Type 5
CyTOF	Cytometry by time-of-flight
DC	Dendritic cell(s)
DCQ	Digital Cell Quantifier
DE	Differentially expressed
Doc	Docile
EDTA	Ethylenediaminetetraacetic acid
FACS	Fluorescence-activated cell sorting
FBS	Fetal Bovine Serum
FC	Fold Change
GO	Gene ontology
GPC	Glycoprotein Precursor
GS	Gene significance
HBV	Hepatitis B Virus
HCV	Hepatitis C Virus
HD	High dose
HIV	Human Immunodeficiency Virus
i.p	Intraperitoneal
IFN	Interferon
IL	Interleukin
IRG	Intergenic Region

ISG	IFN-stimulated genes
LCMV	Lymphocytic Choriomeningitis Virus
LD	Low dose
LIS	Listeria
MCMV	Murine Cytomegalovirus
MDSC	Myeloid derived suppressor cells
ME	Module Eigengene
MFI	Mean fluorescence intensity
MHC	Major Histocompatibility Complex
MS	Module significance
NaCl	Sodium Chloride
NH4Cl	Ammonium Chloride
NK cells	Natural Killer cells
NP	Nucleoprotein
p.i	Postinfection
PBS	Phosphate-buffered saline
PD-1	Programmed Cell Death-1
PD-L1	Programmed Cell Death-1 ligand
pDC	Plasmacytoid dendritic cell(s)
PFU	Plaque-forming unit
RdRP	RNA dependent RNA polymerase
RIN	RNA integrity number
RNA	Ribonucleoprotein
RNPs	Viral Ribonucleoproteins
RPMI	Roswell Park Memorial Institute Medium
SEM	Standard error of the mean
SIV	Simian immunodeficiency virus
TGF-β	Transforming growth factor beta
Th	Helper T cell(s)
TLR7	Toll-like receptor 7

TNF	Tumor Necrosis Factor
TNFSF8	TNF superfamily member 8
Treg	Regulatory T cell(s)
VSV	Vesicular stomatitis virus
WGCNA	Weighted Gene Coexpression Network Analysis
XCL1	X-C motif chemokine ligand 1
XCR1	X-C motif chemokine receptor 1

REFERENCES

A

Aiuti, F., and Mezzaroma, I. (2006). Failure to reconstitute CD4+ T-cells despite suppression of HIV replication under HAART. AIDS Rev. *8*, 88–97.

Allen, T.M., Altfeld, M., Geer, S.C., Kalife, E.T., Moore, C., O'Sullivan, K.M., DeSouza, I., Feeney, M.E., Eldridge, R.L., Maier, E.L., et al. (2005). Selective Escape from CD8 T-Cell Responses Represents a Major Driving Force of Human Immunodeficiency Virus Type 1 (HIV-1) Sequence Diversity and Reveals Constraints on HIV-1 Evolution. J. Virol. *79*, 13239–13249.

Altboum, Z., Steuerman, Y., David, E., Barnett-Itzhaki, Z., Valadarsky, L., Keren-Shaul, H., Meningher, T., Mendelson, E., Mandelboim, M., Gat-Viks, I., et al. (2014). Digital cell quantification identifies global immune cell dynamics during influenza infection. Mol. Syst. Biol. *10*, 720.

Argilaguet, Jordi., Pedragosa,P., Esteve-Codina, A., Riera, G., Vidal., Peligero, P., Andreu, D., Kaisho, T., Bocharov, G., Ludewig, B., Heath,S., Meyerhans, A. (2018). "Systems analysis reveals complex biological processes in virus infection fate decisions". Manuscript submitted for publication.

Asabe, S., Wieland, S.F., Chattopadhyay, P.K., Roederer, M., Engle, R.E., Purcell, R.H., and Chisari, F.V. (2009). The size of the viral inoculum contributes to the outcome of hepatitis B virus infection. J. Virol. *83*, 9652–9662.

B

Barabási, A.-L., and Oltvai, Z.N. (2004). Network biology: understanding the cell's functional organization. Nat. Rev. Genet. *5*, 101–113.

Barber, D.L., Wherry, E.J., Masopust, D., Zhu, B., Allison, J.P., Sharpe, A.H., Freeman, G.J., and Ahmed, R. (2006). Restoring function in exhausted CD8 T cells during chronic viral infection. Nature *439*, 682–687.

Barnaba, V., and Schinzari, V. (2013). Induction, control, and plasticity of Treg cells: the immune regulatory network revised? Eur. J. Immunol. *43*, 318–322.

Battegay, M., Moskophidis, D., Rahemtulla, A., Hengartner, H., Mak, T.W., and Zinkernagel, R.M. (1994). Enhanced establishment of a virus carrier state in adult CD4+ T-cell-deficient mice. J. Virol. *68*, 4700–4704.

Beauvillain, C., Delneste, Y., Scotet, M., Peres, A., Gascan, H., Guermonprez, P., Barnaba, V., and Jeannin, P. (2007). Neutrophils efficiently cross-prime naive T cells in vivo. Blood *110*, 2965–2973.

Belkaid, Y., and Rouse, B.T. (2005). Natural regulatory T cells in infectious disease. Nat. Immunol. *6*, 353–360.

Bengsch, B., Ohtani, T., Khan, O., Setty, M., Manne, S., O'Brien, S., Gherardini, P.F., Herati, R.S., Huang, A.C., Chang, K.-M., et al. (2018). Epigenomic-Guided Mass Cytometry Profiling Reveals Disease-Specific Features of Exhausted CD8 T Cells. Immunity *48*, 1029–1045.e5.

Bergthaler, A., Flatz, L., Hegazy, A.N., Johnson, S., Horvath, E., Löhning, M., and Pinschewer, D.D. (2010). Viral replicative capacity is the primary determinant of lymphocytic choriomeningitis virus persistence and immunosuppression. Proc. Natl. Acad. Sci. U. S. A. *107*, 21641–21646.

Bernhard, C.A., Ried, C., Kochanek, S., and Brocker, T. (2015). CD169+ macrophages are sufficient for priming of CTLs with specificities left out by cross-priming dendritic cells. Proc. Natl. Acad. Sci. U. S. A. *112*, 5461–5466.

Bertoletti, A., and Ferrari, C. (2012). Innate and adaptive immune responses in chronic hepatitis B virus infections: towards restoration of immune control of viral infection. Gut *61*, 1754–1764.

Bjornson, Z.B., Nolan, G.P., and Fantl, W.J. (2013). Single-cell mass cytometry for analysis of immune system functional states. Curr. Opin. Immunol. *25*, 484–494.

Blackburn, S.D., Shin, H., Freeman, G.J., and Wherry, E.J. (2008). Selective expansion of a subset of exhausted CD8 T cells by alpha PD-L1 blockade. Proc. Natl. Acad. Sci. U. S. A. *105*, 15016–15021.

Bocharov, G., Ludewig, B., Bertoletti, A., Klenerman, P., Junt, T., Krebs, P., Luzyanina, T., Fraser, C., and Anderson, R.M. (2004). Underwhelming the immune response: effect of slow virus growth on CD8+-T-lymphocyte responses. J. Virol. *78*, 2247–2254.

Boehm, T. (2016). Form follows function, function follows form: how lymphoid tissues enable and constrain immune reactions. Immunol. Rev. *271*, 4–9.

Brooks, D.G., Trifilo, M.J., Edelmann, K.H., Teyton, L., McGavern, D.B., and Oldstone, M.B.A. (2006). Interleukin-10 determines viral clearance or persistence in vivo. Nat. Med. *12*, 1301–1309.

Brooks, D.G., McGavern, D.B., and Oldstone, M.B.A. (2006). Reprogramming of antiviral T cells prevents inactivation and restores T cell activity during persistent viral infection. J. Clin. Invest. *116*, 1675–1685.

C

Cabrera, R., Tu, Z., Xu, Y., Firpi, R.J., Rosen, H.R., Liu, C., and Nelson, D.R. (2004). An immunomodulatory role for CD4 CD25 regulatory T lymphocytes in hepatitis C virus infection. Hepatology *40*, 1062–1071.

Cahalan, M.D., Parker, I., Wei, S.H., and Miller, M.J. (2002). Two-photon tissue imaging: seeing the immune system in a fresh light. Nat. Rev. Immunol. *2*, 872–880.

Cao, W. (1998). Identification of -Dystroglycan as a Receptor for Lymphocytic Choriomeningitis Virus and Lassa Fever Virus. Science *282*, 2079–2081.

Chakrabarti, A.K., Vipat, V.C., Mukherjee, S., Singh, R., Pawar, S.D., and Mishra, A.C. (2010). Host gene expression profiling in influenza A virus-infected lung epithelial (A549) cells: a comparative analysis between highly pathogenic and modified H5N1 viruses. Virol. J. *7*, 219.

Cheng, L., Ma, J., Li, J., Li, D., Li, G., Li, F., Zhang, Q., Yu, H., Yasui, F., Ye, C., et al. (2017). Blocking type I interferon signaling enhances T cell recovery and reduces HIV-1 reservoirs. J. Clin. Invest. *127*, 269–279.

Chiossone, L., Chaix, J., Fuseri, N., Roth, C., Vivier, E., and Walzer, T. (2009). Maturation of mouse NK cells is a 4-stage developmental program. Blood *113*, 5488–5496.

Clerici, M., Wynn, T.A., Berzofsky, J.A., Blatt, S.P., Hendrix, C.W., Sher, A., Coffman, R.L., and Shearer, G.M. (1994). Role of interleukin-10 in T helper cell dysfunction in asymptomatic individuals infected with the human immunodeficiency virus. J. Clin. Invest. *93*, 768–775.

Cole, G.A., Nathanson, N., and Prendergast, R.A. (1972). Requirement for theta-bearing cells in lymphocytic choriomeningitis virus-induced central nervous system disease. Nature *238*, 335–337.

Cook, K.D., Kline, H.C., and Whitmire, J.K. (2015). NK cells inhibit humoral immunity by reducing the abundance of CD4+ T follicular helper cells during a chronic virus infection. J. Leukoc. Biol. *98*, 153–162.

Cornberg, M., Kenney, L.L., Chen, A.T., Waggoner, S.N., Kim, S.-K., Dienes, H.P., Welsh, R.M., and Selin, L.K. (2013). Clonal exhaustion as a mechanism to protect against severe immunopathology and death from an overwhelming CD8 T cell response. Front. Immunol. *4*, 475.

Crawford, A., and Wherry, E.J. (2009). The diversity of costimulatory and inhibitory receptor pathways and the regulation of antiviral T cell responses. Curr. Opin. Immunol. *21*, 179–186.

D

Davis, M.M., and Shen-Orr, S.S. (2013). Systems Immunology. In Handbook of Systems Biology, pp. 481–497.

Day, C.L., Kaufmann, D.E., Kiepiela, P., Brown, J.A., Moodley, E.S., Reddy, S., Mackey, E.W., Miller, J.D., Leslie, A.J., DePierres, C., et al. (2006). PD-1 expression on HIV-specific T cells is associated with T-cell exhaustion and disease progression. Nature *443*, 350–354.

Diaz-Beltran, L., Cano, C., Wall, D.P., and Esteban, F.J. (2013). Systems biology as a comparative approach to understand complex gene expression in neurological diseases. Behav. Sci. *3*, 253–272.

Diercks, A., and Aderem, A. (2013). Systems approaches to dissecting immunity. Curr. Top. Microbiol. Immunol. *363*, 1–19.

Dietze, K.K., Zelinskyy, G., Gibbert, K., Schimmer, S., Francois, S., Myers, L., Sparwasser, T., Hasenkrug, K.J., and Dittmer, U. (2011). Transient depletion of regulatory T cells in transgenic mice reactivates virus-specific CD8+ T cells and reduces chronic retroviral set points. Proc. Natl. Acad. Sci. U. S. A. *108*, 2420–2425.

van Dinther, D., Veninga, H., Iborra, S., Borg, E.G.F., Hoogterp, L., Olesek, K., Beijer, M.R., Schetters, S.T.T., Kalay, H., Garcia-Vallejo, J.J., et al. (2018). Functional CD169 on Macrophages Mediates Interaction with Dendritic Cells for CD8+ T Cell Cross-Priming. Cell Rep. *22*, 1484–1495.

Di Pilato, M., Mejías-Pérez, E., Zonca, M., Perdiguero, B., Gómez, C.E., Trakala, M., Nieto, J., Nájera, J.L., Sorzano, C.O.S., Combadière, C., et al. (2015). NFκB activation by modified vaccinia virus as a novel strategy to enhance neutrophil migration and HIV-specific T-cell responses. Proc. Natl. Acad. Sci. U. S. A. *112*, E1333–E1342.

Dittmer, U., He, H., Messer, R.J., Schimmer, S., Olbrich, A.R.M., Ohlen, C., Greenberg, P.D., Stromnes, I.M., Iwashiro, M., Sakaguchi, S., et al. (2004). Functional impairment of CD8(+) T cells by regulatory T cells during persistent retroviral infection. Immunity *20*, 293–303.

Doering, T.A., Crawford, A., Angelosanto, J.M., Paley, M.A., Ziegler, C.G., and Wherry, E.J. (2012). Network analysis reveals centrally connected genes and pathways involved in CD8+ T cell exhaustion versus memory. Immunity *37*, 1130–1144.

Draenert, R., Le Gall, S., Pfafferott, K.J., Leslie, A.J., Chetty, P., Brander, C., Holmes, E.C., Chang, S.-C., Feeney, M.E., Addo, M.M., et al. (2004). Immune selection for altered antigen processing leads to cytotoxic T lymphocyte escape in chronic HIV-1 infection. J. Exp. Med. *199*, 905–915.

Duffy, D., Perrin, H., Abadie, V., Benhabiles, N., Boissonnas, A., Liard, C., Descours, B., Reboulleau, D., Bonduelle, O., Verrier, B., et al. (2012). Neutrophils transport antigen from the dermis to the bone marrow, initiating a source of memory CD8+ T cells. Immunity *37*, 917–929.

Dunn, H.S., Haney, D.J., Ghanekar, S.A., Stepick-Biek, P., Lewis, D.B., and Maecker, H.T. (2002). Dynamics of CD4 and CD8 T cell responses to cytomegalovirus in healthy human donors. J. Infect. Dis. *186*, 15–22.

E

Ehl, S., Klenerman, P., Zinkernagel, R.M., and Bocharov, G. (1998). The impact of variation in the number of CD8(+) T-cell precursors on the outcome of virus infection. Cell. Immunol. *189*, 67–73.

Ertl, R., and Klein, D. (2014). Transcriptional profiling of the host cell response to feline immunodeficiency virus infection. Virol. J. *11*, 52.

Fallet, B., Narr, K., Ertuna, Y.I., Remy, M., Sommerstein, R., Cornille, K., Kreutzfeldt, M., Page, N., Zimmer, G., Geier, F., et al. (2016). Interferon-driven deletion of antiviral B cells at the onset of chronic infection. Sci Immunol *1*.

F

Farmer, T.W., and Janeway, C.A. (1942). Infections With The Virus Of Lymphocytic Choriomeningitis. Medicine *21*, 65–94.

Feinberg, M.B., and Ahmed, R. (2012). Born this way? Understanding the immunological basis of effective HIV control. Nat. Immunol. *13*, 632–634.

Fell, D.A. (2001). Beyond genomics. Trends Genet. *17*, 680–682.

Fitzgerald-Bocarsly, P., and Jacobs, E.S. (2010). Plasmacytoid dendritic cells in HIV infection: striking a delicate balance. J. Leukoc. Biol. *87*, 609–620.

Friedman, J., Hastie, T., and Tibshirani, R. (2010). Regularization Paths for Generalized Linear Models via Coordinate Descent. J. Stat. Softw. *33*, 1–22.

Frohlich, A., Kisielow, J., Schmitz, I., Freigang, S., Shamshiev, A.T., Weber, J., Marsland, B.J., Oxenius, A., and Kopf, M. (2009). IL-21R on T Cells Is Critical for Sustained Functionality and Control of Chronic Viral Infection. Science *324*, 1576–1580.

Fukuyama, S., and Kawaoka, Y. (2011). The pathogenesis of influenza virus infections: the contributions of virus and host factors. Curr. Opin. Immunol. *23*, 481–486.

G

Gallaher, W.R., DiSimone, C., and Buchmeier, M.J. (2001). The viral transmembrane superfamily: possible divergence of Arenavirus and Filovirus glycoproteins from a common RNA virus ancestor. BMC Microbiol. *1*, 1.

Geiss, G.K., Bumgarner, R.E., An, M.C., Agy, M.B., van 't Wout, A.B., Hammersmark, E., Carter, V.S., Upchurch, D., Mullins, J.I., and Katze, M.G. (2000). Large-scale monitoring of host cell gene expression during HIV-1 infection using cDNA microarrays. Virology *266*, 8–16.

Gilliet, M., Cao, W., and Liu, Y.-J. (2008). Plasmacytoid dendritic cells: sensing nucleic acids in viral infection and autoimmune diseases. Nat. Rev. Immunol. *8*, 594–606.

Glazer, H.S., Mauro, M.A., Aronberg, D.J., Lee, J.K., Johnston, D.E., and Sagel, S.S. (1983). Computed tomography of laryngoceles. American Journal of Roentgenology *140*, 549–552.

Guo, X., Xiao, H., Guo, S., Dong, L., and Chen, J. (2017). Identification of breast cancer mechanism based on weighted gene coexpression network analysis. Cancer Gene Ther. *24*, 333–341.

Gygi, S.P., Rochon, Y., Robert Franza, B., and Aebersold, R. (1999). Correlation between Protein and mRNA Abundance in Yeast. Mol. Cell. Biol. *19*, 1720–1730.

H

Hangartner, L., Zinkernagel, R.M., and Hengartner, H. (2006). Antiviral antibody responses: the two extremes of a wide spectrum. Nat. Rev. Immunol. *6*, 231–243.

He, R., Hou, S., Liu, C., Zhang, A., Bai, Q., Han, M., Yang, Y., Wei, G., Shen, T., Yang, X., et al. (2016). Follicular CXCR5- expressing CD8(+) T cells curtail chronic viral infection. Nature *537*, 412–428.

Hilpert, C., Sitte, S., Matthies, A., and Voehringer, D. (2016). Dendritic Cells Are Dispensable for T Cell Priming and Control of Acute Lymphocytic Choriomeningitis Virus Infection. The Journal of Immunology *197*, 2780–2786.

Hiroishi, K., Kita, H., Kojima, M., Okamoto, H., Moriyama, T., Kaneko, T., Ishikawa, T., Ohnishi, S., Aikawa, T., Tanaka, N., et al. (1997). Cytotoxic T lymphocyte response and viral load in hepatitis C virus infection. Hepatology *25*, 705–712.

Hohl, T.M., Rivera, A., Lipuma, L., Gallegos, A., Shi, C., Mack, M., and Pamer, E.G. (2009). Inflammatory monocytes facilitate adaptive CD4 T cell responses during respiratory fungal infection. Cell Host Microbe *6*, 470–481.

Hunziker, L., Recher, M., Macpherson, A.J., Ciurea, A., Freigang, S., Hengartner, H., and Zinkernagel, R.M. (2003). Hypergammaglobulinemia and autoantibody induction mechanisms in viral infections. Nat. Immunol. *4*, 343–349.

I

Ibrahim, S.F., and van den Engh, G. (2007). Flow cytometry and cell sorting. Adv. Biochem. Eng. Biotechnol. *106*, 19–39.

Ideker, T., Thorsson, V., Ranish, J.A., Christmas, R., Buhler, J., Eng, J.K., Bumgarner, R., Goodlett, D.R., Aebersold, R., and Hood, L. (2001). Integrated genomic and proteomic analyses of a systematically perturbed metabolic network. Science *292*, 929–934.

Iijima, N., Mattei, L.M., and Iwasaki, A. (2011). Recruited inflammatory monocytes stimulate antiviral Th1 immunity in infected tissue. Proc. Natl. Acad. Sci. U. S. A. *108*, 284–289.

Im, S.J., Hashimoto, M., Gerner, M.Y., Lee, J., Kissick, H.T., Burger, M.C., Shan, Q., Hale, J.S., Lee, J., Nasti, T.H., et al. (2016). Defining CD8+ T cells that provide the proliferative burst after PD-1 therapy. Nature *537*, 417–421.

J

Janeway, C.A., Jr., and Medzhitov, R. (1998). Introduction: The role of innate immunity in the adaptive immune response. Semin. Immunol. *10*, 349–350.

Jin, H.-T., Jeong, Y.-H., Park, H.-J., and Ha, S.-J. (2011). Mechanism of T cell exhaustion in a chronic environment. BMB Rep. *44*, 217–231.

Jin, X., Bauer, D.E., Tuttleton, S.E., Lewin, S., Gettie, A., Blanchard, J., Irwin, C.E., Safrit, J.T., Mittler, J., Weinberger, L., et al. (1999). Dramatic rise in plasma viremia after CD8(+) T cell depletion in simian immunodeficiency virus-infected macaques. J. Exp. Med. *189*, 991–998.

Ju, X., Silveira, P.A., Hsu, W.-H., Elgundi, Z., Alingcastre, R., Verma, N.D., Fromm, P.D., Hsu, J.L., Bryant, C., Li, Z., et al. (2016). The Analysis of CD83 Expression on Human Immune Cells Identifies a Unique CD83+-Activated T Cell Population. J. Immunol. *197*, 4613–4625.

K

Kägi, D., Ledermann, B., Bürki, K., Seiler, P., Odermatt, B., Olsen, K.J., Podack, E.R., Zinkernagel, R.M., and Hengartner, H. (1994). Cytotoxicity mediated by T cells and natural killer cells is greatly impaired in perforin-deficient mice. Nature *369*, 31–37.

Kahan, S.M., Wherry, E.J., and Zajac, A.J. (2015). T cell exhaustion during persistent viral infections. Virology *479-480*, 180–193.

Karrer, U., Althage, A., Odermatt, B., Roberts, C.W., Korsmeyer, S.J., Miyawaki, S., Hengartner, H., and Zinkernagel, R.M. (1997). On the key role of secondary lymphoid organs in antiviral immune responses studied in alymphoplastic (aly/aly) and spleenless (Hox11(-)/-) mutant mice. J. Exp. Med. *185*, 2157–2170.

Katze, M.G. (2013). Systems Biology (Springer Science & Business Media).

Khaitan, A., and Unutmaz, D. (2010). Revisiting Immune Exhaustion During HIV Infection. Curr. HIV/AIDS Rep. *8*, 4–11.

Kidd, B.A., Peters, L.A., Schadt, E.E., and Dudley, J.T. (2014). Unifying immunology with informatics and multiscale biology. Nat. Immunol. *15*, 118–127.

Kim, J.V., Kang, S.S., Dustin, M.L., and McGavern, D.B. (2009). Myelomonocytic cell recruitment causes fatal CNS vascular injury during acute viral meningitis. Nature *457*, 191–195.

Kitano, H. (2001). Foundations of Systems Biology (MIT Press (MA)).

Kityo, C., Makamdop, K.N., Rothenberger, M., Chipman, J.G., Hoskuldsson, T., Beilman, G.J., Grzywacz, B., Mugyenyi, P., Ssali, F., Akondy, R.S., et al. (2018). Lymphoid tissue fibrosis is associated with impaired vaccine responses. J. Clin. Invest. *128*, 2763–2773.

Klenerman, P., and Hill, A. (2005). T cells and viral persistence: lessons from diverse infections. Nat. Immunol. *6*, 873–879.

Kunz, S., Borrow, P., and Oldstone, M.B.A. (2002). Receptor Structure, Binding, and Cell Entry of Arenaviruses. In Current Topics in Microbiology and Immunology, pp. 111–137.

Kunz, S., Edelmann, K.H., de la Torre, J.-C., Gorney, R., and Oldstone, M.B.A. (2003). Mechanisms for lymphocytic choriomeningitis virus glycoprotein cleavage, transport, and incorporation into virions. Virology *314*, 168–178.

L

Landay, A.L., Clerici, M., Hashemi, F., Kessler, H., Berzofsky, J.A., and Shearer, G.M. (1996). In vitro restoration of T cell immune function in human immunodeficiency virus-positive persons: effects of interleukin (IL)-12 and anti-IL-10. J. Infect. Dis. *173*, 1085–1091.

Langfelder, P., and Horvath, S. (2008). WGCNA: an R package for weighted correlation network analysis. BMC Bioinformatics *9*, 559.

Lederer, S., Favre, D., Walters, K.-A., Proll, S., Kanwar, B., Kasakow, Z., Baskin, C.R., Palermo, R., McCune, J.M., and Katze, M.G. (2009). Transcriptional profiling in pathogenic and non-pathogenic SIV infections reveals significant distinctions in kinetics and tissue compartmentalization. PLoS Pathog. *5*, e1000296.

Leong, Y.A., Chen, Y., Ong, H.S., Wu, D., Man, K., Deleage, C., Minnich, M., Meckiff, B.J., Wei, Y., Hou, Z., et al. (2016). CXCR5 follicular cytotoxic T cells control viral infection in B cell follicles. Nat. Immunol. *17*, 1187–1196.

Li, Q., Skinner, P.J., Ha, S.-J., Duan, L., Mattila, T.L., Hage, A., White, C., Barber, D.L., O'Mara, L., Southern, P.J., et al. (2009). Visualizing antigen-specific and infected cells in situ predicts outcomes in early viral infection. Science *323*, 1726–1729.

Lichterfeld, M., Yu, X.G., Mui, S.K., Williams, K.L., Trocha, A., Brockman, M.A., Allgaier, R.L., Waring, M.T., Koibuchi, T., Johnston, M.N., et al. (2007). Selective Depletion of High-Avidity Human Immunodeficiency Virus Type 1 (HIV-1)-Specific CD8 T Cells after Early HIV-1 Infection. J. Virol. *81*, 4199–4214.

López-Pacheco, C., Soldevila, G., Du Pont, G., Hernández-Pando, R., and García-Zepeda, E.A. (2016). CCR9 Is a Key Regulator of Early Phases of Allergic Airway Inflammation. Mediators Inflamm. *2016*, 3635809.

M

Macal, M., Lewis, G.M., Kunz, S., Flavell, R., Harker, J.A., and Zúñiga, E.I. (2012). Plasmacytoid dendritic cells are productively infected and activated through TLR-7 early after arenavirus infection. Cell Host Microbe *11*, 617–630.

Marco-Sola, S., Sammeth, M., Guigó, R., and Ribeca, P. (2012). The GEM mapper: fast, accurate and versatile alignment by filtration. Nat. Methods *9*, 1185–1188.

Martínez-Sobrido, L., Giannakas, P., Cubitt, B., García-Sastre, A., and de la Torre, J.C. (2007). Differential inhibition of type I interferon induction by arenavirus nucleoproteins. J. Virol. *81*, 12696–12703.

Martínez-Sobrido, L., Emonet, S., Giannakas, P., Cubitt, B., García-Sastre, A., and de la Torre, J.C. (2009). Identification of amino acid residues critical for the anti-interferon activity of the nucleoprotein of the prototypic arenavirus lymphocytic choriomeningitis virus. J. Virol. *83*, 11330–11340.

Masson, D., and Tschopp, J. (1985). Isolation of a lytic, pore-forming protein (perforin) from cytolytic T-lymphocytes. J. Biol. Chem. *260*, 9069–9072.

Matloubian, M., Kolhekar, S.R., Somasundaram, T., and Ahmed, R. (1993). Molecular determinants of macrophage tropism and viral persistence: importance of single amino acid changes in the polymerase and glycoprotein of lymphocytic choriomeningitis virus. J. Virol. *67*, 7340–7349.

Matloubian, M., Concepcion, R.J., and Ahmed, R. (1994). CD4+ T cells are required to sustain CD8+ cytotoxic T-cell responses during chronic viral infection. J. Virol. *68*, 8056–8063.

Medzhitov, R., Schneider, D.S., and Soares, M.P. (2012). Disease Tolerance as a Defense Strategy. Science *335*, 936–941.

Moir, S., and Fauci, A.S. (2009). B cells in HIV infection and disease. Nat. Rev. Immunol. *9*, 235–245.

Montoya, M., Edwards, M.J., Reid, D.M., and Borrow, P. (2005). Rapid activation of spleen dendritic cell subsets following lymphocytic choriomeningitis virus infection of mice: analysis of the involvement of type 1 IFN. J. Immunol. *174*, 1851–1861.

Moskophidis, D., Lechner, F., Pircher, H., and Zinkernagel, R.M. (1993). Virus persistence in acutely infected immunocompetent mice by exhaustion of antiviral cytotoxic effector T cells. Nature *362*, 758–761.

Moskophidis, D., Battegay, M., van den Broek, M., Laine, E., Hoffmann-Rohrer, U., and Zinkernagel, R.M. (1995). Role of virus and host variables in virus persistence or immunopathological disease caused by a non-cytolytic virus. J. Gen. Virol. *76 (Pt 2)*, 381–391.

Murali-Krishna, K., Altman, J.D., Suresh, M., Sourdive, D.J., Zajac, A.J., Miller, J.D., Slansky, J., and Ahmed, R. (1998). Counting antigen-specific CD8 T cells: a reevaluation of bystander activation during viral infection. Immunity *8*, 177–187.

N

Ng, C.T., and Oldstone, M.B.A. (2012). Infected CD8α- dendritic cells are the predominant source of IL-10 during establishment of persistent viral infection. Proc. Natl. Acad. Sci. U. S. A. *109*, 14116–14121.

Ng, C.T., Snell, L.M., Brooks, D.G., and Oldstone, M.B.A. (2013). Networking at the Level of Host Immunity: Immune Cell Interactions during Persistent Viral Infections. Cell Host Microbe *13*, 652–664.

Nguyen, L.T., and Ohashi, P.S. (2015). Clinical blockade of PD1 and LAG3 — potential mechanisms of action. Nat. Rev. Immunol. *15*, 45–56.

Nilsson, J., Boasso, A., Velilla, P.A., Zhang, R., Vaccari, M., Franchini, G., Shearer, G.M., Andersson, J., and Chougnet, C. (2006). HIV-1-driven regulatory T-cell accumulation in lymphoid tissues is associated with disease progression in HIV/AIDS. Blood *108*, 3808–3817.

Norris, B.A., Uebelhoer, L.S., Nakaya, H.I., Price, A.A., Grakoui, A., and Pulendran, B. (2013). Chronic but not acute virus infection induces sustained expansion of myeloid suppressor cell numbers that inhibit viral-specific T cell immunity. Immunity *38*, 309–321.

O

Ohta, T., Sugiyama, M., Hemmi, H., Yamazaki, C., Okura, S., Sasaki, I., Fukuda, Y., Orimo, T., Ishii, K.J., Hoshino, K., et al. (2016). Crucial roles of XCR1-expressing dendritic cells and the XCR1-XCL1 chemokine axis in intestinal immune homeostasis. Sci. Rep. *6*, 23505.

Okoye, I.S., Houghton, M., Tyrrell, L., Barakat, K., and Elahi, S. (2017). Coinhibitory Receptor Expression and Immune Checkpoint Blockade: Maintaining a Balance in CD8 T Cell Responses to Chronic Viral Infections and Cancer. Front. Immunol. *8*, 1215.

Oldstone, M.B.A. (2006). Viral persistence: Parameters, mechanisms and future predictions. Virology *344*, 111–118.

Oldstone, M.B.A. (2013). Lessons learned and concepts formed from study of the pathogenesis of the two negative-strand viruses lymphocytic choriomeningitis and influenza. Proc. Natl. Acad. Sci. U. S. A. *110*, 4180–4183.

Oldstone, M.B.A., and Campbell, K.P. (2011). Decoding arenavirus pathogenesis: Essential roles for alpha-dystroglycan-virus interactions and the immune response. Virology *411*, 170–179.

P

Pauken, K.E., and John Wherry, E. (2015). Overcoming T cell exhaustion in infection and cancer. Trends Immunol. *36*, 265–276.

Peligero, C., Argilaguet, J., Güerri-Fernandez, R., Torres, B., Ligero, C., Colomer, P., Plana, M., Knobel, H., García, F., and Meyerhans, A. (2015). PD-L1 Blockade Differentially Impacts Regulatory T Cells from HIV-Infected Individuals Depending on Plasma Viremia. PLoS Pathog. *11*, e1005270.

Penaloza-MacMaster, P., Kamphorst, A.O., Wieland, A., Araki, K., Iyer, S.S., West, E.E., O'Mara, L., Yang, S., Konieczny, B.T., Sharpe, A.H., et al. (2014). Interplay between regulatory T cells and PD-1 in modulating T cell exhaustion and viral control during chronic LCMV infection. J. Exp. Med. *211*, 1905–1918.

Penna, A., Pilli, M., Zerbini, A., Orlandini, A., Mezzadri, S., Sacchelli, L., Missale, G., and Ferrari, C. (2007). Dysfunction and functional restoration of HCV-specific CD8 responses in chronic hepatitis C virus infection. Hepatology *45*, 588–601.

Perez, M., and de la Torre, J.C. (2003). Characterization of the Genomic Promoter of the Prototypic Arenavirus Lymphocytic Choriomeningitis Virus. J. Virol. *77*, 1184–1194.

Petrovas, C., Casazza, J.P., Brenchley, J.M., Price, D.A., Gostick, E., Adams, W.C., Precopio, M.L., Schacker, T., Roederer, M., Douek, D.C., et al. (2006). PD-1 is a regulator of virus-specific CD8 T cell survival in HIV infection. J. Exp. Med. *203*, 2281–2292.

Pipkin, M.E., Sacks, J.A., Cruz-Guilloty, F., Lichtenheld, M.G., Bevan, M.J., and Rao, A. (2010). Interleukin-2 and inflammation induce distinct transcriptional programs that promote the differentiation of effector cytolytic T cells. Immunity *32*, 79–90.

Prame Kumar, K., Nicholls, A.J., and Wong, C.H.Y. (2018). Partners in crime: neutrophils and monocytes/macrophages in inflammation and disease. Cell Tissue Res. *371*, 551–565.

R

Radziewicz, H., Dunham, R.M., and Grakoui, A. (2009). PD-1 tempers Tregs in chronic HCV infection. J. Clin. Invest. *119*, 450–453.

Rehermann, B., and Nascimbeni, M. (2005). Immunology of hepatitis B virus and hepatitis C virus infection. Nat. Rev. Immunol. *5*, 215–229.

Richter, K., Perriard, G., and Oxenius, A. (2013). Reversal of chronic to resolved infection by IL-10 blockade is LCMV strain dependent. Eur. J. Immunol. *43*, 649–654.

Rivière, Y., Gresser, I., Guillon, J.C., and Tovey, M.G. (1977). Inhibition by anti-interferon serum of lymphocytic choriomeningitis virus disease in suckling mice. Proc. Natl. Acad. Sci. U. S. A. *74*, 2135–2139.

Robbins, S.H., Bessou, G., Cornillon, A., Zucchini, N., Rupp, B., Ruzsics, Z., Sacher, T., Tomasello, E., Vivier, E., Koszinowski, U.H., et al. (2007). Natural killer cells promote early CD8 T cell responses against cytomegalovirus. PLoS Pathog. *3*, e123.

Robinson, M.D., and Oshlack, A. (2010). A scaling normalization method for differential expression analysis of RNA-seq data. Genome Biol. *11*, R25.

Robinson, M.D., McCarthy, D.J., and Smyth, G.K. (2010). edgeR: a Bioconductor package for differential expression analysis of digital gene expression data. Bioinformatics *26*, 139–140.

Robinson, S.W., Fernandes, M., and Husi, H. (2014). Current advances in systems and integrative biology. Comput. Struct. Biotechnol. J. *11*, 35–46.

Rydyznski, C., Daniels, K.A., Karmele, E.P., Brooks, T.R., Mahl, S.E., Moran, M.T., Li, C., Sutiwisesak, R., Welsh, R.M., and Waggoner, S.N. (2015). Generation of cellular immune memory and B-cell immunity is impaired by natural killer cells. Nat. Commun. *6*, 6375.

S

Said, E.A., Dupuy, F.P., Trautmann, L., Zhang, Y., Shi, Y., El-Far, M., Hill, B.J., Noto, A., Ancuta, P., Peretz, Y., et al. (2010). Programmed death-1–induced interleukin-10 production by monocytes impairs CD4 T cell activation during HIV infection. Nat. Med. *16*, 452–459.

Schmitz, J.E. (1999). Control of Viremia in Simian Immunodeficiency Virus Infection by CD8 Lymphocytes. Science *283*, 857–860.

Schmitz, I., Schneider, C., Fröhlich, A., Frebel, H., Christ, D., Leonard, W.J., Sparwasser, T., Oxenius, A., Freigang, S., and Kopf, M. (2013). IL-21 restricts virus-driven Treg cell expansion in chronic LCMV infection. PLoS Pathog. *9*, e1003362.

Serin, E.A.R., Nijveen, H., Hilhorst, H.W.M., and Ligterink, W. (2016). Learning from Co-expression Networks: Possibilities and Challenges. Front. Plant Sci. *7*, 444.

Sevilla, N., Kunz, S., McGavern, D., and Oldstone, M.B.A. (2003). Infection of dendritic cells by lymphocytic choriomeningitis virus. Curr. Top. Microbiol. Immunol. *276*, 125–144.

Sevilla, N., McGavern, D.B., Teng, C., Kunz, S., and Oldstone, M.B.A. (2004). Viral targeting of hematopoietic progenitors and inhibition of DC maturation as a dual strategy for immune subversion. J. Clin. Invest. *113*, 737–745.

Shin, H., Blackburn, S.D., Blattman, J.N., and Wherry, E.J. (2007). Viral antigen and extensive division maintain virus-specific CD8 T cells during chronic infection. J. Exp. Med. *204*, 941–949.

Snell, L.M., McGaha, T.L., and Brooks, D.G. (2017). Type I Interferon in Chronic Virus Infection and Cancer. Trends Immunol. *38*, 542–557.

Speranza, E., and Connor, J.H. (2017). Host Transcriptional Response to Ebola Virus Infection. Vaccines (Basel) *5*.

Spiropoulou, C.F., Kunz, S., Rollin, P.E., Campbell, K.P., and Oldstone, M.B.A. (2002). New World arenavirus clade C, but not clade A and B viruses, utilizes alpha-dystroglycan as its major receptor. J. Virol. *76*, 5140–5146.

Subramanian, N., Torabi-Parizi, P., Gottschalk, R.A., Germain, R.N., and Dutta, B. (2015). Network representations of immune system complexity. Wiley Interdiscip. Rev. Syst. Biol. Med. *7*, 13–38.

Sun, X., Hua, S., Chen, H.-R., Ouyang, Z., Einkauf, K., Tse, S., Ard, K., Ciaranello, A., Yawetz, S., Sax, P., et al. (2017). Transcriptional Changes during Naturally Acquired Zika Virus Infection Render Dendritic Cells Highly Conducive to Viral Replication. Cell Rep. *21*, 3471–3482.

Suvas, S., Kumaraguru, U., Pack, C.D., Lee, S., and Rouse, B.T. (2003). CD4+CD25+ T cells regulate virus-specific primary and memory CD8+ T cell responses. J. Exp. Med. *198*, 889–901.

T

Teijaro, J.R., Ng, C., Lee, A.M., Sullivan, B.M., Sheehan, K.C.F., Welch, M., Schreiber, R.D., de la Torre, J.C., and Oldstone, M.B.A. (2013). Persistent LCMV infection is controlled by blockade of type I interferon signaling. Science *340*, 207–211.

Thimme, R., Bukh, J., Spangenberg, H.C., Wieland, S., Pemberton, J., Steiger, C., Govindarajan, S., Purcell, R.H., and Chisari, F.V. (2002). Viral and immunological determinants of hepatitis C virus clearance, persistence, and disease. Proc. Natl. Acad. Sci. U. S. A. *99*, 15661–15668.

Tinoco, R., Alcalde, V., Yang, Y., Sauer, K., and Zuniga, E.I. (2009). Cell-intrinsic transforming growth factor-beta signaling mediates virus-specific CD8+ T cell deletion and viral persistence in vivo. Immunity *31*, 145–157.

de la Torre, J.C. (2009). Molecular and cell biology of the prototypic arenavirus LCMV: implications for understanding and combating hemorrhagic fever arenaviruses. Ann. N. Y. Acad. Sci. *1171 Suppl 1*, E57–E64.

Traub, E. (1936a). An epidemic in a mouse colony due to the virus of acute lymphocytic choriomeningitis. J. Exp. Med. *63*, 533–546.

Traub, E. (1936b). Persistence of lymphocytic choriomeningitis virus in immune animals and its relation to immunity. J. Exp. Med. *63*, 847–861.

V

Virgin, H.W., John Wherry, E., and Ahmed, R. (2009). Redefining Chronic Viral Infection. Cell *138*, 30–50.

Vollbrecht, T., Stirner, R., Tufman, A., Roider, J., Huber, R.M., Bogner, J.R., Lechner, A., Bourquin, C., and Draenert, R. (2012). Chronic progressive HIV-1 infection is associated with elevated levels of myeloid-derived suppressor cells. AIDS *26*, F31–F37.

W

Waggoner, S.N., Cornberg, M., Selin, L.K., and Welsh, R.M. (2011). Natural killer cells act as rheostats modulating antiviral T cells. Nature *481*, 394–398.

Welsh, R.M., and Seedhom, M.O. (2008). Lymphocytic choriomeningitis virus (LCMV): propagation, quantitation, and storage. Curr. Protoc. Microbiol. *Chapter 15*, Unit 15A.1.

Wherry, E.J. (2011). T cell exhaustion. Nat. Immunol. *12*, 492–499.

Wherry, E.J., and John Wherry, E. (2011). T cell exhaustion. Nat. Immunol. *12*, 492–499.

Wherry, E.J., John Wherry, E., and Kurachi, M. (2015). Molecular and cellular insights into T cell exhaustion. Nat. Rev. Immunol. *15*, 486–499.

Wilson, E.B., and Brooks, D.G. (2010). Translating insights from persistent LCMV infection into anti-HIV immunity. Immunol. Res. *48*, 3–13.

Wilson, E.B., Yamada, D.H., Elsaesser, H., Herskovitz, J., Deng, J., Cheng, G., Aronow, B.J., Karp, C.L., and Brooks, D.G. (2013). Blockade of chronic type I interferon signaling to control persistent LCMV infection. Science *340*, 202–207.

X

Xu, D., Fu, J., Jin, L., Zhang, H., Zhou, C., Zou, Z., Zhao, J.-M., Zhang, B., Shi, M., Ding, X., et al. (2006). Circulating and liver resident CD4+CD25+ regulatory T cells actively influence the antiviral immune response and disease progression in patients with hepatitis B. J. Immunol. *177*, 739–747.

Y

Yang, Z.-W., Jiang, Y.-H., Ma, C., Silvestri, G., Bosinger, S.E., Li, B.-L., Jong, A., Zhou, Y.-H., and Huang, S.-H. (2016). Coexpression Network Analysis of Benign and Malignant Phenotypes of SIV-Infected Sooty Mangabey and Rhesus Macaque. PLoS One *11*, e0156170.

Ye, B., Liu, X., Li, X., Kong, H., Tian, L., and Chen, Y. (2015). T-cell exhaustion in chronic hepatitis B infection: current knowledge and clinical significance. Cell Death Dis. *6*, e1694.

Yi, J.S., Du, M., and Zajac, A.J. (2009). A Vital Role for Interleukin-21 in the Control of a Chronic Viral Infection. Science *324*, 1572–1576.

Yue, F.Y., Lo, C., Sakhdari, A., Lee, E.Y., Kovacs, C.M., Benko, E., Liu, J., Song, H., Jones, R.B., Sheth, P., et al. (2010). HIV-specific IL-21 producing CD4+ T cells are induced in acute and chronic progressive HIV infection and are associated with relative viral control. J. Immunol. *185*, 498–506.

Z

Zajac, A.J., Blattman, J.N., Murali-Krishna, K., Sourdive, D.J., Suresh, M., Altman, J.D., and Ahmed, R. (1998). Viral immune evasion due to persistence of activated T cells without effector function. J. Exp. Med. *188*, 2205–2213.

Zak, D.E., and Aderem, A. (2009). Systems biology of innate immunity. Immunol. Rev. *227*, 264–282.

Zehn, D., and Wherry, E.J. (2015). Immune Memory and Exhaustion: Clinically Relevant Lessons from the LCMV Model. In Advances in Experimental Medicine and Biology, pp. 137–152.

Zeng, M., Haase, A.T., and Schacker, T.W. (2012). Lymphoid tissue structure and HIV-1 infection: life or death for T cells. Trends Immunol. *33*, 306–314.

Zhang, B., and Horvath, S. (2005). A general framework for weighted gene co-expression network analysis. Stat. Appl. Genet. Mol. Biol. *4*, Article17.

Zhao, W., Langfelder, P., Fuller, T., Dong, J., Li, A., and Hovarth, S. (2010). Weighted gene coexpression network analysis: state of the art. J. Biopharm. Stat. *20*, 281–300.

Zhen, A., Rezek, V., Youn, C., Lam, B., Chang, N., Rick, J., Carrillo, M., Martin, H., Kasparian, S., Syed, P., et al. (2017). Targeting type I interferon-mediated activation restores immune function in chronic HIV infection. J. Clin. Invest. *127*, 260–268.

Zhou, X., Ramachandran, S., Mann, M., and Popkin, D.L. (2012). Role of lymphocytic choriomeningitis virus (LCMV) in understanding viral immunology: past, present and future. Viruses *4*, 2650–2669.

Zinkernagel, R.M. (1975). H-2 compatibility requirement for T-cell-mediated lysis of target cells infected with lymphocytic choriomeningitis virus. Different cytotoxic T- cell specificities are associated with structures coded for in H-2K or H-2D; J. Exp. Med. *141*, 1427–1436.

Zinkernagel, R.M. (2002). Lymphocytic Choriomeningitis Virus and Immunology. In Current Topics in Microbiology and Immunology, pp. 1–5.

Zinkernagel, R.M., and Doherty, P.C. (1974). Restriction of in vitro T cell-mediated cytotoxicity in lymphocytic choriomeningitis within a syngeneic or semiallogeneic system. Nature *248*, 701–702.

Zuniga, E.I., Macal, M., Lewis, G.M., and Harker, J.A. (2015). Innate and Adaptive Immune Regulation During Chronic Viral Infections. Annual Review of Virology *2*, 573–597.